



## Metal-organic Frameworks Based on Flexible Ligands (FL-MOFs): Structures and Applications

Journal:	<i>Chemical Society Reviews</i>
Manuscript ID:	CS-REV-12-2013-060483.R1
Article Type:	Review Article
Date Submitted by the Author:	05-Mar-2014
Complete List of Authors:	Lin, Zu-Jin; State Key Laboratory of Structural Chemistry, Fujian Institute of Research on the Structure of Matter, Chinese Academy of Sciences, Lü, Jian; Fujian Institute of Research on the Structure of Matter, Hong, Maochun; Fujian Institute of Research on the Structure of Matter,, State Key Laboratory of Structural Chemistry Cao, Rong; Fujian Institute of Research on the Structure of Matter, State Key Laboratory of Structural Chemistry

## ARTICLE

# Metal-organic Frameworks Based on Flexible Ligands (FL-MOFs): Structures and Applications

Cite this: DOI: 10.1039/x0xx00000x

Zu-Jin Lin, Jian Lü, Maochun Hong and Rong Cao\*

Received 00th January 2012,  
Accepted 00th January 2012

DOI: 10.1039/x0xx00000x

[www.rsc.org/](http://www.rsc.org/)

Metal-organic frameworks (MOFs), also known as coordination polymers (CPs), are crystalline materials constructed from metal ions or clusters bridged by organic ligands to form one-, two-, or three-dimensional infinite networks. In contrast with the prolific production of MOFs based on rigid ligands (RL-MOFs), the design, syntheses and applications of MOFs based on flexible ligands (FL-MOFs) are somewhat overlooked. Although sacrificing a measure of control, the use of flexible ligands may provide unique opportunities to obtain novel crystalline framework materials exhibiting desirable attributes. In this review, emphasis has been placed on the design and the structural diversity of FL-MOFs. Homochiral FL-MOFs and dynamic frameworks induced by flexible ligands are also briefly outlined. An overview is also shown to the applications of FL-MOFs as platforms for gas adsorption, heterogeneous catalysis, proton conduction etc.

## 1. Introduction

Metal-organic frameworks (MOFs), also known as coordination polymers (CPs), are crystalline materials constructed from metal ions or clusters bridged by organic ligands to form one-, two-, or three-dimensional infinite networks.<sup>1</sup> MOFs are becoming one of the most rapidly developing fields in chemical and material sciences and emerging as an important family of porous materials not only because of their intriguing network topologies<sup>2</sup> but also exploitable properties for potential applications such as gas adsorption and separation,<sup>3</sup> catalysis,<sup>4</sup> luminescence,<sup>5</sup> sensing,<sup>6</sup> proton conduction<sup>7</sup> and etc.<sup>8</sup> Their crystalline nature, high and permanent porosity, uniform pore sizes, extraordinary surface areas, finely tunable pore surface properties, and potential scalability to industrial scale have made these materials an attractive target for further study.<sup>9</sup>

The design and synthesis of MOFs always begins with the selection of the metallic nodes and the bridging organic spacers. The structure and functionality rely strongly on either the two components or the nature and type of connection between them. Not surprisingly, MOFs design quickly evolved into the use of conformationally rigid organic ligands associated with the secondary building units (SBUs) or supermolecular building blocks (SBBs) with well-defined coordination spheres under the guide of topology.<sup>10</sup> In principle, the use of geometrically fixed organic building blocks allows targeting of frameworks with certain topologies. Such frameworks usually exhibit relatively high thermal and mechanical stability and are capable of retention the porosity upon guest solvents removal. For these reasons, rigid benzene di-, tri-, and tetra-carboxylic acids, azolate-based ligands, as well as their derivatives are

commonly employed as organic building blocks, and this approach has successfully yielded a range of MOFs with desirable attributes.<sup>11</sup>

In contrast with the prolific production of MOFs based on rigid ligands (denoted as RL-MOFs hereafter, which will be highlighted by Zhou in this MOF themed issue), the design, syntheses and applications of MOFs based on flexible ligands (denoted as FL-MOFs hereafter for convenience) have so far attracted unparallel research attention.<sup>12</sup> Indeed, it is more difficult to construct FL-MOFs due to the flexibility of ligands themselves that can adopt different conformations and thus lead to distinct symmetries during the self-assemble process. On the other hand, the structures of FL-MOFs are more dependent to the various and subtle reaction parameters including temperature, time, pH etc. These factors severely hinder the development of knowledge and concepts that allow the rational design and prediction of extended network architectures with flexible organic ligands.<sup>13</sup> In addition, most FL-MOFs turn to fragile and may lose their porosities after guest molecules removal because of the ligand flexibility that can hardly sustain the skeleton of the frameworks. Some unique advantages, however, have been realized from the use of flexible ligands to make MOFs. For example, conformational mobility coupled with coordination preferences of metal ions (clusters) provides a means to generate FL-MOFs with structural diversity in that crystalline structures inaccessible from rigid building blocks may be obtained from more malleable precursors. Due to their versatile coordination modes and conformations, flexible ligands with multi-donors have been extensively used for constructing polynuclear MOFs and transmitting magnetic

exchanges.<sup>14</sup> Besides, many chiral organic molecules, such as amino acids, peptides and their derivatives, are flexible and can be used as chiral organic linkers to construct FL-MOFs with chiral centers. The resulting homochiral FL-MOFs may confer the possibility of porous FL-MOFs with enantioselective separation, asymmetric catalysis and even biological attributes, which is not easily amenable with rigid linkers for the scarcity of rigid chiral organic ligands. Furthermore, the incorporation of flexible components in MOFs may endow the molecular architectures with a “breathing” ability and adaptive recognition properties as a function of coexisting guest or counterions.<sup>15</sup>

It should be clarified that there is obvious difference between flexible MOFs and FL-MOFs. The former is capable of responding to external stimuli and means that the whole framework is dynamic, while the latter represents one of the components of the framework is flexible. There is not direct link between the organic linker’s rigidity/flexibility and that of the resulting frameworks. Flexible MOFs can be built by rigid ligands or flexible ligands and the flexible ligands can be used to build both flexible MOFs and robust MOFs. FL-MOFs are not always required to breathe. Recently, some review articles have focused specially on the theme of dynamic MOFs.<sup>16</sup> In view of few highlights concerning upon the FL-MOFs, herein, we provide a review of FL-MOFs, covering their design, synthesis, structures and some applications.

It also should be noted that there is not an exact or strict definition about rigid/flexible ligands within the realm of crystal engineering. In principle, ligands are flexible once rotating around a single bond. In this contribution, only ligands with at least one  $sp^3$  hybrid atom (usually C, N, or O) on their backbones are discussed, some of which were interpreted as “semi-rigid ligands” in the original literature.<sup>17</sup> Ligands with flexible sections which do not participate in metal-ligand coordination, as in the case of e.g. 2-butylterephthalic acid in which the butyl group is somewhat flexible but not a metal ligating group, are excluded. Some MOFs built by mixed flexible and rigid ligands were also included and denoted as FL-MOFs. Considering the large number of reports, this review is not an exhaustive literature survey of either the structural features or properties of FL-MOFs. Instead, emphasis has been placed on the design and the structural diversity of FL-MOFs. Homochiral FL-MOFs and dynamic frameworks induced by flexible ligands are also briefly outlined. An overview is also shown to the applications of FL-MOFs as platforms for gas adsorption, heterogeneous catalysis, proton conduction etc.

## 2. The structures of FL-MOFs

### 2.1 Structural diversity of FL-MOFs

#### 2.1.1 FL-MOFs based on achiral ligands

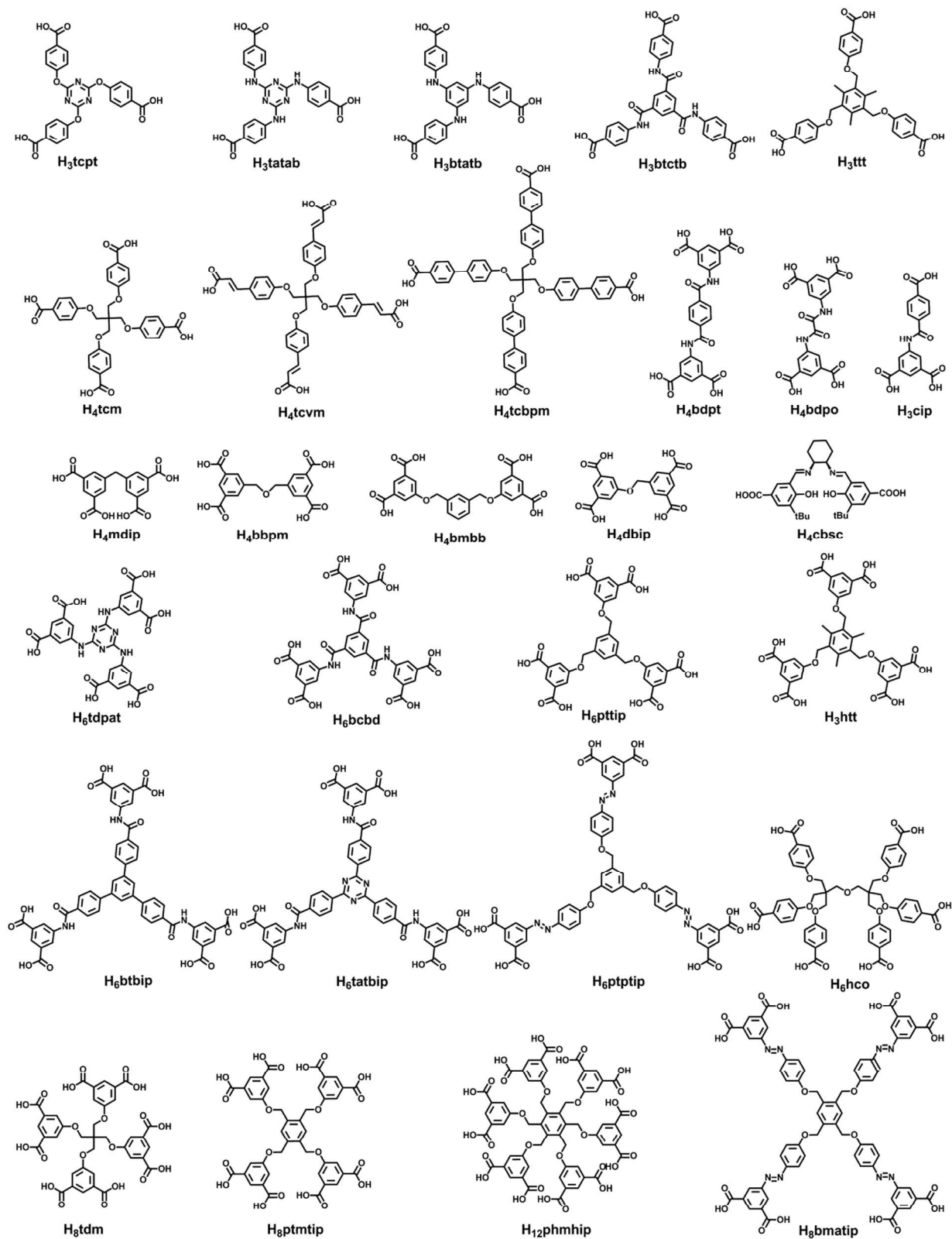
Any discussion of the structural feature of FL-MOFs must touch upon the structural diversity. In principle, the metal ligating functional groups in a flexible ligand can rotate around the single bond thus resulting in its versatile conformations.

Conformational mobility of flexible ligands coupled with coordination preferences of metal ions (clusters) provide a means to generate structural diversity in that crystalline structure inaccessible from rigid building blocks may be obtained from more malleable precursors. An illustrative example is found in a simple flexible ligand 5-(3,5-dicarboxybenzyloxy)isophthalic acid ( $H_4dbip$ ). With two preferential conformations, corresponding to the two phenyl rings in the ligand coplanar or perpendicular to each other (Fig. S1),  $H_4dbip$  can act as planar and tetrahedral nodes, thus resulting in FL-MOFs with **dia**, **flu**, **pts**, **lon**, **msw**, **nbo** topologies.<sup>18</sup> On the contrary, the two phenyl rings in the similar rigid ligands, such as 3,3',5,5'-biphenyltetracarboxylate ( $H_4bpdc$ ) and 1,1'-azobenzene-3,3',5,5'-tetracarboxylic acid ( $H_4azpy$ ), are always coplanar and thus typically serve as 4-connected planar nodes resulting in **nbo**-type MOF materials.<sup>19</sup>

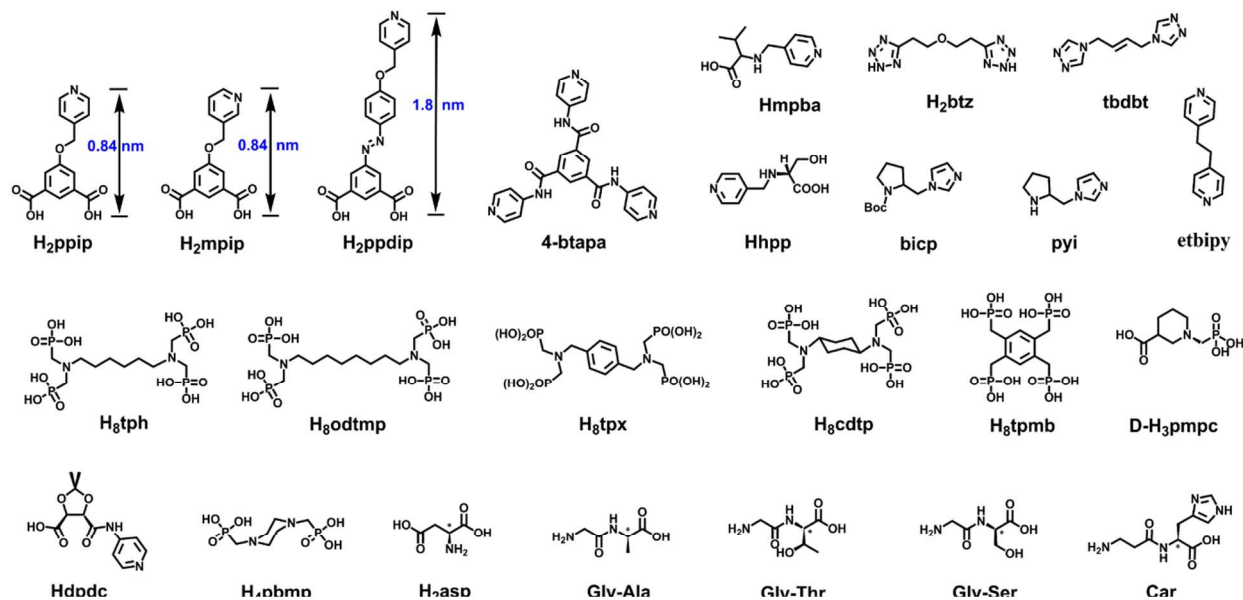
So far, a number of FL-MOFs have been synthesized<sup>20</sup> and some reviews involving the structural diversity of FL-MOFs have been reported.<sup>21</sup> For example, assembly of the *cis*- $H_2CDC$  (1,4-cyclohexanedicarboxylate acid) and Al(III) yielded a layered structure, while that of the *trans*- $H_2CDC$  yielded a MIL-53-like porous network.<sup>22</sup> Combination of the  $H_2obb$  ligands and Co(II) obtained a self-catenated and interdigitated layered framework etc.<sup>23</sup> In consideration of the various flexible ligands being applied in the construction of FL-MOFs, it is truly difficult to survey all of the reported FL-MOF structures. Herein, only tetrakis[4-(carboxyphenyl)oxamethyl]methane acid ( $H_4tcm$ ) was taken as an representative example to elucidate how the diverse structures of FL-MOFs were built by the use of flexible ligands.

As shown in Fig. S2,  $H_4tcm$  is a typical flexible ligand with four 4-methoxybenzoic acid arms linking to a quaternary carbon atom (denoted as  $C_{core}$ ). The relative orientation of the four 4-methoxybenzoic acid arms alters when rotating around -O-CH<sub>2</sub>- moieties, resulting in various conformations. With the carbon atoms in carboxylic groups labelled as  $C_{carboxyl}$ , the conformations of  $H_4tcm$  can be roughly differentiated by a tetrahedron (denoted as  $C_{carboxyl}$  tetrahedra) where the four  $C_{carboxyl}$  atoms in  $H_4tcm$  act as vertexes and the six  $C_{carboxyl}$ - $C_{carboxyl}$  act as edges. To date, more than forty FL-MOFs built by  $H_4tcm$  have been successfully synthesized and characterized. Apart from isomorphous, the conformations of  $H_4tcm$  in these FL-MOFs are distinct to each other (Table S1). The angle of  $C_{carboxyl}$ - $C_{core}$ - $C_{carboxyl}$  ranges from 41° to 174°, and the distance of  $C_{carboxyl}$ - $C_{carboxyl}$  alters from 5.176 Å to 15.341 Å. As a result, the geometries of the  $C_{carboxyl}$  tetrahedron can be approximately regular, irregular or even nearly flattened. The various conformations of  $H_4tcm$  are capable of meeting different coordination environments of metal ions (clusters), leading to structural diversity of the resultant FL-MOFs.

Although  $H_4tcm$  has many conformations, most of them belong to low symmetric point groups (e.g.,  $C_1$  and  $C_2$ ), presumably ascribing to the high rotation degree of -CH<sub>2</sub>-O- moieties. As the symmetric information in organic ligands and inorganic SBUs may be transmit to the whole framework, the low symmetrical molecular conformations may facilitate the



Scheme 1 The selected flexible ligands involving in this paper.



Scheme 1 The selected flexible ligands involving in this paper (continuous).

construction of noncentrosymmetric structures, which is the basic requirement for ferroelectric and second-order non-linear optical (NLO) properties. Based on this approach, Cao and co-workers successfully isolated a noncentrosymmetric diamondoid FL-MOF  $\{[\text{Zn}_2(\text{tcm})(\text{CH}_3\text{CH}_2\text{OH})]\cdot 3\text{H}_2\text{O}\}_n$ .<sup>24</sup> In this structure, the crystallographically independent  $\text{tcm}^{4-}$  ligand ( $C_1$  point group) connects four binuclear zinc units with different complexation modes to form chiral tetrahedral

building units, leading to the generation of the noncentrosymmetric framework. This FL-MOF crystallizes in the point group  $C_s$ , belonging to one of the 10 polar point groups. Ferroelectric and NLO measurements showed that the resulting framework displays interesting ferroelectric and NLO properties ( $\sim 2.5$  times that of potassium dihydrogen phosphate (KDP)). This framework represents the first successful attempt to prepare ferroelectric and NLO-active FL-MOFs with **dia** net from chiral tetracarboxylate building blocks. The authors further isolated another noncentrosymmetric framework  $\{[\text{Zn}_2(\text{tcm})(\text{H}_2\text{O})]_2\cdot \text{H}_2\text{O}\}_n$ , which exhibits intriguing structural features of interpenetration and self-catenation, as well as NLO properties (1.5 times that of KDP).<sup>25</sup> Du and co-workers isolated a FL-MOF  $\{[\text{Zn}_4(\text{tcm})_2(\text{H}_2\text{O})_3(\text{DMA})]\cdot 2\text{H}_2\text{O}\}_n$  (DMA = *N,N*-dimethylacetamide) with  $C_s$  polar point groups by reaction of  $\text{H}_4\text{tcm}$  and  $\text{ZnCl}_2\cdot 2\text{H}_2\text{O}$ .<sup>26</sup> Remarkably, the resulting FL-MOF shows second-harmonic generation (SHG) response (0.6 times that of urea) and ferroelectric properties.

Although several examples of such FL-MOFs were documented (see above), the preparation of noncentrosymmetric FL-MOFs with  $\text{H}_4\text{tcm}$  was somehow serendipitous. It should be noted that most FL-MOFs of  $\text{H}_4\text{tcm}$  were centrosymmetric, no matter which conformations  $\text{H}_4\text{tcm}$  adopted. For example, a centrosymmetric FL-MOF with  $\text{Zn}_4\text{O}(\text{CO}_2)_6$  building units,

$\{[\text{Zn}_4\text{O}(\text{tcm})_{1.5}\cdot 4\text{DMA}\cdot 10\text{DEF}\cdot 10\text{H}_2\text{O}]\}_n$  (DEF = *N,N*-diethylformamide), has been prepared under solvothermal conditions.<sup>27</sup> In this case, the  $\text{tcm}^{4-}$  ligand locates at  $C_2$  axis and belongs to  $C_2$  point group. As shown in Fig. 1a, three carboxylic groups from a  $\text{Zn}_4\text{O}(\text{CO}_2)_6$  cluster serve as a tritopic subunit with angles of  $86^\circ$  and the  $C_{\text{carboxyl}}-C_{\text{core}}-C_{\text{carboxyl}}$  angles in the  $\text{tcm}^{4-}$  ligand are nearly  $90^\circ$ . As a result, two  $\text{Zn}_4\text{O}(\text{CO}_2)_6$  vertices and three  $C_{\text{carboxyl}}-C_{\text{core}}-C_{\text{carboxyl}}$  edges from three ligands build a nanoscale trigonal bipyramidal cage with a diameter of *ca.* 2.0 nm. The curvature needed at the vertices was accomplished by rotation of  $-\text{O}-\text{CH}_2-$  moieties. The remaining two arms from each ligand link the neighbouring cages so that each nanocage is doubly cross-linked to six adjacent nanocages (Fig. 1b). A **pcu** network is generated through the above cage-to-cage connections by considering the cages as nodes. Because of the O-rich environment at wall of the molecular cavities, this FL-MOF shows particular affinity to polar molecules. The adsorption amounts of ethanol, water and methanol vary incrementally from 5.12 wt% to 12.3 wt%. In contrast, the cyclohexane uptake is nearly zero even at the high pressure (0.007 wt%).

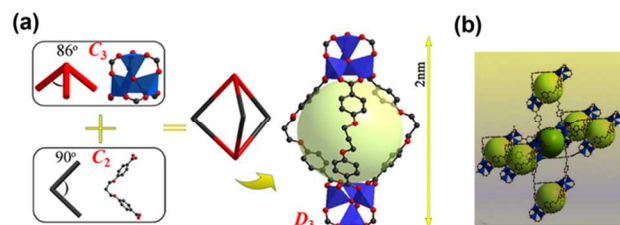


Fig. 1 (a) Trigonal bipyramidal cage built by  $\text{tcm}^{4-}$  and  $\text{Zn}_4\text{O}(\text{CO}_2)_6$  cluster. (b) Representation of nanoscale cages covalently linked into a FL-MOF with **pcu** network. Adapted with permission from ref. <sup>27</sup>. Copyright 2010 Royal Society of Chemistry.

Besides, a series of centrosymmetric FL-MOFs with anionic, cationic, and neutral metal-carboxylate frameworks based on  $H_4tcm$  has also been synthesized.<sup>28</sup> The reactions between divalent transition metal ions and  $H_4tcm$  ligands gave  $\{[M_3(tcm)_2][NH_2(CH_3)_2]_2 \cdot 8DMA\}_n$  ( $M = Co(II), Mn(II), Cd(II)$ ) which have anionic metal-carboxylate frameworks with  $NH_2(CH_3)_2^+$  cations filling in the channels. The reactions of trivalent metal ions  $Y(III), Dy(III),$  and  $In(III)$  with  $H_4tcm$  ligand afforded cationic metal-carboxylate frameworks  $\{[M_3(tcm)_2 \cdot (NO_3) \cdot (DMA)_2 \cdot (H_2O)] \cdot 5DMA \cdot 2H_2O\}_n$  ( $M = Y(III), Dy(III)$ ) and  $\{[In_2(tcm)_3 \cdot (OH)_2] \cdot 3DMA \cdot 6H_2O\}_n$  with the  $NO_3^-$  and  $OH^-$  serving as counterions, respectively. A neutral metal-carboxylate framework  $\{[Pb_2(tcm) \cdot (DMA)_2] \cdot 2DMA\}_n$  was isolated from the reaction of  $Pb(II)$  cations. The charged metal-carboxylate frameworks exhibit selectivity for specific counterions in the reaction system and ion-exchange behaviors.

Supramolecular isomerism is another feather of FL-MOFs because of the inherent conformational diversity derived from the flexibility of the organic ligands. By means of slight adjustment in synthetic parameters, Thallapally, Atwood, and co-workers successfully isolated three centrosymmetric supramolecular isomers, which show 3-fold **pts** topology, 2-fold **dia** topology and 2-fold **lon** topology, respectively (Fig. S3).<sup>29</sup> Activated separately overnight at 200 °C under vacuum, the resulting **pts**, **dia**, and **lon** networks showed  $CO_2$  absorption of 6, 24 and 14 wt%, respectively, at room temperature and 25 bar. The **dia** and **lon** networks sorb  $CO_2$  preferably over  $N_2, H_2$  and methane at room temperature. Additionally, the **pts** and **dia** networks are capable of the catalytic conversion of toluene and biphenyl to a corresponding *p*-*tert*-butyl derivative.<sup>30</sup>

Three novel metal-organic framework isomers based on  $H_4tcm$  with cadmium cations have been synthesized by solvothermal assemble.<sup>31</sup> All three frameworks, having a general formula of  $\{Cd_6(tcm)_3(H_2O)_6 \cdot xsolvent\}_n$ , possess the same **dia** topology but with significant distinct SBUs. In this peculiar case, the choice of solvent exerts a profound influence on both the formation of different type of inorganic clusters/rod SBUs and the way of the organic linker meeting coordination environments of discrete metal cluster (*via* rotating the flexible moieties) in each framework, resulting in supramolecular isomerism.

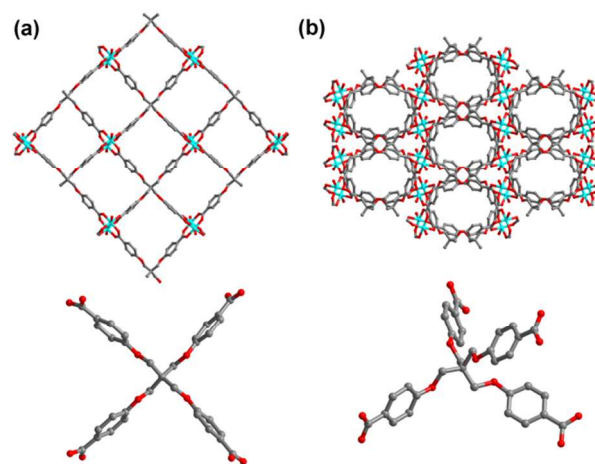


Fig. 2 The channels and  $H_4tcm$  conformations in the *pts*-type networks of (a) SNU-21 and (b)  $\{[Cu_2(tcm)(H_2O)_2] \cdot 4DMA \cdot (H_2O)_2\}_n$ . Colour scheme: Cu, turquoise; C, gray; N, blue; O, red.

As shown in Fig. 2, by combination of  $Cu_2(COOCR)_4$  paddle-wheel SBUs and  $H_4tcm$ , two isomorphous FL-MOFs formulated as  $\{[Cu_2(tcm)(H_2O)_2] \cdot 7DMF \cdot 3(1,4-dioxane) \cdot MeOH\}_n$  (denoted as SNU-21 in the original paper)<sup>32</sup> and  $\{[Cu_2(tcm)(H_2O)_2] \cdot 4DMA \cdot (H_2O)_2\}_n$ <sup>33</sup> have been reported by Suh and Du, respectively. Despite of the same components and topology of the main frameworks (i.e., **pts** topology), the structures of these two FL-MOFs are different to each other. Whilst the geometry of the  $C_{carboxyl}$  tetrahedron in the former structure is nearly flattened, the geometry of that in the latter structure is obvious an irregular tetrahedron (Fig. 2). The differences in  $-CH_2-O-$  space torsion angles in  $tcm^4$  ligand profoundly affect not only in terms of resultant structures, but also in terms of properties of FL-MOFs. In this case, SNU-21 has a larger uptake of  $N_2, CH_4$  and  $CO_2$  than that of the other isomer under the same conditions. Besides, SNU-21 exhibits breathing phenomenon upon adsorption of saturated hydrocarbons.<sup>34</sup>

Upon close inspection into the structure of SNU-21, one can observe that the paddle-wheel SBUs serve as planar nodes, while the flexible  $tcm^4$  ligands act as tetrahedral nodes. The planar nodes arrange in a face-to-face fashion, leading to the axial coordination water molecules pointing into the channels in the same direction. The axial aqua molecules on the paddle-wheel SBUs can be readily replaced by secondary pyridyl or imidazole ligands. In such way, a series of pillared 3D frameworks derived from the parent **pts** networks (i.e., SNU-21) has been designed and synthesized (Fig. 3). Among these pillared FL-MOFs,  $\{[Zn(tcm)(bipy)] \cdot xsolvent\}_n$  ( $bipy = 4,4'$ -bipyridine) shows a 2-fold interpenetrated framework showing breathing effect that absorbs  $CO_2$  preferably over  $N_2$  and  $H_2$ ;<sup>35</sup>  $\{[Co_2(tcm)(etbipy)] \cdot 2DMF \cdot 5H_2O\}_n$  and  $\{[Zn_2(tcm)(etbipy)] \cdot 2.5DMF \cdot 2H_2O\}_n$  ( $etbipy = 1,2$ -bis-(4-pyridyl)ethane) are also 2-fold interpenetrated frameworks with moderate surface areas;<sup>36</sup> Frameworks  $\{[Co_2(tcm)(dib)] \cdot 3DMF\}_n$  ( $dib = 1,4$ -di(1H-imidazol-1-yl)benzene) and  $\{[Co_2(tcm)(dibp)] \cdot 5DMF\}_n$  ( $dibp = 4,4'$ -di(1H-

imidazol-1-yl)-1,1'-biphenyl) exhibit antiferromagnetic behavior.<sup>37</sup>

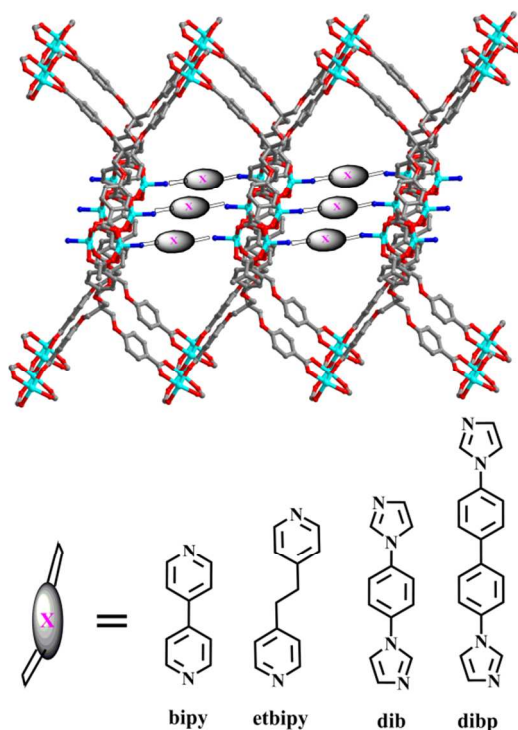


Fig. 3 The  $\text{tcm}^{4-}$ -based pts-net pillared by secondary pyridyl or imidazole ligands. Colour scheme: Cu, turquoise; C, gray; N, blue; O, red.

Recently, Thallapally and co-workers reported that two anionic FL-MOFs  $\{[\text{Mn}_3(\text{tcm})_2]^{2-} \cdot 2[\text{NH}_2(\text{CH}_3)_2]^+ \cdot 9\text{DMF}\}_n$  and  $\{[\text{Mn}_3(\text{tcm})_2]^{2-} \cdot 2(\text{H}_3\text{O})^+ \cdot 12\text{DMF}\}_n$  are capable of sequestering metal cations through cooperative single-crystal-to-single-crystal (SCSC) processes, resulting in novel neutral and heterobimetallic systems with rearranged framework structures.<sup>38</sup> These SCSC transformations are directed by adaptation of the conformation and coordination modes of the flexible organic carboxylate linkers ( $\text{tcm}^{4-}$ ) to meet the coordination environment of inserted/exchanged metal ions, a process involving cooperative breakage/formation of metal-carboxylate coordination bonds in the solid state, resulting in expansion or contraction of the 3D framework by up to 33%. These two anionic FL-MOFs also exhibit exceptional uptake/exchange selectivity for divalent transition-metal cations (e.g.,  $\text{Co}^{2+}$  and  $\text{Ni}^{2+}$ ) in the presence of competing alkali-metal cations (e.g.,  $\text{Li}^+$  and  $\text{Na}^+$ ). In stark contrast to the rigid open 3D frameworks of zeolites, which tend to be less affected by ion exchange, the framework flexibility observed in the anionic FL-MOFs holds great potentials for the design of selective sensors, selective ion-exchange media, and materials for the removal of toxic heavy-metal ions.

## 2.2 Design and synthesis of FL-MOFs

As previous stated, flexible ligands themselves can adopt different conformations with distinct symmetries as a consequence of rotations around single bonds during the self-

assemble process, which greatly deters the ability to design and predict the form of extended network architectures. Although there are so far no effective strategies that are widely applicable to successfully achieve targeting FL-MOFs, it is sensible to develop some common rules to promote the rational design and synthesis of designable FL-MOFs.

A brilliant strategy was demonstrated by Eddaoudi and co-workers who applied a modular pillaring strategy to design and synthesize isorecticular **tbo**-MOFs, including functionalization and expansion of molecular cavities.<sup>39</sup> The unique (3,4)-connected **tbo**-MOFs can be exclusively constructed by utilizing a combination of MOF layers based on the edge-transitive  $4^4$  square lattice (**sql**) and 4-connected (quadrangular) pillars (Fig. 4a). Generally, the **sql** layers can be readily built through square paddle wheel SBUs bridged by ditopic organic ligands such as terephthalate (1,4-bdc) or isophthalate (1,3-bdc). Thus, the surface-decorated **sql**-MOFs (i.e.,  $[\text{M}(\text{R-bdc})]_n$ ) could be employed as supramolecular building layers (SBLs) amenable to pillaring *via* cross-linking through 4-connected organic building blocks to construct the desirable **tbo**-MOFs. To implement this strategy, the authors intelligently designed and synthesized ether linkage 1,3-bdc-based ligands, wherein an ether linkage was chosen to allow flexibility of the pendant bdc arms positioned in a squarelike geometry and retain their ability to freely form the intended SBL (**sql**-MOF). Solvothermal reaction of the flexible rectangle  $5,5',5'',5'''$ -[1,2,4,5-phenyltetramethoxy]tetraisophthalate ( $\text{H}_8\text{ptmtip}$ ) and  $\text{Cu}(\text{NO}_3)_2 \cdot 2.5\text{H}_2\text{O}$  in mixed DMF/water solution yielded  $\{[\text{Cu}_4(\text{ptmtip})(\text{H}_2\text{O})_4 \cdot (\text{solvent})]\}_n$ . As expected, the resulting FL-MOF can be viewed as a pillared **sql**-MOF based on ptmtip cores substituting the interlayer quadrangles and essentially pillaring 2D Cu-(5-R-isophthalate) **sql** SBLs. Alternatively, the structure of this framework can be interpreted as the alternate packing of three types of open polyhedral cages in 3D space (Fig. 4b).

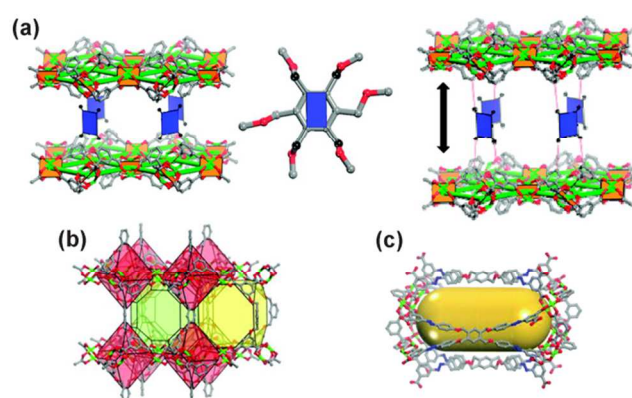


Fig. 4 (a) **tbo**-MOFs can be targeted from **sql** SBLs (green) linked by 4-connected core pillars (blue), which can be functionalized. (b) Three types of polyhedral cage in  $[\text{Cu}_4(\text{ptmtip})(\text{H}_2\text{O})_4 \cdot (\text{solvent})]_n$ : truncated tetrahedron (red), truncated cube (yellow), and truncated cuboctahedron (green). (c) Representation of a nanocapsule cage in  $[\text{Cu}_4(\text{bmatip}_3)(\text{H}_2\text{O})_3(\text{DMF})_3 \cdot (\text{solvent})]_n$ . Reprinted with permission from ref. <sup>39</sup>. Copyright 2011 American Chemical Society.

To further evaluate the efficacy of the strategy, the authors then functionalized  $H_8ptmtip$  with two extra pendant isophthalate arms, which in principle could also potentially coordinate to metal cations and direct the formation of a different network. As projected, the reaction of 5,5',5'',5''',5''''-[1,2,3,4,5,6-phenylhexamethoxy]hexaisophthalic acid ( $H_{12}phmhip$ ) with copper cations under solvothermal reaction yielded another **tbo**-MOF formulated as  $\{Cu_4(H_4phmhip)_2(H_2O)_x(DMF)_4-x(solvent)\}_n$ , which is analogous to  $\{Cu_4(ptmtip)(H_2O)_4(solvent)\}_n$  wherein the two added pendant arms freely point into the generated cavities with no metal coordination. Additionally, the uniqueness of the pillaring approach to **tbo**-MOFs permits the construction of isorecticular FL-MOFs with the identical **tbo** topology *via* the expansion of the flexible organic pillars. Solvothermal reaction between 5,5',5'',5''''-[1,2,4,5-benzenetetrakis(4-methyleneoxyphenylazo)]tetrakisophthalic acid ( $H_8bmatip$ ), and copper cations in mixed DMF/water solution afforded a third isorecticular **tbo**-MOF,  $\{Cu_4(bmatip)_3(H_2O)_3(DMF)_3(solvent)\}_n$ . With expanding quadrangle pillar, the extra-large truncated cuboctahedral cages are more like nanocapsules and possess diameters in the mesoporous range (up to  $29.445 \text{ \AA} \times 18.864 \text{ \AA}$  including vdw radii) (Fig. 4c). The authors further noted that these **tbo**-MOFs exhibit thermal stabilities up to nearly  $300 \text{ }^\circ\text{C}$  and exhibit permanent porosities higher than those observed for the analogous HKUST-1 material.<sup>40</sup> The addition of pendant carboxylic acids enhances the affinity for guest molecules, particularly  $CO_2$ . This approach based on pillaring of SBLs as the main periodic building units will permit the generation of FL-MOFs with larger surface areas that can be readily functionalized for targeted applications prior the assembly process.

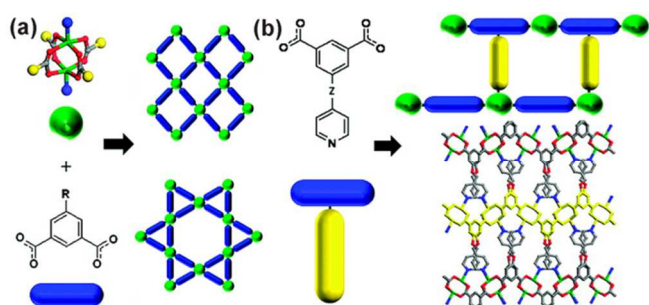


Fig. 5 (a) Scheme showing the derivation of corresponding nets, Kagomé lattice and square lattice, respectively (overhead view). (b) Scheme representing the ligand-to-axial layered MOF (side view) pillaring techniques using exemplary ligands (blue-yellow, "T"-shaped). Reprinted with permission from ref. <sup>41</sup>. Copyright 2011 American Chemical Society.

On the basis of the axial-to-axil and ligand-to-ligand pillaring strategy, Eddaoudi and co-workers developed a new pillaring strategy, ligand-to-axial approach, which permits design, access, and construction of higher dimensional MOFs *via* both rigid and flexible ligands.<sup>41</sup> In this strategy, trigonal bifunctional ligands, in this case isophthalic acid cores functionalized at the 5-position with N-donor (e.g., pyridyl)

moieties, are designed and utilized to pillar pretargeted 2D layers (Fig. 5). Two edge transitive 2D nets, square lattice (**sql**) and Kagomé lattice (**kgm**), have been applied as supramolecular building layers (SBLs), which are cross-linked into predicted 3,6-connected 3D MOFs with tuneable cavities. For example, reaction between copper nitrate and a flexible 5-(4-pyridinylmethoxy)-isophthalic acid ( $H_2ppip$ ) results in an expected ligand-to-axial pillared FL-MOF with **kgm**-SBLs  $\{Cu(ppip):xsolvent\}_n$ , in which  $ppip$  serves as a 3-connected node and the paddlewheel cluster as a 6-connected octahedral node (Fig. 5b). The resultant framework is consistent with the anticipated **ScD**<sub>0.33</sub> (46032), a novel network in MOF chemistry. Addition of a structure-directing agent 1-iodo-4-nitrobenzene in the above system reaction system leads to another type of pillared FL-MOF with **sql** SBLs showing overall **apo** topology,  $\{Cu(ppip):xsolvent\}_n$ . A close inspection indicates that, in the latter structure, the flexible  $H_2ppip$  adopts relatively lower symmetry than that of the former framework, leading to two supramolecular isomers of FL-MOFs. Likewise, reaction between copper nitrate and 5-(3-pyridinylmethoxy)-isophthalic acid ( $H_2mpip$ ), an  $H_2ppip$  isomer, results in an analogous ligand-to-axial pillared FL-MOF with **kgm**-SBLs,  $\{Cu(mpip):xsolvent\}_n$ . The unique nature of these nets and the resultant cavities make them amenable to isorecticular chemistry, allowing the design and synthesis of expanded (3,6)-connected MOFs from various trigonal ligands. To validate this strategy, the authors further designed and synthesized an extended (i.e., longer,  $\sim 18 \text{ \AA}$ ) and functionalized (i.e., azo moiety) ligand, 5-[(1E)-2-[4-(4-pyridinyloxy)phenyl]diazanyl]isophthalic acid ( $H_2ppdip$ ). Self-assembled of  $H_2ppdip$  with copper nitrate successfully affords the desired expanded/functionalized ligand-to-axial pillared FL-MOF with **sql** SBLs,  $\{Cu(ppdip):xsolvent\}_n$ .

Apart from **sql** and **kgm** grids, a cuboctahedral cage, also can be readily constructed by 5R-isophthalate (i.e., 5R-1,3- $H_2bdc$ ) and paddle wheel SBUs. The cuboctahedral cage, also regarded as a small rhombihexahedron when the centres of the phenyl rings in the 5R-isophthalate are considered as vertices and termed "nanoball" by Zaworotko *et al.*, has also been found capable of acting as fundamental building units in the construction of porous MOFs.<sup>42, 10c</sup> For example, when the 1,3- $bdc$  is functionalized at the 5-position with connecting organic moieties, the nanoballs can serve as nano-scale supermolecular building blocks (SBBs) to construct polyhedral frameworks, which should have high pore volume ratio and may process excellent properties in gas storage and separation.

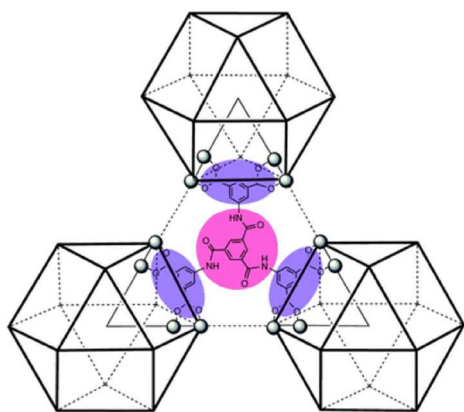


Fig. 6 A **rht** network constructed by a  $C_3$  symmetric carboxylate ligand  $H_6bcbd$  and cuboctahedra. Adapted with permission from ref. <sup>43</sup>. Copyright 2008 Royal Society of Chemistry.

Eddaoudi and Zaworotko presented the first MOF with an **rht**-like network based on the nanoball SBBs.<sup>44</sup> They pointed out the nanoball SBBs could serve as 24-connected nodes if each of 24 vertices could be linked through trigonal 3-connected units, thereby generating a unique **rht**-like network. Since then, many researches have been devoted to the design of various trigonal organic linkers, both rigid and flexible, to prepare **rht**-MOFs.<sup>45, 3h</sup> Lah *et al.* first employed the flexible tripodal ligand,  $5,5',5''$ -[1,3,5-benzenetriyltris(carbonylimino)]tris-1,3-benzene dicarboxylic acid ( $H_6bcbd$ ), to construct a FL-MOF with (3,24)-connected **rht** topology (Fig. 6). Crystals of  $\{Zn_{24}(bcbd)_8(H_2O)_{24}\}_n$  were obtained *via* self-assembly of  $Zn(NO_3)_2 \cdot 6H_2O$  and  $H_6bcbd$  in DMA.<sup>43</sup> In the structure, the four phenyl rings of the flexible  $bcbd^{4-}$  locate nearly in a plane, displaying a  $C_3$  symmetric conformation. The nanoballs, serving as 24-connected nodes, are linked by the tritopic nodes, to construct a 3D network. In such way, each nanoball is connected to 24 tritopic ligands, which results in 12 surrounding nanoballs to the cubic close packing (CCP) arrangement. The CCP arrangement of the nanoballs leads to very large superoctahedra and supertetrahedra, where the nanoballs are used as vertices and  $C_3$  symmetric linkers as faces. Interconnection of the nanoballs and superpolyhedra leads to a solvent-accessible free volume of ~71%. Unfortunately, the FL-MOF framework collapses after the removal of guest molecules, which prevents its further application as absorption materials.

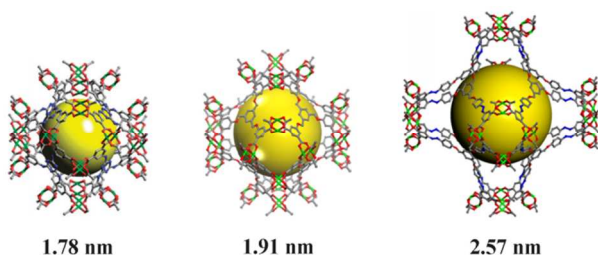


Fig. 7 The superoctahedra of **rht**-MOF-7 (left), **rht**-MOF-4a (middle), and **rht**-MOF-5 (right), respectively. Adapted with permission from ref. <sup>45h</sup> and <sup>46</sup>. Copyright 2012 Royal Society of Chemistry and 2012 Wiley-VCH.

Eddaoudi and co-workers further expanded/functionalized the tripodal flexible ligands to design and synthesize expanded/functionalized **rht**-MOFs. The authors successfully prepared three isoreticular **rht**-MOFs, namely,  $\{Cu_3(tdpat)(H_2O)_3 \cdot xsolvent\}_n$  (**rht**-MOF-7),<sup>45h</sup>  $\{Cu_3(pttip)(H_2O)_3 \cdot xsolvent\}_n$  (**rht**-MOF-4a),  $\{Zn_3(pttip)(H_2O)_3 \cdot xsolvent\}_n$  (**rht**-MOF-5),<sup>46</sup> by employing flexible  $5,5',5''$ -[1,3,5-triazine-2,4,6-triyltriimino]tris-isophthalate hexasodium ( $Na_6tdpat$ ),  $5,5',5''$ -[1,3,5-phenyltris(methoxy)]tris-isophthalic acid ( $H_6pttip$ ),  $5,5',5''$ -[4,4',4''-[1,3,5-phenyltris(methoxy)]tris-phenylazo]tris-isophthalic acid ( $H_6pttip$ ), respectively. Again, the CCP arrangement of nanoballs results in large superoctahedra and supertetrahedra in the **rht** net. With the expanded dimension of the triangular organic cores, the superoctahedra cavity sizes increase from 17.8 (**rht**-MOF-7), 19.1 (**rht**-MOF-4a), to 25.7 Å (**rht**-MOF-5) (Fig. 7); correspondingly, the pore volume ratios of the frameworks increases from 70% (**rht**-MOF-7), 75.2% (**rht**-MOF-4a), to 85.7% (**rht**-MOF-5). As anticipated, the **rht**-MOF-7 shows a high  $CO_2$  uptake capacity (6.52 mmol  $g^{-1}$  at 273 K and 1 bar) and relatively high  $Q_{st}$  at low  $CO_2$  loading, which is likely attributable to the combined size and surface effects pertaining to the exposed free amine groups and triazine nitrogen atoms, promoting stronger  $CO_2$  interaction with nitrogen donor groups decorating the surface of the cavities.

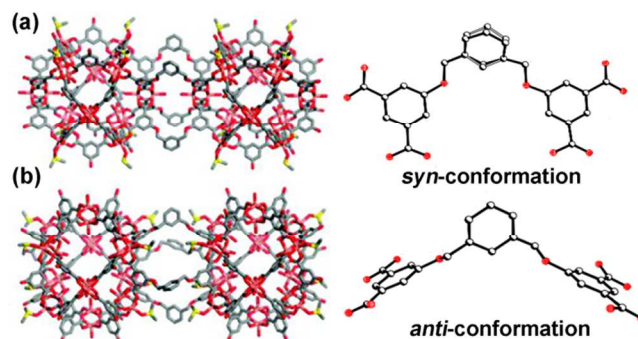


Fig. 8 (a) Nanoball cross-linking as observed along *a*- and *b* axes, note that the ligands adopt a *syn*-conformation. (b) Nanoball cross-linking observed along *c*-axis, note here that the ligands adopt an *anti*-conformation. Adapted with permission from ref. <sup>47</sup>. Copyright 2007 American Chemical Society.

As demonstrated above, the design and synthesis of FL-MOFs can be ideally rationalized, to an extent, comparable to the well-established RL-MOFs through elaborate control of the self-assemble conditions. Additionally, the flexible linking moieties are able to favor the formation of high symmetry structures that cannot be accessed by their rigid analogs. The first **pcu**-type FL-MOF network based on nanoball SBBs has been isolated from the reaction of copper ions and 1,3-bis(5-methoxy-1,3-benzene dicarboxylic acid)benzene ( $H_4bmbb$ ) in a DMSO/*o*-dichlorobenzene solution, formulated as  $\{Cu_{24}(bmbb)_{12}(H_2O)_{16}(DMSO)_8\}_n$ . In the structure, the flexible tetracarboxylate  $bmbb^{4-}$  ligand adopted two conformations that are *syn* and *anti*-conformation, respectively, according to the orientations of functional groups (i.e. 1,3-bdc unit) around the central moieties. As shown in Fig. 8, the two phenyl rings from

the 1,3-bdc moieties are nearly planar with the central phenyl rings in the *syn*-conformational ligand, whereas that is nearly perpendicular in the *anti*-conformational ligand. The *syn*-conformational ligands are cross-linking with nanoballs along the crystallographic *a*, *b*-axes and thus form a cylinder with dimensions of *ca.* 7.24 Å × 10.54 Å (Fig. 8a); the *anti*-conformational ligands are cross-linking with the nanoballs along the crystallographic *c*-axis and form another type of cylinder with sizes of *ca.* 5.86 Å × 17.88 Å (Fig. 8b). The former cylinder is filled with axially coordinated solvent molecules of the paddle-wheel SBUs while the latter cylinder results in a persistent void. Despite of 2-fold interpenetration, the authors note that the framework processes a cavity of *ca.* 18 Å × 18 Å × 14 Å.

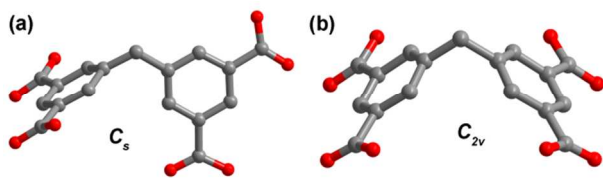


Fig. 9 Two extreme conformations of H<sub>4</sub>mdip (gray C, red O).

Zhou and co-workers utilized flexible 5,5'-methylene-diisophthalic acid (H<sub>4</sub>mdip) and Cu<sup>2+</sup> to synthesize another 3D framework constructed from linking nanoballs into a **pcu**-like network [Cu<sub>6</sub>(mdip)<sub>3</sub>(H<sub>2</sub>O)<sub>6</sub>]-3DMA-6H<sub>2</sub>O (PCN-12).<sup>48</sup> The flexible mdip<sup>4-</sup> ligands adopt two extreme conformations in the structure: a form with C<sub>3</sub> point group symmetry, in which the two benzene rings of mdip<sup>4-</sup> are perpendicular to each other (Fig. 9a), and a C<sub>2v</sub> form that can be generated by symmetry with one-fourth of the ligand (Fig. 9b). The former type of mdip<sup>4-</sup> ligands are cross-linking the nanoballs along the crystallographic *a* and *b* axes, while the latter type of mdip<sup>4-</sup> ligands are cross-linking the nanoballs along *c* axis. Thus, the nanoballs are cross-linked to six neighbouring ones along three orthogonal directions through four bridge ligands. The network was referred to 3.4<sup>4</sup>, consisting of rhombicuboctahedra and cubes or to **pcu** network by considering the nanoballs acting as 6-connected nodes. Due to the short length of the bridge between two 1,3-bdc moieties in an mdip<sup>4-</sup>, PCN-12 does not exhibit framework interpenetration and has a pore volume ratio of *ca.* 70.2% and activated sample shows a BET surface area of 1943 m<sup>2</sup> g<sup>-1</sup>. Due to its high specific surface area and high density of open copper sites, PCN-12 shows an impressive hydrogen uptake of 3.0 wt% at 1 bar and 77 K.

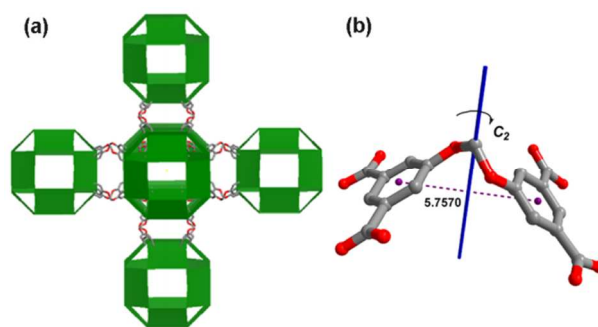


Fig. 10 (a) Schematic representation of the octahedral node from the assembly of nanoballs *via* six square open windows in three orthogonal directions. (b) The conformation of H<sub>4</sub>bbpm ligand in the structure. Adapted with permission from ref. <sup>49</sup>. Copyright 2012 Royal Society of Chemistry.

Very recently, Qiu and co-workers reported a third example of **pcu**-type FL-MOF network built by flexible 1,1-bis-[3,5-bis(carboxy)phenoxy]methane (H<sub>4</sub>bbpm) and nanoball SBBS, {[Cu<sub>6</sub>(bbpm)<sub>3</sub>(DMF)<sub>5</sub>](H<sub>2</sub>O)<sub>5</sub>}(DMF)<sub>x</sub>]<sub>n</sub> from the solvothermal reaction of H<sub>4</sub>bbpm and CuCl<sub>2</sub>·2H<sub>2</sub>O in DMF/water mixed solvent.<sup>49</sup> In the structure, each nanoball SBB connects to six others *via* six square open windows in three orthogonal directions, affording a new porous **pcu** topology, in which the nanoballs serves as 6-connected nodes (Fig. 10a). The connecting fashion leads to the generation of three different types of open cages in the overall framework. Different from the aforementioned two **pcu**-type FL-MOFs, in the case of this framework, bbpm<sup>4-</sup> ligands adopt uniform conformation with C<sub>2</sub> point group symmetry that facilitates the highly symmetrical interconnection of nanoball SBBS (Fig. 10b). The centroid-centroid distance of the phenyl rings in the bbpm<sup>4-</sup> ligand is *ca.* 5.7570 Å and the dihedral angle between them is *ca.* 66.46°. This framework does not exhibit framework interpenetration, presumably due to the short length of the bridge between 1,3-bdc moieties. The framework possesses 70.7% void space, with BET and Langmuir surface areas of 2010 and 2665 m<sup>2</sup> g<sup>-1</sup>, respectively. Gas absorption experiments shows that the framework has a methane uptake of 90 cm<sup>3</sup> g<sup>-1</sup> at 295 K and 8.0 bar, and a CO<sub>2</sub> uptake of 91 cm<sup>3</sup> g<sup>-1</sup> at 273 K and 8.0 bar.

### 2.3 Homochiral FL-MOFs

One of the important subclass of MOFs, homochiral MOFs, is believed to be suited for applications in enantioselective separation and asymmetric catalysis. However, only a few porous homochiral MOFs possessing enantioselective sorption properties or stereoselective catalytic activity have been reported to date, which is directly related to the scarcity of porous homochiral MOFs with functional pore surfaces and appropriate sizes. Although homochiral MOFs can be prepared from totally achiral components *via* self-resolution or chiral influence during crystal growth, the most reliable means for homochiral MOF synthesis is to employ readily available enantiopure ligands as cross-linking ligands.<sup>4b</sup> Fortunately, a large number of flexible organic molecules, such as amino acids, saccharides, peptides, and their derivatives, are chiral and are capable of binding to metal centers, which makes them

suitable organic nodes for the construction of homochiral FL-MOF materials.<sup>50</sup> Some excellent reviews have been recently published concerning on the design, synthesis and applications of homochiral MOFs.<sup>4b-d</sup> Rather than focusing on all homochiral MOFs obtained with chiral ligands, this section will outline only a few recent examples that illustrate the unique advantage of flexible ligands in the construction of homochiral MOFs.

$\alpha$ -Amino acids are representative flexible ligands with chiral centers. They are excellent organic linkers and may coordinate metal ions through both carboxylic and amino groups. In most cases, 1D or 2D homochiral FL-MOFs are often isolated based on pure amino acids.<sup>51</sup> For example, combining L-phenylalanine with Mn(II) salt have obtained a 2D homochiral FL-MOF showing super-exchange antiferromagnetic interactions between the magnetic centers;<sup>52</sup> assembled L-proline with Cd<sup>2+</sup> or Zn<sup>2+</sup> ions have isolated two 2D homochiral layered frameworks.<sup>53</sup>

In contrast, 3D FL-MOFs based on pure amino acids are scarce. Reports are almost wholly confined to aspartic,<sup>54</sup> glutamic,<sup>55</sup> methionine and histidine acids,<sup>56</sup> which have at least a third metal binding groups except for  $\alpha$ -amino and  $\alpha$ -carboxylic groups. Chemists usually employ amino-acid derivatives or introduce auxiliary ligands to construct 3D amino-acid-based homochiral FL-MOFs.<sup>57</sup> As a typical example, Rosseinsky and coworkers reported a 3D amino-acid-based microporous FL-MOF that can afford racemic diols separation.<sup>58</sup> The solvothermal reaction of Ni(L-asp) $\cdot$ 3H<sub>2</sub>O (asp = aspartic acid) with 4,4'-bipy in a water/methanol mixture affords a homochiral porous FL-MOF  $\{[\text{Ni}_2(\text{L-asp})_2(\text{bipy})]\cdot\text{guest}\}_n$ , in which the chiral  $[\text{Ni}(\text{L-asp})]_n$  layers are extended by 4,4'-bipy linkers to form a pillared 3D structure with 1D channels (Fig. 11). The windows of these channels in  $\{[\text{Ni}_2(\text{L-asp})_2(\text{bipy})]\cdot\text{guest}\}_n$  is  $3.8 \times 4.7$  Å, which is determined by the length of the 4,4'-bipy pillars and the nickel centers in the chiral  $[\text{Ni}(\text{L-asp})]_n$  layer. Chiral gas chromatography confirms that the enantiopurity of the starting amino acid is delivered to the product by this route when either D- or L-asp is used as the starting material.

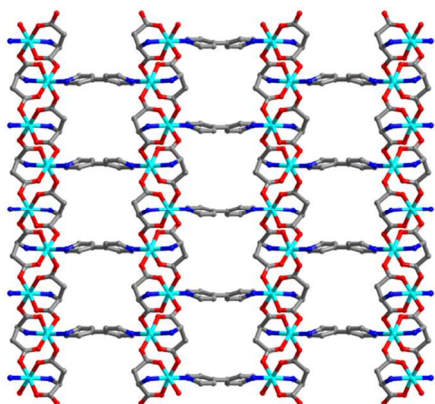


Fig. 11 The structure of  $\{[\text{Ni}_2(\text{L-asp})_2(\text{bipy})]\cdot\text{guest}\}_n$ . Colour scheme: Ni, turquoise; C, gray; N, blue; O, red.

In consideration of the homochiral nature of the internal surface, the enantioselective sorption property of  $\{[\text{Ni}_2(\text{L-asp})_2(\text{bipy})]\cdot\text{guest}\}_n$  was probed by using a spectrum of racemic chiral diols.  $\{[\text{Ni}_2(\text{L-asp})_2(\text{bipy})]\cdot\text{guest}\}_n$  shows some enantioselectivity, but it is the differentiation between diols with similar chain lengths but differing separations between the hydroxyl groups. Considering a fixed chain length of four carbon atoms, 1,2-butanediol (*ee* value, 5.07%) and 2,3-butanediol (*ee* value, 1.5%) display considerably reduced enantioselection relative to 1,3-butanediol (*ee* value, 17.93%). The favorable nature of the 1,3-disposition of the diol units is further demonstrated by the high *ee* value of 2,4-pentanediol (*ee* value, 24.5%), in comparison with those of 1,2-pentanediol (*ee* value, 13.9%) and 2,5-hexanediol (*ee* value, 3.4%). The highest sorption *ee* value observed within the library of diol guests studied was 53.7% for 2-methyl-2,4-pentanediol, a monosubstituted derivative of 2,4-pentanediol with only one chiral center. Further investigations demonstrated that the good match of size and shape between the host and the desired guest, as well as the channel surface chemistry are of significant importance in chiral recognition and separation.

In addition, the pore sizes and free accessible volumes of the homochiral FL-MOF material can be modulated by the replacement of 4,4'-bipyridine with etbipy to form two analogous FL-MOFs  $\{[\text{Cu}\{\text{L/D-asp}\}(\text{etbipy})_{0.5}]\cdot(\text{guest})\}_n$ .<sup>59</sup> The channel topologies of  $\{[\text{Cu}\{\text{L/D-asp}\}(\text{etbipy})_{0.5}]\cdot(\text{guest})\}_n$  are defined by pore windows of  $4.1 \times 4.3$  Å, and elongated pores of  $8.6 \times 3.2$  Å, arising from the increased interlayer separation of the etbipy pillared frameworks. Upon treatment of anhydrous HCl (1 equiv) in diethylether, the protonated frameworks,  $\{[\text{Cu}\{\text{L/D-asp}\}(\text{etbipy})_{0.5}]\cdot(\text{HCl})\cdot(\text{H}_2\text{O})\}_n$ , were obtained, which show Brønsted acid catalytic activity. PXRD studies suggested no major structural changes in the frameworks upon protonation and IR spectroscopy confirmed that the COOH moieties were formed in the protonated frameworks. The resulting protonated frameworks were used to catalyze the methanolysis of *cis*-2,3-epoxybutane. As expected,  $\{[\text{Cu}\{\text{L/D-asp}\}(\text{etbipy})_{0.5}]\cdot(\text{HCl})\cdot(\text{H}_2\text{O})\}_n$  showed some enantioselectivity, however, only moderate yields (32–65%) and very low *ee*'s (6–17%) were obtained. The heterogeneous nature was confirmed by the inactive filtered supernatant. Besides, no conversion was observed for attempted methanolysis of the bulkier epoxide (2, 3-epoxypropyl)-benzene, suggesting catalysis does occur mostly in the channels and pores rather than on the external surfaces.

Peptides are particularly interesting because they have specific recognition properties and intrinsic chirality that may be useful for a wide range of applications. They have the ability to act as organic linkers in MOFs as they have at least one amino and one carboxylic acid terminus that can coordinate metal ions. To date, some peptide-derived FL-MOFs have been reported.<sup>60</sup> Recently, Rosseinsky and coauthors reported a notable peptide-based FL-MOFs  $\{[\text{Zn}(\text{Gly-Ala})_2]\cdot(\text{solvent})\}_n$  based on an flexible oligopeptide linker glycylalanine (Gly-Ala).<sup>61</sup> In this structure, the zinc ions are tetrahedrally coordinated to four dipeptide ligands, in which two dipeptide

ligands are coordinated by the C-terminal Ala carboxylate groups and the other two by N-terminal Gly amine groups. Each Gly-Ala ligand is coordinated to two zinc ions, forming  $[\text{Zn}(\text{Gly-Ala})_2]_n$  layers with a grid-like structure (Fig. 12a). The layers aligned in an AA fashion in the third dimension by hydrogen bonds between all of the amide groups in adjacent layers to form 1D, square-shape pores along the crystallographic *c*-axis (Fig. 12). The experimental isotherms and desorption simulations of the desolvated framework showed that the pores block when no guests are present, gradually and cooperatively opening when triggered by small molecules possessing polar bonds, which is ascribed to the low-energy torsion and displacement of the peptide linkers. The flexible peptide linker plays the vital role for the framework's adaptable porosity. This MOF displayed adaptable porosity as a result of the flexible linker, evoking comparisons to the conformational selection that is characteristic of proteins.

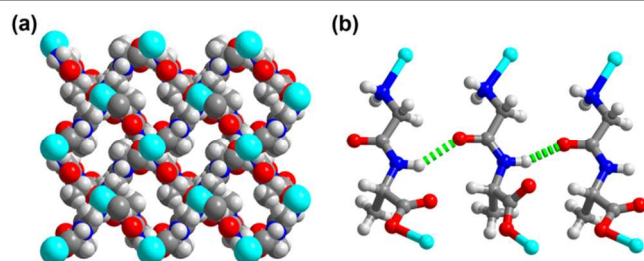


Fig. 12 (a) View of 1D channels in  $\{[\text{Zn}(\text{Gly-Ala})_2] \cdot (\text{solvent})\}_n$  along the crystallographic *c*-axis. (b) The hydrogen bond between  $[\text{Zn}(\text{Gly-Ala})_2]_n$  layers. Colour scheme: Zn, turquoise; C, gray; N, blue; O, red; H, white; Hydrogen bonds, green dash line.

In contrast to the adaptable porosity in  $\{[\text{Zn}(\text{Gly-Ala})_2] \cdot (\text{solvent})\}_n$ , a robust porous FL-MOF  $\{[\text{Zn}(\text{Gly-Thr})_2] \cdot \text{CH}_3\text{OH}\}_n$  has been constructed based on a flexible dipeptide glycylothreonine (Gly-Thr).<sup>62</sup> In this structure, the  $\text{Zn}^{2+}$  ions is six coordinated by four dipeptide molecules, wherein two peptides interact through the monodentate C-terminus Thr carboxylate group and the other two forming a five-membered chelate with the amine and oxo groups belonging to the N-terminus Gly residue. In this way, each dipeptide acts as  $\mu_2$ -linker connecting two metal ions to form 2D grid-like  $[\text{Zn}(\text{Gly-Thr})_2]_n$  layers along the *b* axis, which are packed along the *a* axis following an AA fashion and forming 1D channels. This arrangement is driven by the presence of parallel H-bonds between the peptide N-H and C=O groups belonging to neighboring layers, defining a pattern reminiscent of the parallel  $\beta$ -sheet interconnecting adjacent beta strands in the secondary structure of proteins. The H-bond network is completed by the interaction between the N-terminus amino groups and the -OH groups from the threonine side chain (Fig. 13).  $\{[\text{Zn}(\text{Gly-Thr})_2] \cdot \text{CH}_3\text{OH}\}_n$  exhibits permanent porosity with a surface area of  $200 \text{ m}^2 \text{ g}^{-1}$  after solvent removal and shows selective adsorption of  $\text{CO}_2$  in preference to  $\text{CH}_4$ . This rigidity can be clearly ascribed to the formation a chelate with  $\text{Zn}^{2+}$  and exhibiting additional intralayers hydrogen bonds between the -OH groups in the threonine (Thr) side chain and

the  $\text{NH}_2$  terminal group, which are inaccessible to the  $-\text{CH}_3$  of Ala.

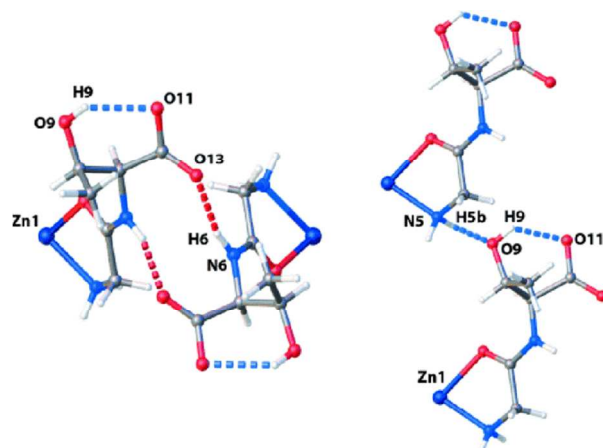


Fig. 13 Interlayer hydrogen bonds between N6-H6...O13 and N5-H5...O9 and intralayer H-bonds (O9-H9...O11) specific to the presence of the threonine side chain. Colour scheme: Zn, dark blue; C, gray; N, blue; O, red; H, white; Hydrogen bonds, blue dash line. Reprinted with permission from ref. <sup>62</sup>. Copyright 2011 Wiley-VCH.

By changing one dipeptide residue and employing of glycyserine (Gly-Ser) as organic linker, a third peptide-based FL-MOF  $\{[\text{Zn}(\text{Gly-Ser})_2]_n\}$ , have been synthesized, which allows ordered torsional change and displacement on guest loss to effect reversible closure of the pores.<sup>63</sup> This torsional change is controlled by the side-chain hydrogen bonding in  $\{[\text{Zn}(\text{Gly-Ser})_2]_n\}$  and coupled with large ordered displacements of the peptide linkers to suppress reversibly 87% of the initial pore volume. The Ser side-chain retains the -OH functionality of Thr, but the change from a secondary to a primary alcohol is sufficient to produce this dramatic change in guest response. The construction of multiple Gly-X dipeptide frameworks from the three X residues (Ala, Thr, Ser), the side chains of which each impose distinct functions, is then demonstrated to control the overall cooperative MOF response in a tuneable way through peptide torsions and side-chain chemistry, attaining responses that are not linear combinations of those of the end-member single-peptide materials.

Rosseinsky and coauthors further presented a new peptide-based FL-MOF,  $\{[\text{ZnCar} \cdot \text{DMF}]_n\}$  by assembling from  $\text{Zn}^{2+}$  and carnosine (Car), a natural dipeptide with the molecular structure of  $\beta$ -alanyl-L-histidine).<sup>64</sup>  $\{[\text{ZnCar} \cdot \text{DMF}]_n\}$  is a 3D framework in which each carnosine molecule links four tetrahedral  $\text{Zn}^{2+}$  cations and each  $\text{Zn}^{2+}$  cation connects four carnosine ligands. The imidazole side chain of the histidine residue is deprotonated to afford Zn-imidazolates chains, with bonding similar to the zeolitic imidazolates framework (ZIF) family of porous materials. The desolvated samples is a microporous material with a surface area of  $448 \text{ m}^2 \text{ g}^{-1}$  and its pores are 1D channels with 5 Å openings and a characteristic chiral shape. This compound is chemically stable in organic solvents and water. Single-crystal X-ray diffraction showed that the  $\{[\text{ZnCar}]_n\}$  framework adapts to MeOH and  $\text{H}_2\text{O}$  guests because of the torsional flexibility of the main His- $\beta$ -Ala chain, while

retaining the rigidity conferred by the Zn-imidazolate chains. The conformation adopted by carnosine is driven by the H bonds formed both to other dipeptides and to the guests, permitting the observed structural transformations. These investigations demonstrate the critical role of the side chain in controlling how the torsional degrees of freedom can be deployed in response to environmental changes.

Besides amino acids, peptides and their derivatives, some other chiral small organic molecules, such as tartronic acid, lactic acid, malic acid etc. have proved successful in the synthesis of homochiral FL-MOFs.<sup>65</sup> For example, the incorporation of chirality has also been considered through the use of *trans*-*R,R*- and *trans*-*S,S*-cyclohexane dicarboxylates by Cheatham *et al.*<sup>66</sup> The thermodynamics versus kinetic aspects of the synthesis of racemic/chiral MOFs were also discussed.<sup>67</sup>

#### 2.4 Dynamic FL-MOFs induced by flexible ligands

Among the numerous reported MOFs, dynamic MOFs (also called flexible/breathing MOFs) are of particular interest.<sup>68</sup> Dynamic MOFs are able to respond to external stimuli such as temperature, pressure, light, electric fields, chemical inclusion etc., but they are also crystalline and can reversibly change their channels with large magnitude while retaining the same or similar topologies. These MOFs are often associated with reversible transformations between two or more states corresponding to expansion (*lp* phase) and contraction (*np* phase), respectively. The phenomenon is often labelled as ‘breathing’,<sup>69</sup> ‘sponge like’,<sup>70</sup> and ‘accordion’ effects.<sup>71</sup> In 1998, MOFs were first classified in three categories and the dynamic MOFs belong to the third generation MOFs.<sup>72</sup> Kitagawa and Uemura differentiated the known behaviours of flexibility into six classes according to the dimension and breathing mechanism of the materials.<sup>73</sup> For 3D breathing MOFs, three situations were subdivided. In the case of pillared-layer MOFs, the reversible phases because of interlayer elongation and shortening could be realized by suitable flexible pillars (Class a, Fig. 14a). For expanding and shrinking MOFs, they can show sponge-like dynamic behaviours (Class b, Fig. 14b). Finally, when the interpenetrated grids are involved, they are densely packed in the absence of guests while the introduction of molecules generates a sliding of one network (Class c, Fig. 14c). To date, many dynamic MOFs built by rigid ligands have been observed. Typically, Férey and Serre have prepared a series of 3D dynamic MOFs (Class b),<sup>74</sup> whose critical feature is a rigid ditopic carboxylate attached to an inorganic SBU that has a mirror plane. The breathing mechanism is activated by rotation around the O-O axis of the carboxylate, which act as a “kneecap” for the system either through a twisting or bending mode. This mechanism requires an opposite rotation on the opposing side of the SBU.<sup>69</sup> Along with incorporation “kneecap” into the metal–ligand interface, an alternative approach to induce flexibility is to incorporate it into the linkers themselves while keeping the MOF skeleton stable. Herein, some selected examples were extracted to discuss the special function of flexible ligands in the construction dynamic MOFs.

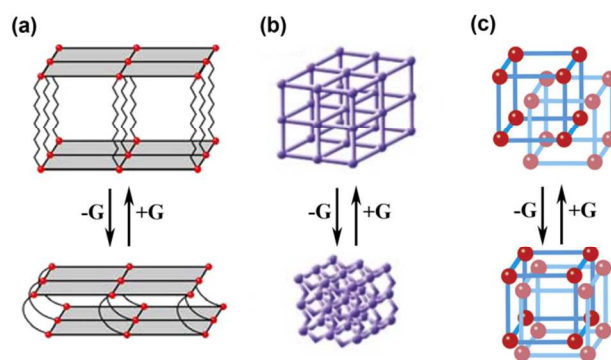


Fig. 14 Three classes of 3D breathing MOFs categorized by Kitagawa and Uemura.

One rational prototype to construct 3D dynamic FL-MOFs is pillaring the layer with flexible linkers (Class b). In this model, the reversible elongation and shortening of pillars in the interlayer results in two (or more) stable MOF phases, thus delivering the flexibility from the linkers to the whole MOF framework. An elegant example has been illustrated by Alberti and coworkers.<sup>71, 69</sup> In view of that the  $[\text{O}_2\text{P}(\text{OH})_2]$  groups in the known layered crystal structures of  $\gamma\text{-ZrPO}_4[\text{O}_2\text{P}(\text{OH})_2]\cdot 2\text{H}_2\text{O}$  can be substituted by various length of alkanediphosphonate ligands, the authors have synthesized a series of pillared-layer  $\gamma\text{-ZrPO}_4[\text{O}_2\text{P}(\text{OH})_2]\cdot 2\text{H}_2\text{O}$  derivatives formulated as  $\text{ZrPO}_4[\text{O}_2\text{P}(\text{OH})_2]_{1-x}(\text{O}_2\text{POH}-(\text{CH}_2)_n\text{-HOPO}_2)_{x/2}\cdot m\text{H}_2\text{O}$  ( $n = 4, 6, 8, 10, 12, \text{ and } 16, x$  arranging from 0 to 1) (Fig. 15). The degree of pillaring ( $x$ ) can be exactly tuned by controlling the reaction time. Breathing was observed for low values of  $x$ , which correspond to situations where two different alkanediphosphonic chains are separated by  $[\text{O}_2\text{P}(\text{OH})_2]$  groups in a direction parallel to the layer. In this case, the derivatives undergo accordion-like transformations which was extensively studied in the 1,10-decanediphosphonate derivative. When fully hydrated, the alkyl chains were in their extended conformations (Fig. 15a). Alternatively, with the removal of water molecules, the interlayer distance was decreased (Fig. 15b). This shrinking and expansion were reversible, and the original expanded network could be readily recovered by the addition of solvent.

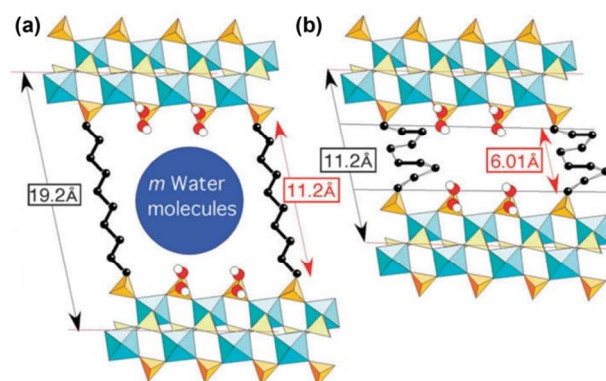


Fig. 15 A schematic view of (a) the fully hydrated phosphate/diphosphonate and of (b) the corresponding dehydrated sample showing the contraction of the carbon chain. Colour scheme: Zr octahedra, pale blue; phosphate tetrahedra,

yellow; OH groups, red and white; C, black. Reprinted with permission from ref. 69, Copyright 2009 Royal Society of Chemistry.

Based on 5-ethyl-pyridine-2,3-dicarboxylic acid ( $H_2epda$ ) and  $etbipy$ , a pillared-layer dynamic FL-MOF  $\{[Co_2(epda)_2(etbipy)(H_2O)_2] \cdot 3H_2O\}_n$  was reported by Wang and Liu.<sup>75</sup> The formation of the framework is accomplished through employing the rigid dicarboxylate linker  $H_2epda$  and divalent cobalt cations to form the 2D Co-carboxylate grids and the flexible  $etbipy$  as pillaring ligands. The framework showing a breathing effect upon dehydration ( $np$  form) and rehydration ( $lp$  form) with a 9% decrease of the cell volume ( $1899 \text{ \AA}^3$  for  $lp$  form vs.  $1728 \text{ \AA}^3$  for  $np$  form) while the crystal system and space group of  $np$  and  $lp$  forms remain the same (Fig. 16). Additionally, the structures of  $lp$  and  $np$  forms are very similar with the only differences being the distance between 2D Co-carboxylate layers shortening slightly ( $15.77 \text{ \AA}$  for  $lp$  form vs.  $14.35 \text{ \AA}$  for  $np$  form). The decrease of the interlayer distance is attributed to the rotation of the C–C single bonds of the flexible  $etbipy$  ligands with minor changes in the length of the pillars, resulting in the relative gliding between the adjacent layers. The two pyridyl rings of an  $etbipy$  ligand are nearly perpendicular to each other in the  $lp$  form, whereas they are nearly coplanar in the  $np$  form.

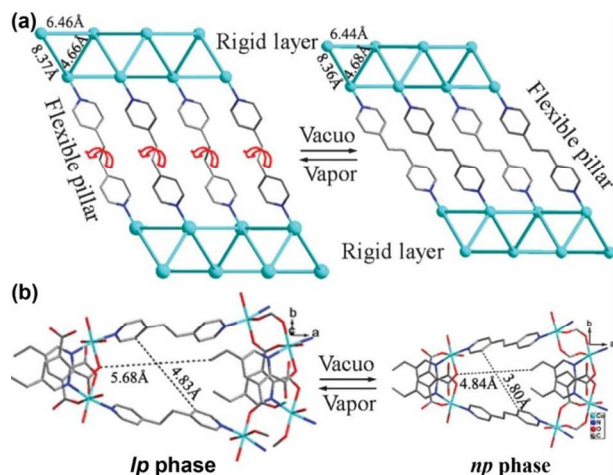


Fig. 16 Structures of pillared FL-MOF  $\{[Co_2(epda)_2(etbipy)(H_2O)_2] \cdot 3H_2O\}_n$  showing the rotation of the flexible ligand upon desolvation. (b) Front view of the channels showing reversible contraction and expansion of the pore. Only Co atoms (blue balls) for each layer are shown for clarity. Reprinted with permission from Ref. 75. Copyright 2012 Royal Society of Chemistry.

The expanding and shrinking MOF is another prototype particularly suitable for construction of dynamic FL-MOFs. In this model, the reversible conformational changes of flexible linkers may lead to expansion and shrinking of a FL-MOF when the two FL-MOF states are stable. A remarkable example is the reversible transformation between the structure of  $\{KCe(pbmp) \cdot 4H_2O\}_n$  ( $H_4pbmp = N,N'$ -piperazinebis(methylenephosphonic acid)) and its dehydrated form demonstrated by synchrotron X-ray crystallography.<sup>76</sup> As shown in Fig. 17, the hydrated FL-

MOF consists of Ce-phosphate chains composed of edge sharing  $CeO_8$  polyhedra. Each Ce-phosphate chain is linked to four other parallel chains *via* the flexible  $pbmp^{4-}$  ligands in which the piperazine rings adopt chair configurations (Fig. 17a). Upon dehydration of the above FL-MOF material at  $160 \text{ }^\circ\text{C}$ , the piperazine rings turn to chair configurations (Fig. 17b). As a result, the dehydrated form is non-porous. However, it can reversibly adsorb water molecules and recover the hydrated structure upon exposing to moist air.

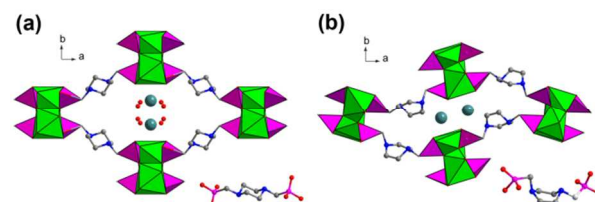


Fig. 17 Transformation of the structure  $\{KCe(pbmp) \cdot 4H_2O\}_n$  and its dehydrated form, view along the crystallographic  $c$ -axis. Colour scheme: Ce octahedra, bright green; P and P tetrahedra, pink; K, sea green; C, gray; N, blue; O, red; P, pink.

Costantino and co-workers have prepared three isorecticular FL-MOFs showing a ligand-flexibility depended breathing effect based on flexible tetraphosphonates and N-donor heterocyclic co-ligands.<sup>77</sup> Structures of the three FL-MOFs contain 1D inorganic chains along the crystallographic  $a$ -axis, which are cross-linked to each other by the organic moieties forming rhombic 1D channels. As shown in Fig. 18, based on  $N,N,N',N'$ -tetrakis(phosphonomethyl)hexamethylenediamine ( $H_8tph$ ) and  $etbipy$ , FL-MOF  $\{Cu_3(H_2tph)(etbipy)_2 \cdot 24H_2O\}$  shows a strong breathing effect upon hydration ( $lp$  form) and dehydration ( $np$  form). The volume difference between  $lp$  form and  $np$  form is remarkably high, being around 26% of the volume of the  $lp$  phase. In contrast, there were no breathing effects being observed when either of the flexible  $H_8tph$  or  $etbipy$  was substituted by a more rigid ligand. For example, with the  $etbipy$  was replaced by  $bipy$ , the isorecticular FL-MOF  $\{Cu_3(H_2tph)(bipy)_2 \cdot 11H_2O\}_n$  could be prepared, for which both  $lp$  and  $np$  phases were also observed. However, the transformations between  $lp$  and  $np$  phases are irreversible. Built by more rigid  $N,N,N',N'$ -tetrakis(phosphonomethyl)- $\alpha,\alpha'$ - $p$ -xylylenediamine ( $H_8tpx$ ) and  $bipy$ , the third isorecticular FL-MOF  $\{Cu_3(H_2tpx)(bipy)_2 \cdot 9H_2O\}_n$  doesn't show  $np$  phase under the same conditions.

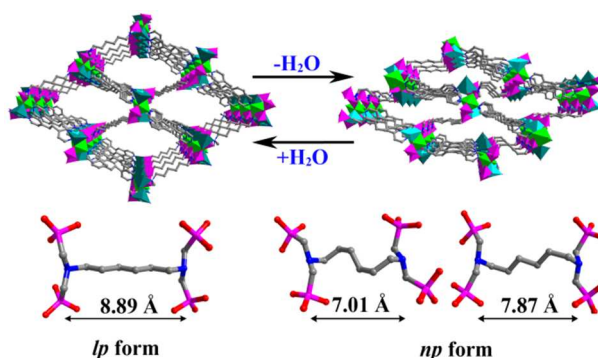


Fig. 18 Polyhedral representation of the structure transition of FL-MOF  $\{Cu_2(H_2tph)(etbipy)_2 \cdot 24H_2O\}_n$  between its *lp* form and *np* form. Colour scheme: Cu Octahedra, green; Cu square pyramidal, dark blue; P and P tetrahedra, pink; C, gray; N, blue.

Recently, Jenkins and co-workers have prepared a dynamic FL-MOF  $\{[Cu_2(tdbbt)_2(SO_4)(Br)_2] \cdot xH_2O\}_n$  based on a flexible ligand 4,4'-(1,4-(trans-2-butene)diyl)bis(1,2,4-triazole) (tdbdt).<sup>78</sup> The asymmetric unit of the framework contains two crystal dependent tdbdt ligands, two copper(II) cations, a sulfate anion and a bromide anion. The adjacent copper atoms are bridged by two triazole fragments and a bridging bromide to form a linear chain SBUs along the crystallographic *a*-axis. The 1D chains are further linked in the other two directions by the secondary triazole moieties of the ligands, forming a 3D network with rhombic 1D channels (Fig. 19a). The flexible di-1,2,4-triazole ligand can act like a “screw”, which twists so that the shapes of the rhombus shift without any significant effects at the metal-ligand binding points. Upon partial dehydration, one of the two 2-butene subunits of the bridging ligand has rotated to become the mirror image of the other one, and they are no longer crystallographically distinct (Fig. 19b, c). The distances between opposite 1D chains in a rhombus turn from  $18.99 \text{ \AA} \times 15.14 \text{ \AA}$  for the hydrated form to  $18.56 \text{ \AA} \times 12.81 \text{ \AA}$  for partial dehydration form (Fig. 19b). Due to the flexibility of the 2-butene portion in the linker, the FL-MOF could further shrink when it is completely dehydrated.

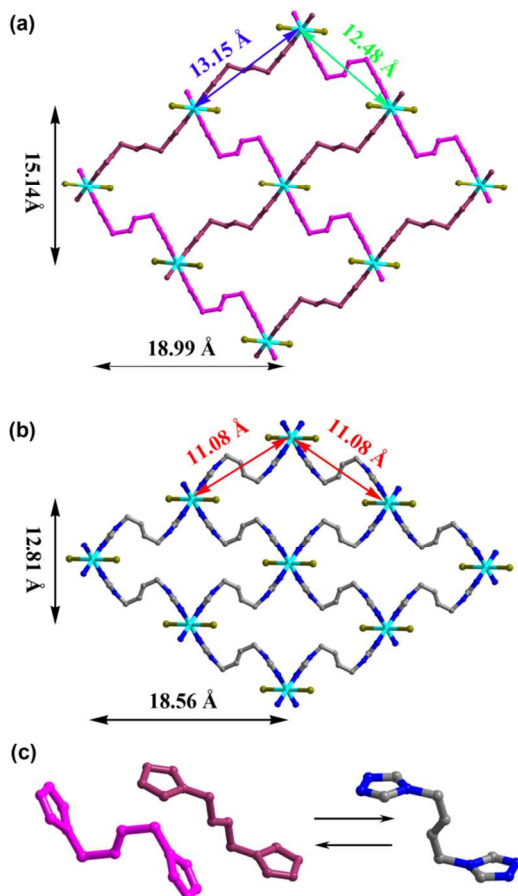


Fig. 19 (a) Crystal structure of  $\{[Cu_2(tdbbt)_2(SO_4)(Br)_2] \cdot xH_2O\}_n$  and (b) its partial dehydrated phase viewed along to the crystallographic *a* and *c*-axis, respectively. (c) The conformations of the tdbdt ligands in the structure  $\{[Cu_2(tdbbt)_2(SO_4)(Br)_2] \cdot xH_2O\}_n$  (pink and plum) and its partial dehydrated phase. Colour scheme: Cu, turquoise; Br, Dark yellow; C, gray; N, blue.

### 3. The applications of FL-MOFs

#### 3.1 Gas adsorption of FL-MOFs

Due to their low densities, high surface areas, large pore volumes, as well as adjustable pore sizes and tunable pore functionalities, MOFs have been widely explored for the gas adsorption (e.g.,  $H_2$ ,  $CH_4$ , and  $CO_2$ ) and separation (e.g.,  $CO_2/N_2$ ,  $CO_2/CH_4$ ).<sup>79</sup> So far, great efforts have been dedicated to quest for strategies to enhance gas adsorption capacity and selectivity in porous MOF materials and lots of vital results have been reported and reviewed.<sup>80</sup> In the cases of FL-MOFs, researches focused on the incensement of pore void ratio, retention of porosity after guest removal, and enhancement of gas-binding affinity for their better application in gas adsorption and separation.

##### 3.1.1 Increasing pore void ratio

Both theoretical calculations and experimental results show that higher specific surface area and higher pore volume should be created in MOFs to increase their high-pressure gas uptake capacities.<sup>81</sup> Given that a large pore volume ratio is a fundamental requirement for high surface area and large pore volume, many researches have been devoted to construction FL-MOFs with large potential solvent-accessible volumes.

A common strategy to enlarge the pore void ratio is the introduction of elongated ligands to construct isorecticular FL-MOFs.<sup>82</sup> For example, a series of non-interpenetrating FL-MOFs formulated as  $\{[Cd_4(tdm)(L_{pillar})_4] \cdot xsolvent\}_n$  ( $H_8tdm =$  tetrakis[(3,5-dicarboxyphenoxy)methyl]methane;  $L_{pillar} =$  bipy, 4,4'-azopyridine (azpy), and etbipy) have been prepared based on the pillaring strategy.<sup>83</sup> As shown in Fig. 20, the binuclear  $\{Cd_2(\mu-O)_2O_6N_4\}$  units are linked by  $tdm^{8-}$  to give rise to neutral 2D sheets with square windows of  $10 \times 10 \text{ \AA}^2$  in the *ab* plane, which are further pillared by various secondary pyridyl ligands ( $L_{pillar}$ ) in AA stacking fashions along *c* axis giving rise to **nbo** networks. With the increase of the pillar lengths, e.g., from bipy to etbipy, the openings of the network cavities along the *c* axis change from *ca.* 11.7 to 14.0 Å and the pore volume ratios of these frameworks vary from *ca.* 59% to 62.6% accordingly.

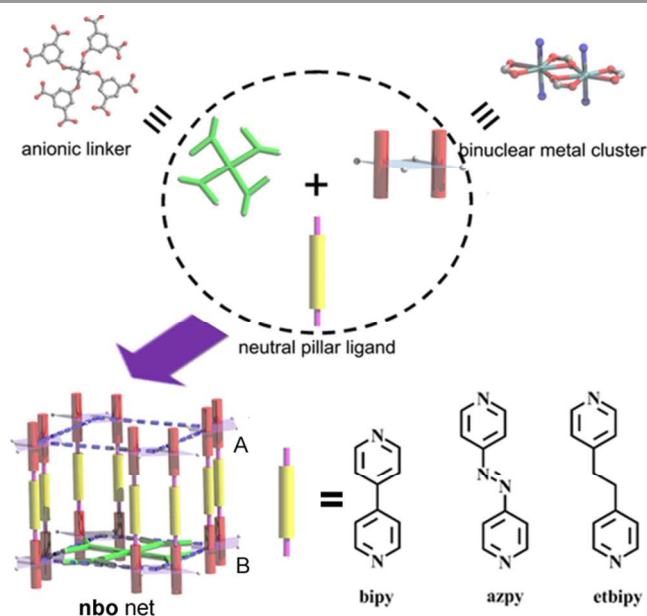


Fig. 20 Simplified representation of the pillaring strategy for synthesis of FL-MOFs  $\{[\text{Cd}_4(\text{tdm})(\text{L}_{\text{pillar}})_4]\cdot x\text{solvent}\}_n$ . Adopted with permission from ref. <sup>83</sup>. Copyright 2011 Royal Society of Chemistry.

In view of the fact that (4,6)-connected MOFs are seldom interpenetrated, Xu and co-workers designed a series of isorecticular FL-MOFs  $\{\text{Zn}_4\text{O}(\text{X})_{1.5}\cdot x\text{solvent}\}_n$  ( $\text{H}_4\text{X} = 4,4'$ -(2,2-bis((4-carboxy-2-methoxyphenoxy)methyl)propane-1,3-diyl)bis(oxy)bis(3-methoxybenzoic acid) ( $\text{H}_4\text{tcom}$ ), 3,3'-(4,4'-(2,2-bis((4-(2-carboxyvinyl)-2-methoxyphenoxy)methyl)propane-1,3-diyl)bis(oxy)bis(3-methoxy-4,1-phenylene))diacrylic acid ( $\text{H}_4\text{tcvom}$ ), and 6,6'-(2,2-bis((6-carboxynaphthalen-2-yl)oxy)methyl)propane-1,3-diyl)bis(oxy)di-2-naphthoic acid ( $\text{H}_4\text{tcnm}$ )) with **cor** topology (Fig. 21).<sup>84</sup> In these structures, each  $\text{Zn}_4\text{O}$  cluster connects to six  $\text{X}^{4-}$  tetratopic ligands and each  $\text{X}^{4-}$  tetratopic ligand connects to four  $\text{Zn}_4\text{O}$  clusters, leading to a series highly porous 3D frameworks with the expecting (4,6)-connected **cor** topology. The resultant FL-MOFs feature a quadrangular opening and two types of microporous and mesoporous cages, the sizes of which gradually increase along with ligand extension in the fixed framework. With such assembly, each microporous cage is surrounded by eight mesoporous cages, which results in very high free porosities of 75.7, 83.7, and 84.6% in these three isorecticular FL-MOFs, respectively. The  $\text{N}_2$  uptakes for these FL-MOFs are very low at 77 K with respect to the calculated accessible surface area, presumably due to the distorted framework upon removal of the solvent molecules. Further investigation shows that these FL-MOFs exhibit high and selective  $\text{CO}_2/\text{N}_2$  adsorptions.

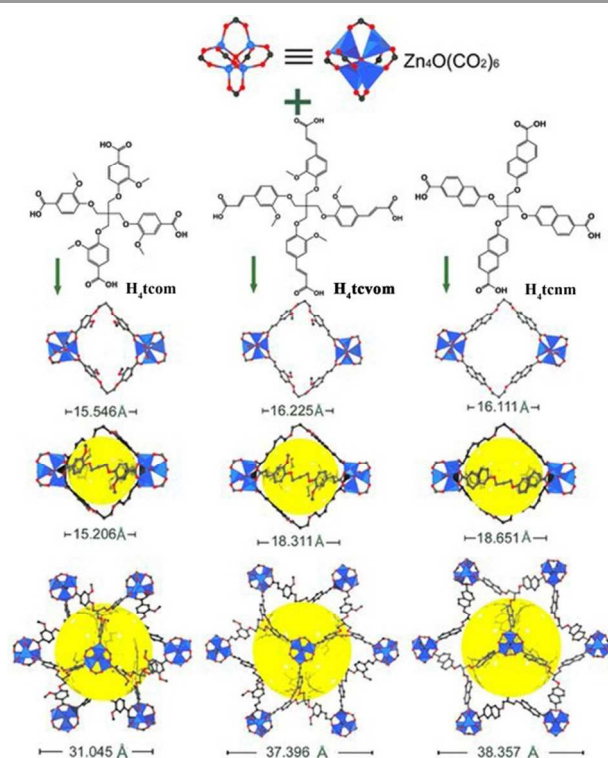


Fig. 21 A view of **cor**-MOFs  $\{\text{Zn}_4\text{O}(\text{X})_{1.5}\cdot x\text{solvent}\}_n$  constructed by  $\text{Zn}_4\text{O}(\text{CO}_2)_6$  SBU and extendable tetratopic ligands. Reprinted with permission from ref. <sup>84</sup>. Copyright 2011 Wiley-VCH.

Besides, a series of non-interpenetrated FL-MOFs with elongated flexible ligands were prepared. For example, Wu and co-workers have synthesized a series of FL-MOFs with pore ratios ranging from *ca.* 21.1% to 50.8% by using 4,4',4''-(2,4,6-trimethylbenzene-1,3,5-triyl)tris(methylene)tris(oxy)tribenzoic acid ( $\text{H}_3\text{ttt}$ ).<sup>85</sup> Zaworotko *et al.* have employed 4,4',4''-[1,3,5-benzenetriyltris(carbonylimino)] trisbenzoic acid ( $\text{H}_3\text{btctb}$ ) to construct the first **asc**-MOF  $\{[\text{Zn}_3(\text{btctb})_2\{\text{Cr}_3\text{O}(\text{isonic})_6(\text{H}_2\text{O})_2(\text{OH})\}]\cdot x\text{DMF}\}_n$  (tp-PMBB-**asc**-3, isonic = pyridine-4-carboxylate) with a pore volume ratio more than 80%.<sup>86</sup> Sun *et al.* using hexa[4-(carboxyphenyl)oxamethyl]-3-oxapentane ( $\text{H}_6\text{hco}$ ) constructed a FL-MOF  $\{\text{Mn}_6(\text{hco})_2(\text{dibp})_{1.5}(\text{H}_2\text{O})_5\}_n$  with a pore volume ratio of *ca.* 56.5%.<sup>87</sup> Hong *et al.* have utilized 5,5',5''-(2,4,6-trimethylbenzene-1,3,5-triyl)tris(methylene)tris(oxy)triisophthalic acid ( $\text{H}_6\text{htt}$ ) to build a polyhedral FL-MOF  $\{[\text{Zn}_7(\text{H}_6\text{htt})_2(\text{OH})_2(\text{H}_2\text{O})_9]\cdot 12.25\text{H}_2\text{O}\}_n$  with a high pore volume ratio of *ca.* 71.7%.<sup>88</sup>

In principle, the use of longer ligands risks to bring in framework interpenetration which likely reduces solvent-accessible voids in the framework materials and leads to less porous or even to nonporous structures. However, some reports have shown that large pore volume ratio can also be realized regardless of the frameworks interpenetration. For example, although 2-fold interpenetrated, NJU-Bai-9 has a pore volume ratio of 78.1% and a BET surface area of  $4258 \text{ m}^2 \text{ g}^{-1}$ .<sup>89</sup> In addition, moderately pore volume ratios (*ca.* 49.2%-64.4%) were found in a family of 2- or 3-fold interpenetrated

diamondoid FL-MOFs (DMOF-*n*, *n* = 1-15) based on the elongated and functionalized tetratopic ligands.<sup>90</sup>

### 3.1.2 Retention of porosity after guest removal

As already mentioned, the pore volume ratios of FL-MOFs could be comparable to that of RL-MOFs. As shown in Table S2, however, the BET surface areas and gas uptake capacities of most FL-MOFs are relatively low comparing with the estimations by computational studies. This phenomenon can be reasonably explained by channel collapse (or partially collapse) upon solvent removal or channel blockage on account of partial solvent retention. On one hand, FL-MOFs have been found particularly susceptible to incomplete activation or loss of porosity owing to the flexibility of the bridging organic linkers which can hardly sustain the frameworks. On the other, however, it is necessary to retain FL-MOFs porosity after the removal of guest solvent molecules for their application in gas adsorption and separation. Therefore, porosity retention of FL-MOFs after guest removal thus presents a major challenge and bottleneck for their applications.

An effective strategy to implement permanent porosity of FL-MOFs is to employ mild activation methods to minimize the damage of the framework. Liang and co-workers have synthesized a FL-MOF based on the flexible H<sub>4</sub>dbip ligand, formulated as {[Cu<sub>2</sub>(dbip)·(H<sub>2</sub>O)<sub>2</sub>]·*x*solvent}<sub>*n*</sub>.<sup>91</sup> As expected, the copper cations form binuclear paddle wheel Cu<sub>2</sub>(COO)<sub>4</sub> SBUs serving as 4-connected square-planar nodes, which are linked by the 4-connected tetracarboxylate ligand dbip<sup>4-</sup>, resulting in a 3D **nbo**-type framework with a potential pore void of 67.2%. The activated sample, prepared by solvent exchange with CH<sub>2</sub>Cl<sub>2</sub> and then evacuated at 65 °C, shows a BET surface area of 1773 m<sup>2</sup> g<sup>-1</sup>, a high CO<sub>2</sub> uptake of 170 cm<sup>3</sup> g<sup>-1</sup> (at 273 K and 0.95 bar) as well as high selectivity of CO<sub>2</sub>/N<sub>2</sub> (20.6, at 273 K). However, activation *via* directly heating the fresh sample at 100 °C only yielded a BET surface area of 232 m<sup>2</sup> g<sup>-1</sup>.<sup>18c</sup>

Based on a flexible tetrapodal octacarboxylate ligand H<sub>8</sub>tdm, a 4,8-connected **scu**-MOF {[Cu<sub>4</sub>(tdm)(H<sub>2</sub>O)<sub>4</sub>]·*x*solvent}<sub>*n*</sub> have been independently designed and synthesized by several research groups.<sup>92</sup> The structure can be viewed as the alternative packing of octahedra and cuboctahedra, leading to a pore void ratio of *ca.* 64.0%. The activated sample prepared by mild solvent exchange shows a BET surface area of 1854 m<sup>2</sup> g<sup>-1</sup>, a total pore volume of 0.84 cm<sup>3</sup> g<sup>-1</sup>, and a H<sub>2</sub> uptake capacity of 2.57 wt % (at 77 K and 1 bar), Henry selectivity of 49 for CO<sub>2</sub>/N<sub>2</sub> and that of 8.4 for CO<sub>2</sub>/CH<sub>4</sub> at 273 K. Directly heating the material at 120 °C under dynamic vacuum, in contrast, only yielded a BET surface area of 1115 m<sup>2</sup> g<sup>-1</sup> and a total pore volume of 0.612 cm<sup>3</sup> g<sup>-1</sup>.

Hupp and co-workers have used supercritical carbon dioxide drying (SCD) as an alternative method to activate MOFs, with the results of permanent internal surface areas and microporosity. SCD drying could eliminate the surface tension, and therefore capillary forces, thus lessening the detriment of the main frameworks.<sup>93</sup> The SCD drying has also successfully been applied in activation of FL-MOFs. A highly porous FL-

MOF {[In<sub>2</sub>(tdm)·(Me<sub>2</sub>NH<sub>2</sub>)<sub>2</sub>]·*x*solvent}<sub>*n*</sub> has been prepared based on H<sub>8</sub>tdm.<sup>94</sup> The framework is comprised of octahedral and cuboctahedral cages, leading to high potential free volume of 65.1%. Activation by SCD drying, the framework shows a BET surface area of 1555 m<sup>2</sup> g<sup>-1</sup>, a total pore volume of 0.62 cm<sup>3</sup> g<sup>-1</sup>, a H<sub>2</sub> uptake of 1.49 wt % at 1 bar and 77 K and 3.05 wt % at 16 bar and 77 K. With the sample activated by evacuation at 80 °C overnight, by contrast, the framework shows a BET surface area of 752 m<sup>2</sup> g<sup>-1</sup> and a pore volume of 0.612 cm<sup>3</sup> g<sup>-1</sup>.<sup>94</sup>

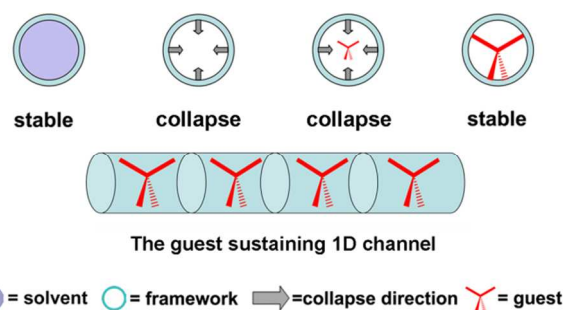


Fig. 22 A scheme of the guest-dependent strategy to increase the stability of MOFs. Adapted with permission from ref. <sup>95</sup>. Copyright 2012 Wiley-VCH.

An alternative strategy to achieve permanent porosity is enhancing the mechanical and thermal stability of the FL-MOFs to resist the detriment of the frameworks during the activated process. For example, Cao and co-workers reported a guest-dependent approach to retain permanent pores in MOFs.<sup>95</sup> In this approach, suitable tetraalkylammonium cations serving as guest species were introduced into the channels to sustain the main frameworks, thus enhancing the framework mechanical and thermal stability. As shown in Fig. 22, taking a FL-MOF with 1D channel as a representative example, the solvated LF-MOF was usually stable. Owing to the ligand flexibility which hardly sustains the framework morphology, however, the framework likely collapses or shrinks after removal of the solvent. To sustain the framework, but not completely block the channel, suitable tetrapodal guests, such as tetraalkylammonium cations, were determined to be the best choice. The guest-strategy was successfully validated in two pre-designed anionic FL-MOFs namely, {[In(dibp)·(Me<sub>2</sub>NH<sub>2</sub>)]*x*solvent}<sub>*n*</sub> and {[In<sub>2</sub>(tdm)·(Me<sub>2</sub>NH<sub>2</sub>)<sub>2</sub>]·*x*solvent}<sub>*n*</sub>. Gas adsorption measurements and variable-temperature PXRD showed that these two fresh FL-MOF frameworks fully collapsed after the guest removal. However, as expected, the porosities were well retained (even activated at 100 °C) and thermal stability were largely enhanced (e.g., stable at 300 °C) after introduction of suitable sizes of the guest tetraalkylammonium cations to sustain the skeleton of the frameworks.

Expanding this strategy, Zhang and co-workers have successfully increased FL-MOF stability and porosity *via* adding rigid pillars into the pores.<sup>96</sup> As shown in Fig. 23, an FL-MOF, {[Cu<sub>2</sub>(obb)<sub>2</sub>(DMF)<sub>2</sub>]·2DMF}<sub>*n*</sub>, has been prepared by 4,4'-oxybis(benzoic acid) (H<sub>2</sub>obb) and paddle-wheel Cu<sub>2</sub>(COO)<sub>4</sub> SBUs. Albeit 3-fold framework interpenetration,

this framework still has a moderate pore volume ratio (53.8 % without coordinated DMF). The single net has a rhombic channel with a window composed of eight  $\text{Cu}_2(\text{COO})_4$  units and eight  $\text{obb}^{2-}$  ligands, which shows a large dimension about  $47.8 \times 27.3 \text{ \AA}^2$ . With half coordinated DMF molecules in the rhombic channels replaced by the bridging  $4,4'$ -bpy ligands, another framework  $\{[\text{Cu}_2(\text{obb})_2(\text{bpy})_{0.5}(\text{DMF})] \cdot 2\text{DMF}\}_n$  has also been isolated (Fig. 23). Gas adsorption experiments shown that the former framework has no appreciable gas sorption while the latter (pillaring framework) exhibits moderate surface areas ( $829 \text{ m}^2 \text{ g}^{-1}$ ) and selective gas uptake for the adsorption of  $\text{CO}_2$  over  $\text{N}_2$  and  $\text{CH}_4$  under 273 K. In this case, the  $4,4'$ -bipy pillars serving as guest species effectively sustain the main framework, resulting in the permanent porosity of the pillaring framework.

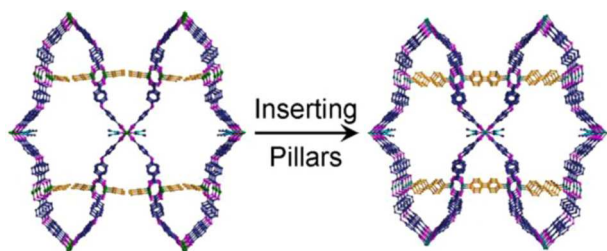


Fig. 23 The structures of  $\{[\text{Cu}_2(\text{obb})_2(\text{DMF})_2] \cdot 2\text{DMF}\}_n$  (left) and  $[\text{Cu}_2(\text{obb})_2(\text{bpy})_{0.5}(\text{DMF})] \cdot 2\text{DMF}$  (right). Reprinted with permission from ref. <sup>96</sup>. Copyright 2011 American Chemical Society.

### 3.1.3 Enhancing gas-binding affinity

To improve the capacity (e.g.,  $\text{CO}_2$ ,  $\text{H}_2$ ,  $\text{CH}_4$ ) and selectivity of a specific gas (e.g.,  $\text{CO}_2/\text{N}_2$ ,  $\text{CO}_2/\text{CH}_4$ ), current efforts are devoted to enhancing the gas-binding affinity in MOFs. Strategies reported include pore size control,<sup>97</sup> incorporation of open metal sites (OMSs),<sup>98</sup> grafting of amines into the frameworks,<sup>80a, 99</sup> employment of nitrogen-rich organic linkers,<sup>100</sup> introduction of metal cations<sup>101</sup> etc. Among these strategies, the last two approaches were frequently-used for the FL-MOFs.

Generally, the elongated amine- or amide-functional organic ligands are typical flexible ligands with Lewis basic nitrogen atoms, which were commonly adopted to improve the gas (particular for  $\text{CO}_2$ ) uptake capacity and selectivity. For example, Bai and co-workers have successfully prepared an amide-inserted FL-MOF  $\{[\text{Cu}_3(\text{cip})_2(\text{H}_2\text{O})_5] \cdot x\text{Guest}\}_n$  (NJU-Bai3,  $\text{H}_3\text{cip} = 5$ -(4-carboxybenzoylamino)-isophthalic acid).<sup>102</sup> The overall structure of NJU-Bai3 is well packed by three types of cages (bowl-like cage, trigonal bipyramidal and hexagonal bipyramidal) with densely decorated amide units that are directly exposed to each individual cavity. The cages have inner sphere diameters of *ca.* 1.1, 1.4 and 1.6 nm, respectively. The total accessible volume of the fully desolvated NJU-Bai3 is *ca.* 76.9%. NJU-Bai3 has a BET surface of about  $2690 \text{ m}^2 \text{ g}^{-1}$ . The  $\text{CO}_2$  uptake of NJU-Bai3 is  $6.21 \text{ mmol g}^{-1}$  at 273 K and 1 bar, while the corresponding  $\text{N}_2$  and  $\text{CH}_4$  uptake measured at the same conditions is only  $3.96 \text{ mmol g}^{-1}$  and  $6.9 \text{ mmol g}^{-1}$ , respectively. NJU-Bai3 exhibits a strong binding affinity for

$\text{CO}_2$  (e.g.,  $36.5 \text{ kJ mol}^{-1}$  at zero coverage) and high  $\text{CO}_2$  uptake (e.g.,  $22.12 \text{ mmol g}^{-1}$  at 273 K and 20 bar). The selectivity of  $\text{CO}_2$  over  $\text{N}_2$  ranges from 25.1 to 60.8 and the value of  $\text{CO}_2$  over  $\text{CH}_4$  are 13.7–46.6 in the range of 0–20 bar as predicted by IAST for equimolar gas mixtures.

Based on an acylamide functionalized ligand bis(3,5-dicarboxyphenyl)terephthalamide ( $\text{H}_4\text{bdpt}$ ), a new expanded microporous **nbo**-type FL-MOF  $\{\text{Cu}_2(\text{bdpt})\}_n$  (HNUST-1) with inserted acylamide groups has been designed and synthesized, which is composed of a spherical (Fig. 24a) and an ellipsoidal cage (Fig. 24b).<sup>103</sup> HNUST-1 shows both a large  $\text{CO}_2$  uptake capacity ( $156.4 \text{ cm}^3 \text{ g}^{-1}$  at 1 bar and 273 K) and high selectivity for  $\text{CO}_2$  over  $\text{N}_2$  (39.8) and  $\text{CH}_4$  (7.2) at 273 K. Another acylamide functionalized **nbo**-type FL-MOF  $\{[\text{Cu}_2\text{bdpo}] \cdot x\text{solvent}\}_n$  (HNUST-3) has been designed and isolated by self-assembling  $[\text{Cu}_2(\text{COO})_4]$  paddle wheel SBUs and a novel tetracarboxylate ligand with linking oxalamide groups  $\text{H}_4\text{bdpo}$  ( $\text{H}_4\text{bdpo} = N,N'$ -bis(3,5-dicarboxyphenyl)oxalamide).<sup>104</sup> Again, the structure of HNUST-3 could be seen as alternative packing of a spherical (Fig. 24c) and an ellipsoidal cage (Fig. 24d) in 3D space, resulting in a high potential void volume of *ca.* 73.2%. HNUST-3 represents the first example of a porous oxalamide-functionalized MOF, which exhibits a high BET surface area of  $2412 \text{ m}^2 \text{ g}^{-1}$ , large  $\text{H}_2$  uptake (6.1 wt % at 20 bar and 77 K), and high  $\text{CO}_2$  adsorption capacity ( $20.2 \text{ mmol g}^{-1}$  at 20 bar and 298 K) with good selectivities for  $\text{CO}_2$  over  $\text{CH}_4$  (7.9) and  $\text{N}_2$  (26.1) at 298 K.

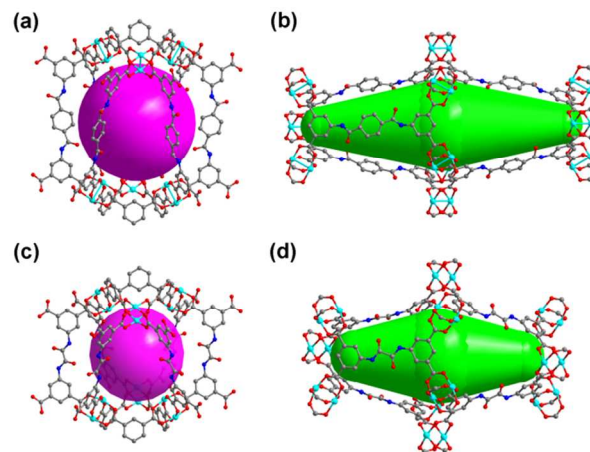


Fig. 24 Ellipsoidal and spherical cages in (a) HNUST-1 and (b) HNUST-3. Adapted with permission from Ref. <sup>103</sup> and <sup>104</sup>. Copyright 2013 Royal Society of Chemistry and 2013 American Chemical Society.

Bai and co-workers have successfully inserted amide functional groups into a **rht**-type FL-MOF  $\{[\text{Cu}_{24}(\text{cbcd})_8(\text{H}_2\text{O})_{24}] \cdot x\text{solvent}\}_n$ ,<sup>105</sup> which is isomorphous with  $\{[\text{Zn}_{24}(\text{cbcd})_8(\text{H}_2\text{O})_{24}] \cdot x\text{solvent}\}_n$  reported by Lah and co-workers.<sup>43</sup> This FL-MOF has a BET surface area of *ca.*  $3160 \text{ m}^2 \text{ g}^{-1}$ , an excess  $\text{CO}_2$  uptake of  $23.53 \text{ mmol g}^{-1}$  at 298 K and 20 bar, high  $\text{CO}_2$  adsorption enthalpy (*ca.*  $26.3 \text{ kJ mol}^{-1}$  at zero loading), and good  $\text{CO}_2/\text{N}_2$  selectivity (*ca.* 22 at 1 bar and 33 at 20 bar, predicted by IAST for equimolar mixtures). To further improve

the CO<sub>2</sub> storage capacity of these materials, Bai and co-workers further designed and synthesized two expanded isorecticular **rht**-type FL-MOFs, {Cu<sub>3</sub>(btbip)}<sub>n</sub> and {Cu<sub>3</sub>(tatbip)}<sub>n</sub> based on nano-sized triangular acylamide-bridging hexacarboxylate linkers H<sub>6</sub>btb and H<sub>6</sub>tatb (Scheme 1), respectively.<sup>106</sup> {Cu<sub>3</sub>(btbip)}<sub>n</sub> and {Cu<sub>3</sub>(tatbip)}<sub>n</sub> almost have the same gas sorption behaviors, despite that the surface of latter framework is decorated by nitrogen containing triazine rings. The activated frameworks exhibit large surface area (i.e., 3288 for {Cu<sub>3</sub>(btbip)}<sub>n</sub> and 3360 m<sup>2</sup> g<sup>-1</sup> for {Cu<sub>3</sub>(tatbip)}<sub>n</sub>) and exceptionally high CO<sub>2</sub> uptake capacities (157 wt% at 20 bar and 273 K) as well as good selectivities of CO<sub>2</sub>/CH<sub>4</sub> (8.6) and CO<sub>2</sub>/N<sub>2</sub> (34.3). In addition, the advantages of acylamide groups for CO<sub>2</sub> capture have been further supported by Grand Canonical Monte Carlo (GCMC) and first-principles calculations.

Shi and Li employed a high density of Lewis basic sites (LBSs) hexacarboxylate ligand 2,4,6-tris(3,5-dicarboxylphenylamino)-1,3,5-triazine (H<sub>6</sub>tdpat) to construct a **rht**-type FL-MOF {[Cu<sub>3</sub>(tdpat)(H<sub>2</sub>O)<sub>3</sub>]·10H<sub>2</sub>O·5DMA}<sub>n</sub> (Cu-tdpat),<sup>107</sup> which is also independently isolated by Eddaoudi *et al.*, who denoted it as **rht**-MOF-7.<sup>45h</sup> Cu-tdpat may be the smallest member of **rht**-nets and represents the first example of MOF that possesses a high density of both open metal sites (OMSs, 1.76 nm<sup>3</sup>) and LBSs (3.52 nm<sup>3</sup>) (Fig. 25). Cu-tdpat shows a very high CO<sub>2</sub> adsorption enthalpy (42.2 kJ mol<sup>-1</sup> at zero loading), high low-pressure CO<sub>2</sub> uptake (i.e., 44.5% at 1 bar and 273 K), extremely large high-pressure gas uptake capacity [i.e., CO<sub>2</sub> (excess): 310 v/v, 298 K, 48 bar; H<sub>2</sub> (total): 6.77 wt %, 77 K, 67 bar; CH<sub>4</sub> (total): 181 v/v, 298 K, 35 bar]. These values place it among the leading MOF materials to date for CO<sub>2</sub>, H<sub>2</sub>, and CH<sub>4</sub> storage. At a total pressure of 1 atm and CO<sub>2</sub> concentration of 10 % (partial pressure of 0.1 atm) and 298 K, a remarkable CO<sub>2</sub>/N<sub>2</sub> selectivity of *ca.* 79 is predicted by IAST.

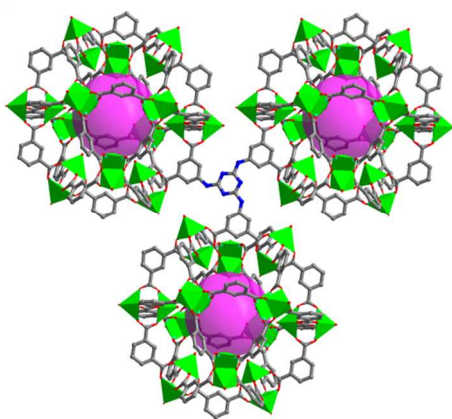


Fig. 25 Representation of the (3, 24)-connected **rht**-net built on the shortest linker H<sub>6</sub>tdpat.

Based on 1,5-bis(5-tetrazolo)-3-oxapentane (H<sub>2</sub>btz), a novel N-rich microporous FL-MOF {[Zn(btzt)]·DMF·0.5H<sub>2</sub>O}<sub>n</sub> with a sodalite (**sod**) topology has been isolated.<sup>108</sup> In this structure, 24 Zn(II) ions and 36 Tz (tetrazolate) rings stitch into a 24 nuclear

zinc **sod** cage with a ~7.2 Å diameter cavity, which exhibits truncated octahedral geometry with eight hexagonal windows on its surface (Fig. 26a). The cage as a repeat unit is further extended into microporous zeolite-like 3D framework with a potential solvent void of *ca.* 45.6% (Fig. 26b). This framework exhibits high CO<sub>2</sub> adsorption capacity up to 35.6 wt % (8.09 mmol g<sup>-1</sup>) and an excellent CO<sub>2</sub>/CH<sub>4</sub> selectivity of 21.1 at 273 K and 1 bar, being among the highest values known to date. Theoretical calculations based on simulated annealing techniques and periodic DFT revealed that CO<sub>2</sub> is predominantly located around the inner surface of the cages through multipoint interactions, in particular, around the aromatic tetrazolate rings (Fig. 26c). Importantly, the authors further noted that it is the first time that multipoint interactions between CO<sub>2</sub> molecules and frameworks resulting in high CO<sub>2</sub> uptake are observed.

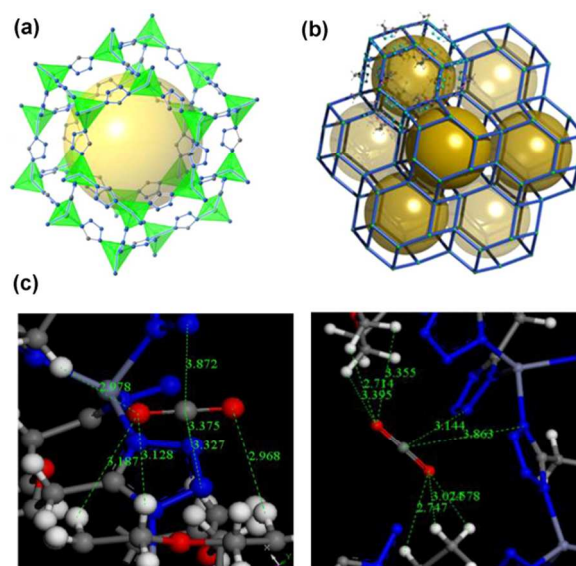


Fig. 26 (a) The Zn<sub>24</sub>(Tz)<sub>36</sub> cage. (b) The **sod** topological net of {[Zn(btzt)]·DMF·0.5H<sub>2</sub>O}<sub>n</sub>. (c) Preferred CO<sub>2</sub> adsorption site configurations by annealing simulations. Close contact distances, in Å, are marked. Adapted with permission from ref. <sup>108</sup>. Copyright 2012 American Chemical Society.

Suh and co-workers reported an example for CO<sub>2</sub> uptake capacity and selectivity enhancement through introducing metal cations into {[Zn<sub>3</sub>(tcpt)<sub>2</sub>(HCOO)][NH<sub>2</sub>(CH<sub>3</sub>)<sub>2</sub>]·5DMF}<sub>n</sub> (SNU-100, H<sub>3</sub>tcpt = 2,4,6-tris-(4-carboxyphenoxy)-1,3,5-triazine).<sup>109</sup> In the structure, three hourglass Zn<sub>3</sub>(COO)<sub>6</sub> SBUs are connected by two tcpt<sup>3-</sup> linkers infinitely to form 2D layers running parallel to the *ab* plane (Fig. 27b). The 2D layers are further pillared by formate species along the *c* axis, giving rise to a 3D anionic framework (Fig. 27a). The counterions NH<sub>2</sub>(CH<sub>3</sub>)<sub>2</sub><sup>+</sup> can be readily exchanged with Li<sup>+</sup>, Mg<sup>2+</sup>, Ca<sup>2+</sup>, Co<sup>2+</sup>, and Ni<sup>2+</sup>, resulting in various metal cations impregnated frameworks namely SUN-100-M (M = Li<sup>+</sup>, Mg<sup>2+</sup>, Ca<sup>2+</sup>, Co<sup>2+</sup>, and Ni<sup>2+</sup>). As shown in Table S2, the BET surface areas and the H<sub>2</sub> uptake (at 1 atm and 77 K) of activated SUN-100-M are slightly higher than that of activated SNU-100. However, the isosteric heat (*Q*<sub>st</sub>), selectivity, and uptake capacity of the CO<sub>2</sub>

adsorption in the SNU-100-M at room temperature were significantly enhanced due to the electrostatic interactions between CO<sub>2</sub> and the impregnated extra-framework metal ions.

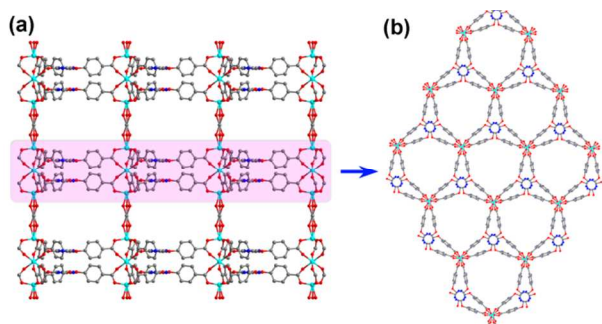


Fig. 27 3D anionic framework formed from the 2D layers pillared by formate species along the *c* axis. (b) A 2D layer running parallel to the *ab* plane.

### 3.2 Heterogeneous catalysis of FL-MOFs

The ability to incorporate guest-accessible functional sites into the channel of MOFs makes them excellent candidates as heterogeneous catalysts. In principle, the pore size and functionality of the framework can be rationally adjusted over a wide range for a variety of catalytic reactions. However, it is really difficult to obtain thermally stable MOFs with suitable cavities in association with the generation of catalyst active sites. Since the first utility of a crystalline porous coordination polymer as a heterogeneous Lewis acid catalyst by Fujita *et al.* in 1994,<sup>110</sup> only several dozen successful MOFs concerning MOF-based heterogeneous catalysis have thus far been reported and the MOF-based catalysis is still in its infancy. Several review articles on MOF-based heterogeneous catalysis have been appeared recently.<sup>111</sup> Whilst some RL-MOFs exhibit zeolite-like high thermal stability and permanent microporosity, FL-MOFs have relatively low thermal stability and chemical robustness, increasing the likelihood of framework collapse under harsh evacuated conditions or post-synthetic process. Therefore, the design and synthesis of FL-MOF catalysts mainly focuses on direct incorporation the pre-designed functional ligands into channel surface of framework in a one-pot synthesis.

An attractive and straightforward strategy to acquire FL-MOF catalysts is incorporation Lewis bases into the pre-designed ligands so that the resultant FL-MOFs may act as base-type catalysts. Kitagawa and co-authors have designed a novel flexible ligand 1,3,5-benzene tricarboxylic acid tris[*N*-(4-pyridyl)amide] (4-btapa).<sup>112</sup> As anticipated, the ligand contains three amide groups that are responsible for catalytic activity, and three pyridyl groups that coordinate to Cd<sup>2+</sup> ions to form a 3D porous framework {Cd(4-btapa)<sub>2</sub>(NO<sub>3</sub>)<sub>2</sub>·6H<sub>2</sub>O·2DMF}<sub>n</sub>. The as-prepared framework, which embeds amide groups on the surface of the channels, is capable of base-catalyzing the Knoevenagel condensation between benzaldehyde and malononitrile in 98% conversion. Reactions with larger nitriles, including ethyl cyanoacetate and cyano-acetic acid *tert*-butyl ester, however, show only negligibly conversions, implying that

catalysis takes place chiefly within the material's channels rather than on its surface. The simultaneous lack of porosity and catalysis of the evacuated material, further confirms the assumption of the occurrence of the catalytic activity inside the material's channels. The authors further demonstrated that this FL-MOF is amenable to uniformly disperse the catalytic sites since that the free strut is catalytically inert in homogeneous solution due to intermolecular H-bonding between 4-btapa molecules. Subsequently, other FL-MOFs or macrocycles based on amide-containing ligands have also been reported, which show the similar size-selective heterogeneous catalysis of the Knoevenagel condensation reaction.<sup>113</sup>

Two isostructural mesoporous FL-MOFs referred to as PCN-100 and PCN-101 have been constructed by using Zn<sub>4</sub>O(CO<sub>2</sub>)<sub>6</sub> as SBUs and two flexible amino functional ligands, namely, 4,4',4''-(benzene-1,3,5-triyltris(azanediyl))tribenzoic acid (H<sub>3</sub>tatab) and 4,4',4''-(1,3,5-triazine-2,4,6-triyl)tris(azanediyl)tribenzoic acid (H<sub>3</sub>btatb), respectively.<sup>114</sup> Again, due to the uniform distribution of amino groups in the channel surface serving as Lewis bases, both PCN-100 and -101 exhibit size-selective catalytic activity toward the Knoevenagel condensation reaction.

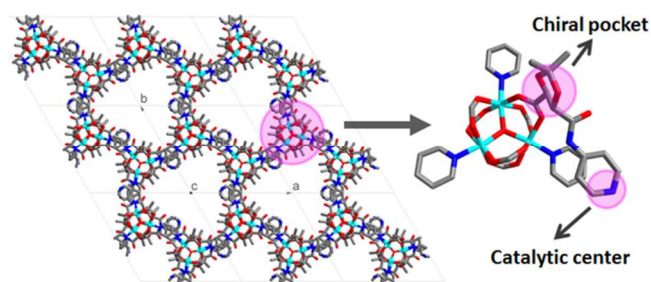
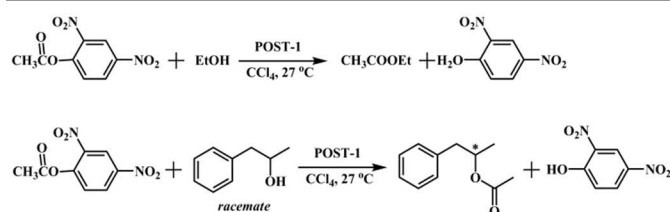


Fig. 28 Large triangular shape chiral channels of POST-1 along the *c* axis (left); coordination environment of POST-1, showing the catalytic centre and the chiral pocket (right). Colour scheme: Zn, turquoise; C, gray; N, blue; O, red.

Another compelling and widely used strategy is *in situ* incorporation chiral ligands such as amino acids and their derivatives into FL-MOFs to produce potentially useful solid materials for asymmetric catalysis. To achieve strong asymmetric induction and a high enantioselectivity in products, the catalytic centres and chiral induction sites should be in close proximity with proper relative orientation. Based on this approach, Kim and co-workers reported the first homochiral MOF that can catalyze a chemical reaction in an enantioselective manner in 2000.<sup>115</sup> The authors first designed a flexible enantiopure chiral ligand [(4*R*,5*R*)-2,2-dimethyl-5-[(pyridin-4-ylamino)carbonyl]-1,3-dioxolane-4-carboxylic acid (Hdpdc), which is a derivative of D-tartaric acid. Self-assembled D-Hdpdc with zinc cations readily produced a homochiral porous FL-MOF whose formula is {[Zn<sub>3</sub>(μ<sub>3</sub>-O)(Hdpdc)<sub>6</sub>]·2H<sub>2</sub>O·12H<sub>2</sub>O}<sub>n</sub>, known as D-POST-1. The enantiomeric L-POST-1 was also obtained from the enantiomer of Hdpdc and the zinc cations under the same reaction conditions. In the structure of POST-1, three zinc cations are held together with six carboxylate groups and a

bridging oxo oxygen, to form a typical planar oxo-bridged trinuclear cluster  $[Zn_3(\mu_3-O)(COO)_6]$  (Fig. 28). The trinuclear clusters, serving as SBUs, are further interconnected *via* coordinate covalent bonds between the zinc cations and the pyridyl groups of Hdpdc, thus generating 2D infinite layers. The 2D layers are stacked along the *c* axis to form large triangular-shaped chiral 1D channels with a side length of 13.4 Å (Fig. 28). In the structure, every SBU has six pyridyl groups, one half of that is coordinated to the zinc cations from three neighboring SBUs and the remaining of that are free and direct toward the channel interior. These exposed pyridine groups show catalytic activity in the transesterification of ester. Reaction of 2,4-dinitrophenyl acetate and ethanol in the presence of POST-1 yielded ethyl acetate in 77% yield (Scheme a). Control experiments showed that in the absence of POST-1, or in the present of POST-1 with N-methylated free pyridyl units, however, very little conversion was observed, demonstrating the catalytic activity of the pyridyl units of POST-1. Transesterification of 2,4-dinitrophenyl acetate with bulkier alcohols such as 2-butanol, neopentanol, and 3,3,3-triphenyl-1-propanol occurs with a much slower or even negligible rate under otherwise identical reaction conditions, suggesting that the catalysis mainly occurred in the channels rather than on the material's surfaces.



Scheme 2 Transesterifications catalyzed by POST-1.

Owing to the presence of the free pyridyl groups and the chiral environment of the channel, enantioselective catalysis can also be achieved. The reaction of 2,4-dinitrophenyl acetate with a large excess of *rac*-1-phenyl-2-propanol in the presence of D-POST-1 or the enantiomeric L-POST-1 produced corresponding esters with  $\sim 8\%$  in favor of *S* or *R* enantiomer (Scheme 2), respectively. The low enantioselectivity was presumably due to the fact that the catalytically active units (free pyridyl groups) are too far from the chiral sites of the pores. Although modest, the enantioselectivity of this process is noteworthy because it was the first example of catalytic asymmetric induction mediated by well-defined modular porous materials.

Expanding this strategy, Wu and co-workers reported a serine-based homochiral FL-MOF that can catalyze 1,2-addition of  $\alpha,\beta$ -unsaturated ketones in an enantioselective manner in 2009.<sup>116</sup> Reaction of copper chloride with (*S*)-3-hydroxy-2-(pyridine-4-ylmethylamino)propanoic acid (Hhpp) afforded a 2D homochiral FL-MOF,  $\{[Cu_2(hpp)_2Cl_2] \cdot H_2O\}_n$ . Each ligand chelates one copper atom through hydroxyl, carboxyl and amino groups further bridges a neighbouring copper atom *via* the pyridyl group to extend into 1D polymeric

chains running along two different orientations. The chains are further coupled by one of the two chlorides to form a thick bilayer framework structure. All thick lamellar frameworks are stacked together *via* supramolecular interactions to form a 3D porous framework with 1D chiral channels ( $5.1 \times 2.9 \text{ \AA}^2$ ) filled with water molecules. The as-prepared framework catalyzed the Biginelli reaction of benzaldehyde, urea and ethyl acetoacetate to give dihydropyrimidinone in a 90% yield yet without any enantioselectivity. However, it could catalyze 1,2-addition of Grignard reagent to  $\alpha,\beta$ -unsaturated ketones in excellent conversion (88%-98%) and good to moderate enantioselectivity (51%-99%). Control experiments show that the free ligand can also promote the reaction, whereas the copper chloride did not show any catalytic activity, suggesting that the reaction was promoted by the ligand of the framework. The supernatant from the solid cannot promote the transformation under otherwise identical conditions, confirming the heterogeneous behaviour of the catalyst system. However, due to small pore sizes of the catalyst, the catalytic process was believed to occur in the surface of the materials.

A more rational synthetic approach is used the so-called privileged asymmetric ligands, such as organocatalysts and their analogies, chiral salen ligands etc., which can catalyze a wide range of chemical reactions with high enantioselectivity, as organic linkers to construct catalytically active homochiral MOFs. Through this strategy, Duan and co-workers reported a direct incorporation of chiral organocatalysts units at metal nodes of an achiral framework in a one-pot synthesis.<sup>117</sup> Solvothermal reaction of  $Cd(ClO_4)_2 \cdot 6H_2O$ ,  $H_3btb$  (1,3,5-tris(4-carboxyphenyl)benzene), and *N-tert*-butoxy-carbonyl-2-(imidazole)-1-pyrrolidine (L-bcip) afforded a catalytically active FL-MOF  $\{Cd_3(btbt)_2(L-pyi)\}_n$  (*pyi* = pyrrolidine-2-yl-imidazole), which exhibits stereochemical catalysis toward the Aldol reactions. Through incorporating the stereoselective organocatalyst L- or D-*pyi* and a triphenylamine photoredox group into a single framework, the authors have further developed two enantiomeric FL-MOFs, Zn-PY11 and Zn-PY12, to prompt the asymmetric  $\alpha$ -alkylation of aliphatic aldehydes in a heterogeneous manner (Fig. 29).<sup>118</sup> The strong reductive excited state of the triphenylamine moiety within these FL-MOFs initiated a photoinduced electron transfer, rendering an active intermediate for the  $\alpha$ -alkylation. The chiral *pyi* moieties acted as cooperative organocatalytic active sites to drive the asymmetric catalysis with significant stereoselectivity. Further investigations demonstrated that the integration of both photocatalyst and asymmetric organocatalyst into a single FL-MOF makes the enantioselection superior to that of simply mixing the corresponding FL-MOFs with the chiral adduct.

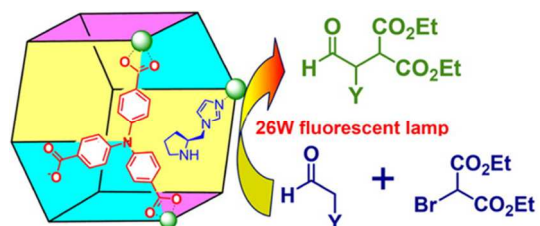


Fig. 29 The asymmetric  $\alpha$ -alkylation of aliphatic aldehydes catalyzed by Zn-PYI. Adapted with permission from ref. <sup>118</sup>. Copyright 2012 American Chemical Society.

Pyridyl or carboxyl-functionalized chiral salen ligands are of particular to construct homochiral FL-MOFs. Generally, the flexible salen ligands always link to metallic cations via  $N_2O_2$  in a one pot synthesis, thus turning to rigid metallsalens struts. In 2012, Cui and co-worker<sup>119</sup> reported the synthesis of dicarboxyl-functionalized chiral salen complexes of Co to make a homochiral FL-MOF  $\{[Cd_4(Co(cbc)s)_4(DMF)_4(OAc)_4] \cdot 4H_2O\}_n$  ( $H_4cbcs = 1,2$ -cyclohexanediamine- $N,N'$ -bis-(3-tert-butyl-5-(carboxyl)salicylide), which showed an efficient heterogeneous catalyst for HKR of epoxides. In the structure, a square-planar tetrameric  $[Cd_4(COO)_8]$  unit serving as SBU, was clustered by six bidentate and two tridentate carboxylate groups of eight Co(cbc)s units (Fig. 30a). All Co(cbc)s units exhibit an *exo*-pentadentate coordination mode including one bridging bidentate and one chelating-bridging tridentate carboxylate groups. Each tetranuclear Cd<sub>4</sub> cluster is thus linked by eight Co(cbc)s ligands, and each Co(cbc)s ligand is linked to three cadmium cations to generate a chiral porous 3D framework with channel cross sections of  $12 \times 8 \text{ \AA}^2$  along the *a* axis (Fig. 30b). Consequently, the channel surfaces are uniformly lined with chiral Co(cbc)s units with coordinatively unsaturated  $Co^{3+}$  cations that are available for guest molecules.

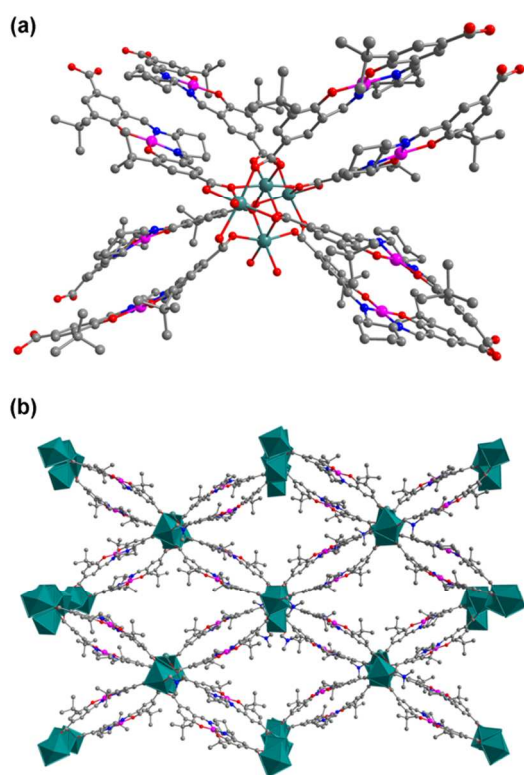


Fig. 30 (a) Building block in  $\{[Cd_4(Co(cbc)s)_4(DMF)_4(OAc)_4] \cdot 4H_2O\}_n$  (only the O atoms of DMF molecules are shown for clarity) and (b) view of 3D porous structure of  $[Cd_4(Co(cbc)s)_4(DMF)_4(OAc)_4] \cdot 4H_2O$  along the *a*-axis. Colour scheme: Cd and Cd octahedral, teal; Co, pink; C, gray; N, blue; O, red.

The catalytic activity of  $\{[Cd_4(Co(cbc)s)_4(DMF)_4(OAc)_4] \cdot 4H_2O\}_n$  was examined by the catalysis of HKR of epoxides. As shown in Table 1 (entries 1-6), a 0.5 mol % loading of the as-prepared framework with regard to the racemic substrates afforded the resolved target epoxides in 87–98% ee and 54–57% conversions within 48 h with a range of benzyloxy epoxide derivatives bearing both electron-donating and electron-withdrawing substituents. The resolutions of 1- and 2-naphthyl glycidyl ethers required a little higher catalyst loading (0.7 mol %), and within 48 h, 95 and 94% ee and 53 and 56% conversions of the epoxides were obtained, respectively. Increasing the reaction time to 60 h led to 99.5 and 99% ee and 57 and 62% conversions, respectively (Table 1, entries 7 and 8). Noteworthy, the examined epoxides exhibited good to excellent kinetic resolution selectivities ( $K_{rel} = 13$ -43, the ratio of relative rates of the two substrate enantiomers). Due to bulky substrate cannot access the catalytic sites in the porous structure, the catalysis of HKR of racemic triphenyl glycidyl ether, however, suffered from low conversion (5%) compared with homogeneous Co(cbc)s catalysts, which demonstrates the epoxide species chiefly occurs inside the pores rather than on the surface of the solid catalyst. The authors further pointed out, because the MOF structure brings Co(cbc)s units into a highly dense arrangement and close proximity that enhances bimetallic cooperative interactions, the catalytic activity and enantioselectivity in HKR was improved compared with its homogeneous analogues.

Table 1 HKR of Terminal Epoxides<sup>a</sup>

entry	R	cat. load (mol %) <sup>b</sup>	Reaction time (h)	ee <sub>ep</sub> (%) <sup>c</sup>	conv (%) <sup>d</sup>	$K_{rel}$ <sup>e</sup>
1	CH <sub>2</sub> O <sup>f</sup> Ph	0.5	48	95	56	25
2	CH <sub>2</sub> O( <i>o</i> -NO <sub>2</sub> C <sub>6</sub> H <sub>4</sub> )	0.5	48	92	54	27
3	CH <sub>2</sub> O( <i>p</i> -MeC <sub>6</sub> H <sub>4</sub> )	0.5	48	87	57	13
4	CH <sub>2</sub> O( <i>p</i> -OMeC <sub>6</sub> H <sub>4</sub> )	0.5	48	94	55	27
5	CH <sub>2</sub> O( <i>o</i> -MeC <sub>6</sub> H <sub>4</sub> )	0.5	48	97	54	43
6	CH <sub>2</sub> O( <i>m</i> -ClC <sub>6</sub> H <sub>4</sub> )	0.5	48	98	55	41
7	CH <sub>2</sub> O(1-naphthyl)	0.7	48/60	95/9	53/5	43/4
8	CH <sub>2</sub> O(2-naphthyl)	0.7	48/60	94/9	56/62	23/2
9	CH <sub>2</sub> O(triphenylethane)	0.7	72	n.d.	<5 <sup>f</sup>	n.d.

<sup>a</sup>Solvents: THF for entries 2, 3, and 7; CH<sub>2</sub>Cl<sub>2</sub>/CH<sub>3</sub>CN for other entries.

<sup>b</sup>Catalyst loading based on racemic epoxide. <sup>c</sup>ee values determined by HPLC.

<sup>d</sup>Isolated yield based on racemic epoxide. <sup>e</sup> $K_{rel} = \ln[1-c(1+ee)]/\ln[1-c(1-ee)]$ , where ee is the enantiomeric excess of the epoxide, and *c* is the conversion of the epoxide. <sup>f</sup>Estimated by <sup>1</sup>H NMR. Reprinted with permission from ref. <sup>119</sup>. Copyright 2012 American Chemical Society.

Very recently, Cui and co-workers further a chiral porous zeolite-like FL-MOF which is constructed by using mixed ligands of dipyridyl-functionalized chiral Ti(salen) and biphenyl-4,4'-dicarboxylate.<sup>120</sup> The framework containing

salen-bound  $\text{Ti}_4\text{O}_6$  clusters consists of both hydrophobic and amphiphilic mesocages and is shown to be an efficient and recyclable heterogeneous catalyst for the oxidation of thioethers to sulfoxides by aqueous  $\text{H}_2\text{O}_2$  (up to 82% ee), displaying markedly enhanced enantioselectivity over the homogeneous catalyst by providing a cavity confinement effect.

### 3.3 Proton conduction of FL-MOFs

Proton conductivity in solid-state materials is important due to potential applications in transport dynamics, electrochemical devices, and fuel cells, and also important to understand the complex biological ion channels. From the view of structure, in principle, proton conductivity requires proton carriers such as  $\text{H}_3\text{O}^+$  or  $\text{H}^+$ , given by acid or -OH groups, whereas conducting pathways are usually based on hydrogen-bonded networks. The crystallinity and highly tuneable nature of MOFs makes them a good candidate for solid-state proton conductor and an excellent platform to develop structure-activity relationships. Relative to the tremendous efforts directed at gas storage and separation and etc., proton conduction has only recently received attention. To date, only a few articles related to proton conductivity of MOFs has been reported, where some of them have shown excellent proton conductivity.<sup>7</sup>

Kitagawa and co-workers first employed 2D MOFs derived from dithiooxamide derivatives<sup>121</sup> and oxalate-bridged anionic layer frameworks<sup>122</sup> as MOF-based proton conductors. Subsequently, some research groups adopted flexible ligands to construct 2D to 3D FL-MOFs with proton conductivity. For example, Zhu and co-workers have synthesized a chiral 2D FL-MOF formulated as  $\{[\text{Ca}(\text{D-Hpmpc})(\text{H}_2\text{O})_2] \cdot 2\text{H}_2\text{O}_{0.5}\}_n$  based on a flexible ligand D-1-(phosphonomethyl) piperidine-3-carboxylic acid (D-H<sub>3</sub>pmpc), showing proton conductivity.<sup>123</sup> In the structure, protonated tertiary amines act as proton carriers and hydrogen-bonding chains serve as proton-conducting pathways. MOF-polymer composite membranes have been fabricated *via* assembling polymer PVP with different contents of the as-prepared framework. Interestingly, the proton conductivity of the composite membrane containing 50 wt% of the framework at room temperature is rapidly increased from  $2.8 \times 10^{-5} \text{ S cm}^{-1}$  at ~53% Relative humidity (RH) to  $5.7 \times 10^{-5} \text{ S cm}^{-1}$  at ~65% RH.

Sahoo and Banerjee investigated the influence of halogens (especially halogens coordinated to metals) in proton conduction in MOFs. They first synthesized four new homochiral FL-MOFs isomers  $\{[\text{Zn}(\text{L-mpba})(\text{Cl})](\text{H}_2\text{O})_2\}_n$ ,  $\{[\text{Zn}(\text{L-mpba})(\text{Br})](\text{H}_2\text{O})_2\}_n$ ,  $\{[\text{Zn}(\text{D-mpba})(\text{Cl})](\text{H}_2\text{O})_2\}_n$ , and  $\{[\text{Zn}(\text{D-mpba})(\text{Br})](\text{H}_2\text{O})_2\}_n$  by using flexible D/L-Hmpba·HX (Hmpba = 3-methyl-2-(pyridin-4-ylmethylamino)-butanoic acid; X = Cl or Br) ligands and  $\text{Zn}(\text{CH}_3\text{COO})_2 \cdot 2\text{H}_2\text{O}$ .<sup>124</sup> In each case, two lattice water molecules (one H-bonded to halogen atoms and lattice water molecules stronger than that between Br atoms and lattice water molecules, FL-MOFs  $\{[\text{Zn}(\text{L-mpba})(\text{Cl})](\text{H}_2\text{O})_2\}_n$  and  $\{[\text{Zn}(\text{D-mpba})(\text{Cl})](\text{H}_2\text{O})_2\}_n$  show higher water holding capacity than two other frameworks. Consequently, FL-MOFs

$\{[\text{Zn}(\text{L-mpba})(\text{Cl})](\text{H}_2\text{O})_2\}_n$  and  $\{[\text{Zn}(\text{D-mpba})(\text{Cl})](\text{H}_2\text{O})_2\}_n$  show high proton conductivity of  $4.45 \times 10^{-5}$  and  $4.42 \times 10^{-5} \text{ S cm}^{-1}$  at 304 K and 98% RH, respectively, while the other two frameworks show zero proton conductivity.

Except for carboxylic ligands, phosphonate ligands are alternative organic linkers particularly suitable for construction proton-conducting materials. Each phosphonic acid group possess three oxygen atoms which are only partly bonded to metal ions, whereas the remaining ones could expose to the MOFs cavities. Serving as acid and hydrophilic sites, the remaining oxygen atoms and free  $-\text{PO}_3\text{H}_2$  groups may increase the proton conductivity of MOFs. For this reason, efforts have devoted to synthesize proton conducting MOF materials *via* phosphonate organic ligands. In 2012, Cabeza and co-workers employed a flexible tetrakisphosphonates H<sub>8</sub>tph to construct a FL-MOF  $\{[\text{La}(\text{H}_5\text{tph}) \cdot 7\text{H}_2\text{O}]\}_n$  with coordinated hydrogen phosphonate where acidic conditions were employed to mediate protic state and obtained conductivities of  $8 \times 10^{-3} \text{ S cm}^{-1}$  at 297 K and 98% RH.<sup>125</sup> Extending the carbon chain of ligand, the authors further using another flexible tetrakisphosphonates octamethylenediamine-*N,N,N',N'*-tetrakis(methylenephosphonic acid) (H<sub>8</sub>odtmp) to build a 3D porous FL-MOF  $\{[\text{Mg}(\text{H}_6\text{odtmp}) \cdot 6\text{H}_2\text{O}]\}_n$ , which shows a proton conductivity of  $1.6 \times 10^{-3} \text{ S cm}^{-1}$  at 292 K and ~100% RH.<sup>126</sup> Based on another flexible linker cyclohexyl-*N,N,N',N'*-diamino tetrakisphosphonates (H<sub>8</sub>cdtp), Costantino and co-workers construct a zirconium-based FL-MOF, which displays varied proton conductivity associated with phase transitions.<sup>127</sup>

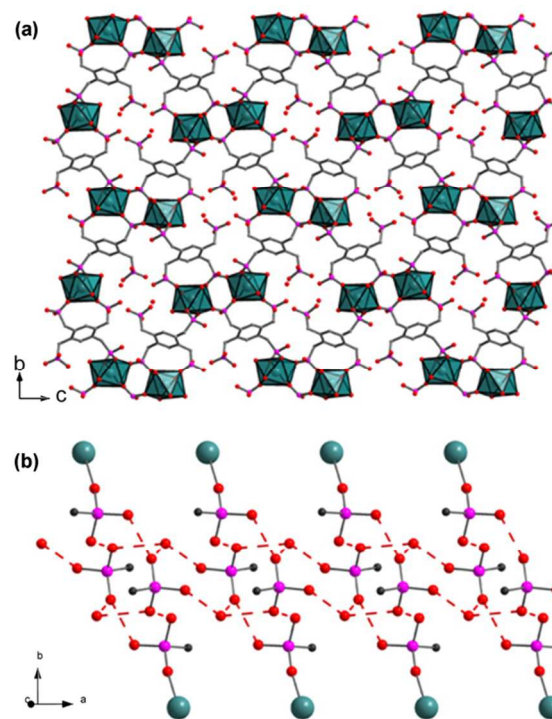


Fig. 31 (a) Structure of PCMOF-5 as viewed down the *a*-axis. Free phosphonic acid groups and uncoordinated water molecules are located in each pore. (b) View showing the 1D hydrogen-bonding array formed between phosphonic acid

groups and free water molecules in the direction of the *a*-axis. Reprinted with permission from ref. <sup>128</sup>. Copyright 2013 American Chemical Society.

Recently, Shimizu reported a new water-stable 3D FL-MOF  $\{\text{La}(\text{H}_5\text{tpmb})(\text{H}_2\text{O})_4\}_n$  (PCMOF-5) derived from a flexible phosphonate linker 1,2,4,5-tetrakisphosphonomethylbenzene ( $\text{H}_8\text{tpmb}$ ).<sup>128</sup> As shown in Fig. 31a, PCMOF-5 adopts a modified pillared-layered motif, where a hydrophobic tpmb pillars hydrophilic 1D columns of La(III) phosphonate along the *a*-axis. Alternating between the columns along the *a*-axis are acidic channels housing a single column of water molecules. The 1D La(III) phosphonate chains are connected into a 3D framework through three of the four phosphonate groups on tpmb, leaving the fourth group, a diprotic phosphonic acid, uncoordinated and protruding into the hydrated channel (Fig. 31). The hydrated channel is completely lined with phosphonic acid groups, with one coordinated monodentate hydrogen phosphonate per formula unit along the *b*-axis and one uncoordinated phosphonic acid per formula unit along the *c*-axis (Fig. 31b); three coordinated water molecules do not line the channel and appear to be involved in structural hydrogen bonds with the 1D La(III) phosphonate columns. Free water molecules fill the channel, alternating between and bridging the phosphonic acid groups through hydrogen bonds.

PCMOF-5 shows structural stability to high RH and dilute acidic solutions. Analysis on PCMOF-5 at 98% RH gave very good conductivity of  $1.3 \times 10^{-3} \text{ S cm}^{-1}$  at 21.5°C that rose to  $2.5 \times 10^{-3} \text{ S cm}^{-1}$  at 60.1 °C with a very low activation energy (0.16 eV). Reducing the humidity to 90% gave conductivity values between  $2 \times 10^{-5}$  and  $2 \times 10^{-4} \text{ S cm}^{-1}$  from 20 to 85°C, with an activation energy calculated at 0.32 eV. The high conductivity, with corresponding low activation energy at 98% RH, is likely due to the highly acidic, hydrated nature of the channel, along with the existence of a potential hydrogen bond pathway within PCMOF-5 under the highly humid conditions. It noteworthy that PCMOF-5 represents the first coordination polymer with a 3D structure to have uncoordinated phosphonic acid groups.

#### 4. Conclusion

In the last few decades, numerous FL-MOFs have been synthesized by using various flexible ligands. The conformational variations of flexible linkers combining with different coordination preferences of metal ions (clusters) result in the structural diversity of FL-MOFs. As an exemplary flexible ligand ( $\text{H}_4\text{tcm}$ ), more than forty FL-MOFs have been documented, which corresponds to about forty conformations of  $\text{H}_4\text{tcm}$  induced *via* fine control of the synthetic parameters. In terms of the structures of FL-MOFs built by  $\text{H}_4\text{tcm}$  ligands, FL-MOFs with versatile topologies (i.e., **pts**, **dia**, **lon**, **pcu**, **sxa**) were readily prepared using the same precursors, e.g. the case of zinc ions and  $\text{H}_4\text{tcm}$ , as a result of the intelligent conformational changes of the organic ligands. Meanwhile, both centrosymmetric structures with high permanent porosity for gas adsorption/separation and noncentrosymmetric

structures with excellent ferroelectric and second-order non-linear optical properties were successfully isolated. More interestingly, even in the cases of FL-MOFs with the same components and topology (such as zinc-based **dia** frameworks, copper-based **pts** networks), slight conformational differences of the  $\text{H}_4\text{tcm}$  ligands profoundly influence not just in terms of the FL-MOF structures (e.g., different pore sizes and shapes) but also their properties (e.g., different gas uptake capacities and selectivities), which could offer brilliant platforms to investigate the structure–property relationship on a molecule level.

The metal ligating functional groups in flexible ligands are not rigidly fixed which severely impacts the ability to rationally design and prediction in the formation of extended network architectures. In most cases, however, the flexible ligands can be idealized as the corresponding rigid ligands (i.e., preferential conformations) in the design and synthesis of desirable FL-MOFs. The ligand-to-axial pillaring strategy based on square layer (**sql**) or Kagomé layered (**kgm**) subunits (serving as SBLs), is a typical platform to construct 3,6-connected networks in isorecticular synthesis for both rigid and flexible ligands. The 3,24-connected **rht** networks based on nanoball SBBs and tripodal hexacarboxylic ligands is another representative platform for isorecticular synthesis. A series of isorecticular **rht**-type FL-MOFs with tuneable pore sizes and properties were successfully synthesized *via* both the elongated/functionalized flexible and rigid tripodal hexacarboxylic ligands. Additionally, the malleable ligands provide a means to the design and synthesis of structures that are hardly accessible, sometimes even inaccessible, from rigid organic building blocks. Eddaoudi and co-workers demonstrated that the unique (3,4)-connected **tbo**-type FL-MOFs can be exclusively constructed by utilizing a combination of the edge-transitive 4,4-square lattice (**sql**) SBLs and 4-connected (quadrangular) pillars. In this **tbo**-type FL-MOF platform, the 1,3-bdc-based pillaring ligands with a measure of flexibility are indispensable. The malleable pillars allow the pendant bdc arms to be positioned in a square geometry and retain their ability to freely form the expecting SBL (**sql** subunits). Likewise, the flexibility of 1,3-bdc-based tetracarboxylic ligands are essential in the construction of isorecticular **pcu**-type FL-MOFs based on the nanoballs.

Many chiral organic molecules, such as amino acids and peptides, are flexible. As the use of chiral ligands is the most reliable means to construct homochiral MOFs, employing flexible ligands somewhat facilitate MOFs with chiral centers. Some amino-acid-based FL-MOFs with enantioselective separation and asymmetric catalysis have been successfully prepared. Through controlling the side-chain of dipeptides, both the adaptable and rigid FL-MOFs were isolated. The extent of framework's rigidity was driven by the H-bonds formed both to other dipeptides and to the guests, which opens the door for the development of protein-like biomimetic materials with biological functions.

Many non-interpenetrating dynamic MOFs built by rigid ligands have been reported based on a so-called “kneecap” mechanism. In some cases, the flexibility of the components

(i.e., ligands) can be transferred to the MOF frameworks, and leads to interesting dynamic FL-MOFs. In this context, flexible ligands are particularly suitable for the construction 3D pillared-layer type and expanding-shrinking type dynamic frameworks. In these dynamic FL-MOFs, the reversible transformations observed for *lp* and *np* phases are attributable to the conformational changes of the organic ligands presence.

On the other hand, FL-MOFs have been widely explored for their applications in gas adsorption. Large research efforts have been dedicated to explore feasible strategies to enhance gas adsorption capacity of FL-MOFs materials. The use of elongated flexible ligands has generated a series of FL-MOFs with large pore volume ratios, which are normally required for better performing MOFs as adsorbents. However, the BET surface areas and gas uptake capacities of most FL-MOFs are always relatively low, comparing with the theoretical estimations from computational studies. A rational explanation is that, in most cases, the FL-MOFs exhibit relatively low mechanical stability and thus the frameworks collapse (or partially collapses) upon solvent removal. To retain the porosity of FL-MOFs, strategies include minimizing the detriment of MOF frameworks during the activation processes and increasing the mechanical stability of MOF frameworks before sample activation. The former can be readily achieved by utilizing mild activation methods such as solvent-exchange or SCD drying method, while the latter can be implemented by “guest-dependent” strategy where the guest molecules effectively sustain the skeleton of the frameworks. Besides, various amine- or amide-functional organic ligands were adopted in the construction FL-MOFs to enhance the gas-binding affinity (especially for CO<sub>2</sub>). The resulting amine- or amide-functional FL-MOFs show considerably high CO<sub>2</sub> uptake capacities and isosteric heat ( $Q_{st}$ ) as well as excellent selectivity of CO<sub>2</sub>/CH<sub>4</sub> and CO<sub>2</sub>/N<sub>2</sub>.

Considering the relatively low mechanical and thermal stability of FL-MOFs, the design and synthesis of FL-MOFs as catalysts mainly focus on direct incorporation the pre-designed functional ligands into channels of the FL-MOF frameworks. Successful examples including incorporation amine or amide as Lewis base sites for size-selective heterogeneous catalysis of the Knoevenagel condensation reaction; incorporation chiral ligands such as amino acids and their derivatives adjacent to active sites for potential asymmetric catalysis; incorporation privileged asymmetric ligands such as organocatalysts, chiral salen ligands etc. for enantioselective catalysis.

The crystalline and highly tuneable nature of FL-MOFs makes them ideal as candidates for solid-state proton conduction and an excellent platform to investigate structure-function relationships. Although proton conduction is still an emerging research area in MOF chemistry, some of FL-MOFs have shown impressive proton conductivities. It has been demonstrated that the phosphonate ligands could be particularly suitable for construction proton-conducting materials. Moreover, FL-MOFs have been found promising applications in luminescent, thermal/photochromic applications and so on.

Although dramatic advancement has been made, FL-MOF research is still at an early stage of development. As the synthetic conditions such as reaction temperature, solvents, counter-anions, organic templates, pH etc. can influence the conformations of flexible ligands and therefore the final structures of FL-MOFs, a high degree of predictability must be integrated prior to synthesis. Further research efforts are indispensable to fully understand the structural features and structure-property relationship in framework materials, in order to establish reliable strategies for design and synthesis of targeting FL-MOFs. Additionally, considering the relatively low mechanical stability nature of FL-MOFs, the FL-MOF applications in the solvate phase such as liquid phase catalysis, proton conduction, luminescence, sensing etc. will surely assume increasingly important roles in future investigations.

## Acknowledgements

We acknowledge the financial support from the 973 Program (2011CB932504 and 2013CB933200), NSFC (21331006, 21303205, 21273238 and 21221001).

## Notes

State Key Laboratory of Structural Chemistry, Fujian Institute of Research on the Structure of Matter, Chinese Academy of Sciences, Fujian, Fuzhou, 350002, P. R. China.

E-mail: rcao@fjirsm.ac.cn; Fax: (+86) 591-8379-6710; Tel: (+86) 591-8379-6710.

Tables representation of the conformations of H<sub>4</sub>tem and the selected adsorption and separation of FL-MOFs.

## Abbreviations

MOF	metal organic framework
RL-MOF	MOF built by rigid ligands
FL-MOF	MOF built by flexible ligands
CP	coordination polymer
1D, 2D, and 3D	one-, two-, and three-dimensional
KDP	potassium dihydrogen phosphate
SBU	secondary building units
SBB	supramolecular building blocks
SBL	supramolecular building layers
CCP	cubic close packing
DMA	<i>N,N</i> -dimethylacetamide
DEF	<i>N,N</i> -diethylformamide
DMF	<i>N,N</i> -dimethylformamide
MeOH	methanol
BET	Brunauer-Emmett-Teller
Relative humidity	RH
ee	enantiomeric excess
Boc	<i>N-tert</i> -butoxy-carbonyl
NLO	non-linear optical
SHG	second-harmonic generation
Asp	aspartic acid
Gly-Ala	glycylalanine
Gly-Thr	glycylthreonine

Gly-Ser	glycylserine	H <sub>4</sub> tcom	4,4'-(2,2-bis((4-carboxy-2-methoxyphenoxy)methyl)propane-1,3-diyl)bis(oxy)bis(3-methoxybenzoic acid)
Carcarnosine		H <sub>4</sub> tcvm	3,3'-(4,4'-(2,2-bis((4-(2-carboxyvinyl)phenoxy)methyl)propane-1,3-diyl)bis(oxy)bis(4,1-phenylene))diacrylic acid
PCN	porous coordination network	H <sub>4</sub> tcvom	3,3'-(4,4'-(2,2-bis((4-(2-carboxyvinyl)-2-methoxyphenoxy)methyl)propane-1,3-diyl)bis(oxy)bis(3-methoxy-4,1-phenylene))diacrylic acid
USTA	University of Texas at San Antonio	H <sub>4</sub> tcnm	6,6'-(2,2-bis((6-carboxynaphthalen-2-yloxy)methyl)propane-1,3-diyl)bis(oxy)di-2-naphthoic acid
POST	Pohang University of Science and Technology	H <sub>4</sub> tc bpm	4',4''-(2,2-bis((4'-carboxybiphenyl-4-yloxy)methyl)propane-1,3-diyl)bis(oxy)dibiphenyl-4-carboxylic acid
HNUST	Hunan University of Science and Technology	H <sub>6</sub> hco	hexa[4-(carboxyphenyl)oxamethyl]-3-oxapentane
NJU-Bai	Nanjing University Bai group	H <sub>3</sub> ttt	4,4',4''-(2,4,6-trimethylbenzene-1,3,5-triyl)tris(methylene)tris(oxy)tribenzoic acid
H <sub>4</sub> dbip	5-(3,5-dicarboxybenzyloxy)isophthalic acid	H <sub>6</sub> htt	5,5',5''-(2,4,6-trimethylbenzene-1,3,5-triyl)tris(methylene)tris(oxy)trisophthalic acid
H <sub>4</sub> bpdc	3,3',5,5'-biphenyltetracarboxylate	H <sub>3</sub> btctb	4,4',4''-[1,3,5-benzenetriyltris(carbonylimino)]trisbenzoic acid
H <sub>4</sub> azpy	1,1'-azobenene-3,3',5,5'-tetracarboxylic acid	H <sub>3</sub> tcpt	2,4,6-tris-(4-carboxyphenoxy)-1,3,5-triazine
H <sub>4</sub> tem	tetrakis[4-(carboxyphenyl)oxamethyl]methane acid	H <sub>6</sub> tdpat	2,4,6-tris(3,5-dicarboxylphenylamino)-1,3,5-triazine
bipy	4,4'-bipyridine	H <sub>3</sub> cip	5-(4-carboxybenzoylamino)-isophthalic acid
etbipy	1,2-bis-(4-pyridyl)ethane	H <sub>4</sub> bdpt	bis(3,5-dicarboxyphenyl)terephthalamide
dib	1,4-di(1H-imidazol-1-yl)benzene	H <sub>4</sub> pbmp	<i>N,N'</i> -piperazinebis(methylenephosphonic acid)
dibp	4,4'-di(1H-imidazol-1-yl)-1,1'-biphenyl	H <sub>4</sub> bdpo	<i>N,N'</i> -bis(3,5-dicarboxyphenyl)oxalamide
H <sub>4</sub> tem	tetrakis[4-(carboxyphenyl)oxamethyl]methane acid	H <sub>2</sub> btz	1,5-bis(5-tetrazolo)-3-oxapentane
1,4-bdc	terephthalate	H <sub>3</sub> btctb	4,4',4''-[1,3,5-benzenetriyltris(carbonylimino)]trisbenzoic acid
1,3-bdc	isophthalate	H <sub>2</sub> obb	4,4'-oxybis(benzoic acid)
H <sub>4</sub> bmbb	1,3-Bis(5-methoxy-1,3-benzene dicarboxylic acid)benzene	4-btapa	1,3,5-benzene tricarboxylic acid tris[ <i>N</i> -(4-pyridyl)amide]
H <sub>4</sub> mdip	5,5'-methylene-diisophthalic acid	H <sub>3</sub> btatb	4,4',4''-(benzene-1,3,5-triyltris(azanediy))tribenzoic acid
H <sub>4</sub> bbpm	1,1-bis-[3,5-bis(carboxy)phenoxy]methane	H <sub>3</sub> tatab	4,4',4''-(1,3,5-triazine-2,4,6-triyl)tris(azanediy)tribenzoic acid
H <sub>6</sub> bcbd	5,5',5''-[1,3,5-benzenetriyltris(carbonylimino)]tris-1,3-benzene dicarboxylic acid	Hdpdc	[(4 <i>R</i> ,5 <i>R</i> )-2,2-dimethyl-5-[(pyridin-4-ylamino)carbonyl]-1,3-dioxolane-4-carboxylic acid
H <sub>8</sub> ptmtip	5,5',5'',5''''-[1,2,4,5-phenyltetramethoxy]tetraisophthalate	Hhpp	( <i>S</i> )-3-hydroxy-2-(pyridine-4-ylmethylamino)propanoic acid
H <sub>12</sub> phmhip	5,5',5'',5''',5''''-[1,2,3,4,5,6-phenylhexamethoxy]hexaisophthalic acid	bcip	<i>N-tert</i> -butoxy-carbonyl-2-(imidazole)-1-pyrrolidine
H <sub>8</sub> bmatip	5,5',5'',5''''-[1,2,4,5-benzenetetrakis(4-methyleneoxyphenylazo)]tetraisophthalic acid	pyi	pyrrolidine-2-yl-imidazole
H <sub>2</sub> ppip	5-(4-pyridinylmethoxy)-isophthalic acid	H <sub>3</sub> btb	1,3,5-tris(4-carboxyphenyl)benzene
H <sub>2</sub> mpip	5-(3-pyridinylmethoxy)-isophthalic acid	H <sub>4</sub> cbcs	1,2-cyclohexanediamine- <i>N,N'</i> -bis-(3- <i>tert</i> -butyl-5-(carboxyl)salicylide
H <sub>2</sub> ppdip	5-[(1 <i>E</i> )-2-[4-(4-pyridinyloxy)phenyl]diazanyl]isophthalic acid	D-H <sub>3</sub> pmpe	D-1-(phosphonomethyl) piperidine-3-carboxylic acid
H <sub>6</sub> pttip	5,5',5''-[1,3,5-phenyl-tris(methoxy)]tris-isophthalic acid	Hmpba	3-methyl-2-(pyridin-4-ylmethylamino)-butanoic acid
H <sub>6</sub> ptptip	5,5',5''-{4,4',4''-[1,3,5-phenyltris(methoxy)]tris-phenylazo}tris-isophthalic acid	H <sub>8</sub> cdtp	Cyclohexyl- <i>N,N,N',N'</i> -diamino tetraphosphonates
Na <sub>6</sub> tdpat	5,5',5''-(1,3,5-triazine-2,4,6-triyltriimino)tris-isophthalate hexasodium	H <sub>8</sub> tpmb	1,2,4,5-tetrakisphosphonomethylbenzene
H <sub>2</sub> epda	5-ethyl-pyridine-2,3-dicarboxylic acid	H <sub>8</sub> odtmp	Octamethylenediamine- <i>N,N,N',N'</i> -tetrakis(methylenephosphonic acid)
etbipy	1,2-bi(4-pyridyl)ethane		
H <sub>4</sub> pbmp	<i>N,N'</i> -piperazinebis(methylenephosphonic acid)		
H <sub>8</sub> tph	<i>N,N,N',N'</i> -tetrakis(phosphonomethyl)hexamethylenediamine		
H <sub>8</sub> tpx	<i>N,N,N',N'</i> -tetrakis(phosphonomethyl)- $\alpha,\alpha'$ - <i>p</i> -xylylenediamine		
tbdbt	4,4'-(1,4-(trans-2-butene)diyl)bis(1,2,4-triazole)		
IAST	the ideal adsorbed solution theory		
OMSs	open metal sites		
LBSs	Lewis basic sites		
bpb	1,4-bis(4-pyridyl)benzene		
azpy	4,4'-azopyridine		
isonic	pyridine-4-carboxylate		
H <sub>8</sub> tdm	tetrakis[(3,5-dicarboxyphenoxy)methyl]methane		

## References

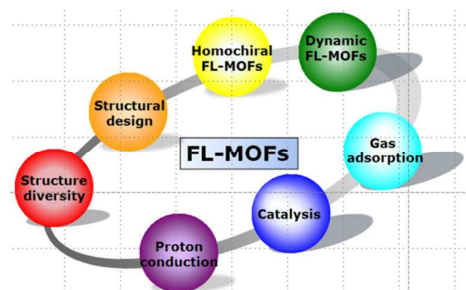
- 1 (a) B. F. Hoskins and R. Robson, *J. Am. Chem. Soc.*, 1989, **111**, 5962; (b) B. F. Hoskins and R. Robson, *J. Am. Chem. Soc.*, 1990, **112**, 1546; (c) B. Moulton and M. J. Zaworotko, *Chem. Rev.*, 2001, **101**, 1629; (d) A. Y. Robin and K. M. Fromm, *Coord. Chem. Rev.*, 2006, **250**, 2127.
- 2 (a) D. Zhao, D. J. Timmons, D. Q. Yuan and H. C. Zhou, *Acc. Chem. Res.*, 2011, **44**, 123; (b) M. O'Keeffe and O. M. Yaghi, *Chem. Rev.*, 2012, **112**, 675; (c) H.-L. Jiang, T. A. Makal and H.-C. Zhou, *Coord. Chem. Rev.*, 2013, **257**, 2232; (d) M. Li, D. Li, M. O'Keeffe and O. M. Yaghi, *Chem. Rev.*, 2013, 10.1021/cr400392k; (e) Q. Chen, F. Jiang, D. Yuan, G. Lyu, L. Chen and M. Hong, *Chem. Sci.*, 2014, 483.
- 3 (a) D. M. D'Alessandro, B. Smit and J. R. Long, *Angew. Chem., Int. Ed.*, 2010, **49**, 6058; (b) J.-R. Li, Y. Ma, M. C. McCarthy, J. Sculley, J. Yu, H.-K. Jeong, P. B. Balbuena and H.-C. Zhou, *Coord. Chem. Rev.*, 2011, **255**, 1791; (c) J.-R. Li, J. Sculley and H.-C. Zhou, *Chem. Rev.*, 2012, **112**, 869; (d) J. Liu, P. K. Thallapally, B. P. McGrail, D. R. Brown and J. Liu, *Chem. Soc. Rev.*, 2012, **41**, 2308; (e) K. Sumida, D. L. Rogow, J. A. Mason, T. M. McDonald, E. D. Bloch, Z. R. Herm, T.-H. Bae and J. R. Long, *Chem. Rev.*, 2012, **112**, 724; (f) S. Chaemchuen, N. A. Kabir, K. Zhou and F. Verpoort, *Chem. Soc. Rev.*, 2013, 9304; (g) J.-R. Li, J. Yu, W. Lu, L.-B. Sun, J. Sculley, P. B. Balbuena and H.-C. Zhou, *Nat. Commun.*, 2013, **4**, 1538; (h) Y. Yan, S. Yang, A. J. Blake and M. Schröder, *Acc. Chem. Res.*, 2013, 10.1021/ar400049h; (i) J. A. Mason, M. Veenstra and J. R. Long, *Chem. Sci.*, 2014, **5**, 32.
- 4 (a) J. Lee, O. K. Farha, J. Roberts, K. A. Scheidt, S. T. Nguyen and J. T. Hupp, *Chem. Soc. Rev.*, 2009, **38**, 1450; (b) L. Ma, C. Abney and W. Lin, *Chem. Soc. Rev.*, 2009, **38**, 1248; (c) Y. Liu, W. M. Xuan and Y. Cui, *Adv. Mater.*, 2010, **22**, 4112; (d) M. Yoon, R. Srirambalaji and K. Kim, *Chem. Rev.*, 2011, **112**, 1196; (e) A. Dhakshinamoorthy and H. Garcia, *Chem. Soc. Rev.*, 2012, **41**, 5262; (f) H. R. Moon, D.-W. Lim and M. P. Suh, *Chem. Soc. Rev.*, 2013, **42**, 1807.
- 5 (a) Q. Zhu, C. Shen, C. Tan, T. Sheng, S. Hu and X. Wu, *Chem. Commun.*, 2012, **48**, 531; (b) J. Heine and K. Muller-Buschbaum, *Chem. Soc. Rev.*, 2013, **42**, 9232; (c) H.-L. Jiang, D. Feng, K. Wang, Z.-Y. Gu, Z. Wei, Y.-P. Chen and H.-C. Zhou, *J. Am. Chem. Soc.*, 2013, **135**, 13934; (d) C.-Y. Sun, X.-L. Wang, X. Zhang, C. Qin, P. Li, Z.-M. Su, D.-X. Zhu, G.-G. Shan, K.-Z. Shao, H. Wu and J. Li, *Nat. Commun.*, 2013, **4**, 10.1038/ncomms3717.
- 6 L. E. Kreno, K. Leong, O. K. Farha, M. Allendorf, R. P. Van Duyne and J. T. Hupp, *Chem. Rev.*, 2012, **112**, 1105.
- 7 (a) T. Yamada, K. Otsubo, R. Makiura and H. Kitagawa, *Chem. Soc. Rev.*, 2013, **42**, 6655; (b) M. Yoon, K. Suh, S. Natarajan and K. Kim, *Angew. Chem., Int. Ed.*, 2013, **52**, 2688.
- 8 (a) Q.-L. Zhu, T.-L. Sheng, R.-B. Fu, S.-M. Hu, L. Chen, C.-J. Shen, X. Ma and X.-T. Wu, *Chem.-Eur. J.*, 2011, **17**, 3358; (b) H. Miyasaka, *Acc. Chem. Res.*, 2012, **46**, 248; (c) J.-K. Sun, P. Wang, Q.-X. Yao, Y.-J. Chen, Z.-H. Li, Y.-F. Zhang, L.-M. Wu and J. Zhang, *J. Mater. Chem.*, 2012, **22**, 12212; (d) M.-S. Wang, C. Yang, G.-E. Wang, G. Xu, X.-Y. Lv, Z.-N. Xu, R.-G. Lin, L.-Z. Cai and G.-C. Guo, *Angew. Chem., Int. Ed.*, 2012, **51**, 3432; (e) W. Zhang and R.-G. Xiong, *Chem. Rev.*, 2012, **112**, 1163; (f) E. Coronado and G. Minguez Espallargas, *Chem. Soc. Rev.*, 2013, **42**, 1525; (g) Y.-N. Gong and T.-B. Lu, *Chem. Commun.*, 2013, **49**, 7711; (h) S.-L. Li and Q. Xu, *Energ Environ. Sci.*, 2013, **6**, 1656.
- 9 H. Furukawa, K. E. Cordova, M. O'Keeffe and O. M. Yaghi, *Science*, 2013, **341**, 10.1126/science.1230444.
- 10 (a) M. O'Keeffe, M. A. Peskov, S. J. Ramsden and O. M. Yaghi, *Acc. Chem. Res.*, 2008, **41**, 1782; (b) D. J. Tranchemontagne, Z. Ni, M. O'Keeffe and O. M. Yaghi, *Angew. Chem., Int. Ed.*, 2008, **47**, 5136; (c) J. J. Perry, J. A. Perman and M. J. Zaworotko, *Chem. Soc. Rev.*, 2009, **38**, 1400; (d) D. J. Tranchemontagne, J. L. Mendoza-Cortes, M. O'Keeffe and O. M. Yaghi, *Chem. Soc. Rev.*, 2009, **38**, 1257.
- 11 (a) H.-L. Jiang and Q. Xu, *Chem. Commun.*, 2011, **47**, 3351; (b) F. A. Almeida Paz, J. Klinowski, S. M. F. Vilela, J. P. C. Tome, J. A. S. Cavaleiro and J. Rocha, *Chem. Soc. Rev.*, 2012, **41**, 1088; (c) D. Feng, Z.-Y. Gu, J.-R. Li, H.-L. Jiang, Z. Wei and H.-C. Zhou, *Angew. Chem., Int. Ed.*, 2012, **51**, 10307; (d) D. Feng, W.-C. Chung, Z. Wei, Z.-Y. Gu, H.-L. Jiang, Y.-P. Chen, D. J. Darensbourg and H.-C. Zhou, *J. Am. Chem. Soc.*, 2013, **135**, 17105; (e) R.-B. Lin, F. Li, S.-Y. Liu, X.-L. Qi, J.-P. Zhang and X.-M. Chen, *Angew. Chem., Int. Ed.*, 2013, **52**, 13429; (f) Y. Peng, V. Krungleviciute, I. Eryazici, J. T. Hupp, O. K. Farha and T. Yildirim, *J. Am. Chem. Soc.*, 2013, **135**, 11887; (g) H.-L. Zhou, R.-B. Lin, C.-T. He, Y.-B. Zhang, N. Feng, Q. Wang, F. Deng, J.-P. Zhang and X.-M. Chen, *Nat. Commun.*, 2013, **4**, 10.1038/ncomms3534.
- 12 (a) M. Hong, Y. Zhao, W. Su, R. Cao, M. Fujita, Z. Zhou and A. S. C. Chan, *Angew. Chem., Int. Ed.*, 2000, **39**, 2468; (b) Y. Gong, Y.-C. Zhou, T.-F. Liu, J. Lu, D. M. Proserpio and R. Cao, *Chem. Commun.*, 2011, **47**, 5982; (c) N. Li, F. Jiang, L. Chen, X. Li, Q. Chen and M. Hong, *Chem. Commun.*, 2011, **47**, 2327; (d) B. Xu, X. Lin, Z. He, Z. Lin and R. Cao, *Chem. Commun.*, 2011, **47**, 3766; (e) X.-J. Li, F.-L. Jiang, M.-Y. Wu, S.-Q. Zhang, Y.-F. Zhou and M.-C. Hong, *Inorg. Chem.*, 2012, **51**, 4116; (f) K. Zhou, F.-L. Jiang, L. Chen, M.-Y. Wu, S.-Q. Zhang, J. Ma and M.-C. Hong, *Chem. Commun.*, 2012, **48**, 12168; (g) Q. Chen, F. Jiang, D. Yuan, L. Chen, G. Lyu and M. Hong, *Chem. Commun.*, 2013, **49**, 719.
- 13 (a) C. A. Fernandez, P. K. Thallapally, R. K. Motkuri, S. K. Nune, J. C. Sumrak, J. Tian and J. Liu, *Cryst. Growth Des.*, 2010, **10**, 1037; (b) T.-F. Liu, J. Lu and R. Cao, *CrystEngComm*, 2010, **12**, 660; (c) F. C. Pigge, *CrystEngComm*, 2011, **13**, 1733.
- 14 (a) P. Dechambenoit and J. R. Long, *Chem. Soc. Rev.*, 2011, **40**, 3249; (b) L.-F. Ma, M.-L. Han, J.-H. Qin, L.-Y. Wang and M. Du, *Inorg. Chem.*, 2012, **51**, 9431; (c) H.-L. Tsai, C.-I. Yang, W. Wernsdorfer, S.-H. Huang, S.-Y. Jhan, M.-H. Liu and G.-H. Lee, *Inorg. Chem.*, 2012, **51**, 13171; (d) Q. Zhu, S. Xiang, T. Sheng, D. Yuan, C. Shen, C. Tan, S. Hu and X. Wu, *Chem. Commun.*, 2012, **48**, 10736; (e) Y. Z. Zheng, Z. P. Zheng and X. M. Chen, *Coord. Chem. Rev.*, 2014, **258**, 1.
- 15 C.-L. Chen, J.-Y. Zhang and C.-Y. Su, *Eur. J. Inorg. Chem.*, 2007, 2997.
- 16 (a) S. Kitagawa and R. Matsuda, *Coord. Chem. Rev.*, 2007, **251**, 2490; (b) G. Ferey, *Chem. Soc. Rev.*, 2008, **37**, 191; (c) G. Ferey, *Dalton Trans.*, 2009, 4400; (d) S. Horike, S. Shimomura and S. Kitagawa, *Nat. Chem.*, 2009, **1**, 695; (e) C. R. Murdock, B. C. Hughes, Z. Lu and D. M. Jenkins, *Coord. Chem. Rev.*, 2014, **258–259**, 119.
- 17 (a) Z. J. Lin, X. Lin and R. Cao, *Acta Chim. Sinica*, 2012, **70**, 2012; (b) L.-L. Qu, Y.-L. Zhu, J. Zhang, Y.-Z. Li, H.-B. Du and X.-Z. You, *CrystEngComm*, 2012, **14**, 824; (c) F. Yu and B. Li, *CrystEngComm*, 2012, **14**, 6049; (d) W. Yang, F.-Y. Yi, X.-D. Li, L. Wang, S. Dang and Z.-M. Sun, *RSC Adv.*, 2013, **3**, 25065; (e) L. Zhou, J. Zhang, Y.-Z. Li and H.-B. Du, *CrystEngComm*, 2013, **15**, 8989.
- 18 (a) Z.-J. Lin, L.-W. Han, D.-S. Wu, Y.-B. Huang and R. Cao, *Cryst. Growth Des.*, 2012, **13**, 255; (b) M.-L. Ma, C. Ji and S.-Q. Zang,

- Dalton Trans.*, 2013, **42**, 10579; (c) R. Patra, H. M. Titi and I. Goldberg, *CrystEngComm*, 2013, **15**, 2853.
- 19 (a) B. Chen, N. W. Ockwig, F. R. Fronczek, D. S. Contreras and O. M. Yaghi, *Inorg. Chem.*, 2004, **44**, 181; (b) Y. Liu, J. F. Eubank, A. J. Cairns, J. Eckert, V. C. Kravtsov, R. Luebke and M. Eddaoudi, *Angew. Chem., Int. Ed.*, 2007, **46**, 3278; (c) A. J. Cairns, J. A. Perman, L. Wojtas, V. C. Kravtsov, M. H. Alkordi, M. Eddaoudi and M. J. Zaworotko, *J. Am. Chem. Soc.*, 2008, **130**, 1560; (d) Y.-G. Lee, H. R. Moon, Y. E. Cheon and M. P. Suh, *Angew. Chem., Int. Ed.*, 2008, **47**, 7741; (e) W. Liu, L. Ye, X. Liu, L. Yuan, J. Jiang and C. Yan, *CrystEngComm*, 2008, **10**, 1395; (f) X.-S. Wang, S. Ma, K. Rauch, J. M. Simmons, D. Yuan, X. Wang, T. Yildirim, W. C. Cole, J. J. López, A. d. Meijere and H.-C. Zhou, *Chem. Mater.*, 2008, **20**, 3145; (g) M. Xue, G. Zhu, Y. Li, X. Zhao, Z. Jin, E. Kang and S. Qiu, *Cryst. Growth Des.*, 2008, **8**, 2478; (h) S. Yang, X. Lin, A. J. Blake, K. M. Thomas, P. Hubberstey, N. R. Champness and M. Schroder, *Chem. Commun.*, 2008, **44**, 6108; (i) H.-S. Choi and M. P. Suh, *Angew. Chem., Int. Ed.*, 2009, **48**, 6865.
- 20 (a) M.-S. Chen, M. Chen, S. Takamizawa, T.-a. Okamura, J. Fan and W.-Y. Sun, *Chem. Commun.*, 2011, **47**, 3787; (b) Q.-Y. Yang, K. Li, J. Luo, M. Pan and C.-Y. Su, *Chem. Commun.*, 2011, **47**, 4234; (c) Q. Yang, X. Chen, Z. Chen, Y. Hao, Y. Li, Q. Lu and H. Zheng, *Chem. Commun.*, 2012, **48**, 10016; (d) C. A. Allen, J. A. Boissonnault, J. Cirera, R. Gulland, F. Paesani and S. M. Cohen, *Chem. Commun.*, 2013, **49**, 3200; (e) L. Sun, H. Xing, Z. Liang, J. Yu and R. Xu, *Chem. Commun.*, 2013, **49**, 11155.
- 21 (a) Z. Lin and M.-L. Tong, *Coord. Chem. Rev.*, 2011, **255**, 421; (b) N. N. Adarsh and P. Dastidar, *Chem. Soc. Rev.*, 2012, **41**, 3039; (c) M. Du, C.-P. Li, C.-S. Liu and S.-M. Fang, *Coord. Chem. Rev.*, 2013, **257**, 1282.
- 22 F. Niekel, M. Ackermann, P. Guerrier, A. Rothkirch and N. Stock, *Inorg. Chem.*, 2013, **52**, 8699.
- 23 (a) D. P. Martin, R. M. Supkowski and R. L. LaDuca, *Inorg. Chem.*, 2007, **46**, 7917; (b) P. Mahata, C.-M. Draznieks, P. Roy and S. Natarajan, *Cryst. Growth Des.*, 2012, **13**, 155.
- 24 Z. Guo, R. Cao, X. Wang, H. Li, W. Yuan, G. Wang, H. Wu and J. Li, *J. Am. Chem. Soc.*, 2009, **131**, 6894.
- 25 T.-F. Liu, J. Lu, Z. Guo, D. M. Proserpio and R. Cao, *Cryst. Growth Des.*, 2010, **10**, 1489.
- 26 L.-L. Liang, S.-B. Ren, J. Zhang, Y.-Z. Li, H.-B. Du and X.-Z. You, *Dalton Trans.*, 2010, **39**, 7723.
- 27 T.-F. Liu, J. Lu, X. Lin and R. Cao, *Chem. Commun.*, 2010, **46**, 8439.
- 28 T.-F. Liu, J. Lue, C. Tian, M. Cao, Z. Lin and R. Cao, *Inorg. Chem.*, 2011, **50**, 2264.
- 29 M. R. Kishan, J. Tian, P. K. Thallapally, C. A. Fernandez, S. J. Dalgarno, J. E. Warren, B. P. McGrail and J. L. Atwood, *Chem. Commun.*, 2010, **46**, 538.
- 30 P. K. Thallapally, C. A. Fernandez, R. K. Motkuri, S. K. Nune, J. Liu and C. H. F. Peden, *Dalton Trans.*, 2010, **39**, 1692.
- 31 J. Tian, R. K. Motkuri, P. K. Thallapally and B. P. McGrail, *Cryst. Growth Des.*, 2010, **10**, 5327.
- 32 T. K. Kim and M. P. Suh, *Chem. Commun.*, 2011, **47**, 4258.
- 33 L.-L. Liang, J. Zhang, S.-B. Ren, G.-W. Ge, Y.-Z. Li, H.-B. Du and X.-Z. You, *CrystEngComm*, 2010, **12**, 2008.
- 34 R. K. Motkuri, P. K. Thallapally, S. K. Nune, C. A. Fernandez, B. P. McGrail and J. L. Atwood, *Chem. Commun.*, 2011, **47**, 7077.
- 35 P. K. Thallapally, J. Tian, M. R. Kishan, C. A. Fernandez, S. J. Dalgarno and et al., *J. Am. Chem. Soc.*, 2008, **130**, 16842.
- 36 L. Zhou, Y.-S. Xue, J. Zhang, H.-B. Du and X.-Z. You, *CrystEngComm*, 2013, **15**, 6199.
- 37 W. Yang, M. Guo, F.-Y. Yi and Z.-M. Sun, *Cryst. Growth Des.*, 2012, **12**, 5529.
- 38 J. Tian, L. V. Saraf, B. Schwenzler, S. M. Taylor, E. K. Brechin, J. Liu, S. J. Dalgarno and P. K. Thallapally, *J. Am. Chem. Soc.*, 2012, **134**, 9581.
- 39 J. F. Eubank, H. Mouttaki, A. J. Cairns, Y. Belmabkhout, L. Wojtas, R. Luebke, M. Alkordi and M. Eddaoudi, *J. Am. Chem. Soc.*, 2011, **133**, 14204.
- 40 S. S.-Y. Chui, S. M.-F. Lo, J. P. H. Charmant, A. G. Orpen and I. D. Williams, *Science*, 1999, **283**, 1148.
- 41 J. F. Eubank, L. Wojtas, M. R. Hight, T. Bousquet, V. C. Kravtsov and M. Eddaoudi, *J. Am. Chem. Soc.*, 2011, **133**, 17532.
- 42 B. Moulton, J. Lu, A. Mondal and M. J. Zaworotko, *Chem. Commun.*, 2001, 863.
- 43 Y. Zou, M. Park, S. Hong and M. S. Lah, *Chem. Commun.*, 2008, 2340.
- 44 F. Nouar, J. F. Eubank, T. Bousquet, L. Wojtas, M. J. Zaworotko and M. Eddaoudi, *J. Am. Chem. Soc.*, 2008, **130**, 1833.
- 45 (a) M. Xue, Y. Liu, R. M. Schaffino, S. Xiang, X. Zhao, G.-S. Zhu, S.-L. Qiu and B. Chen, *Inorg. Chem.*, 2009, **48**, 4649; (b) Y. Yan, X. Lin, S. Yang, A. J. Blake, A. Dailly, N. R. Champness, P. Hubberstey and M. Schroder, *Chem. Commun.*, 2009, 1025; (c) D. Zhao, D. Yuan, D. Sun and H.-C. Zhou, *J. Am. Chem. Soc.*, 2009, **131**, 9186; (d) O. K. Farha, A. Özgür Yazaydin, I. Eryazici, C. D. Malliakas, B. G. Hauser, M. G. Kanatzidis, S. T. Nguyen, R. Q. Snurr and J. T. Hupp, *Nat. Chem.*, 2010, **2**, 944; (e) Y. Yan, I. Telepeni, S. Yang, X. Lin, W. Kockelmann, A. Dailly, A. J. Blake, W. Lewis, G. S. Walker, D. R. Allan, S. A. Barnett, N. R. Champness and M. Schröder, *J. Am. Chem. Soc.*, 2010, **132**, 4092; (f) D. Yuan, D. Zhao, D. Sun and H.-C. Zhou, *Angew. Chem., Int. Ed.*, 2010, **49**, 5357; (g) D. Yuan, D. Zhao and H.-C. Zhou, *Inorg. Chem.*, 2011, **50**, 10528; (h) R. Luebke, J. F. Eubank, A. J. Cairns, Y. Belmabkhout, L. Wojtas and M. Eddaoudi, *Chem. Commun.*, 2012, **48**, 1455; (i) L. Li, S. Tang, X. Lv, M. Jiang, C. Wang and X. Zhao, *New J. Chem.*, 2013, **37**, 3662; (j) Y. Yan, M. Suyetin, E. Bichoutskaia, A. J. Blake, D. R. Allan, S. A. Barnett and M. Schroder, *Chem. Sci.*, 2013, **4**, 1731.
- 46 J. F. Eubank, F. Nouar, R. Luebke, A. J. Cairns, L. Wojtas, M. Alkordi, T. Bousquet, M. R. Hight, J. Eckert, J. P. Embs, P. A. Georgiev and M. Eddaoudi, *Angew. Chem., Int. Ed.*, 2012, **51**, 10099.
- 47 Perry, V. C. Kravtsov, G. J. McManus and M. J. Zaworotko, *J. Am. Chem. Soc.*, 2007, **129**, 10076.
- 48 X.-S. Wang, S. Ma, P. M. Forster, D. Yuan, J. Eckert, J. J. López, B. J. Murphy, J. B. Parise and H.-C. Zhou, *Angew. Chem., Int. Ed.*, 2008, **47**, 7263.
- 49 C. Li, W. Qiu, W. Shi, H. Song, G. Bai, H. He, J. Li and M. J. Zaworotko, *CrystEngComm*, 2012, **14**, 1929.
- 50 R. A. Smaldone, R. S. Forgan, H. Furukawa, J. J. Gassensmith, A. M. Z. Slawin, O. M. Yaghi and J. F. Stoddart, *Angew. Chem., Int. Ed.*, 2010, **49**, 8630.
- 51 I. Imaz, M. Rubio-Martinez, J. An, I. Sole-Font, N. L. Rosi and D. Maspocho, *Chem. Commun.*, 2011, **47**, 7287.

- 52 J. B. Weng, M. C. Hong, R. Cao, Q. Shi and A. S. C. Chan, *Chinese J. Struct. Chem.*, 2003, **22**, 195.
- 53 M. J. Ingleson, J. Bacsá and M. J. Rosseinsky, *Chem. Commun.*, 2007, 3036.
- 54 E. V. Anokhina, Y. B. Go, Y. Lee, T. Vogt and A. J. Jacobson, *J. Am. Chem. Soc.*, 2006, **128**, 9957.
- 55 C. Gramaccioli, *Acta Cryst.*, 1966, **21**, 600.
- 56 T.-T. Luo, L.-Y. Hsu, C.-C. Su, C.-H. Ueng, T.-C. Tsai and K.-L. Lu, *Inorg. Chem.*, 2007, **46**, 1532.
- 57 T. Kundu, S. C. Sahoo and R. Banerjee, *CrystEngComm*, 2013, **15**, 9634.
- 58 R. Vaidhyanathan, D. Bradshaw, J.-N. Rebilly, J. P. Barrio, J. A. Gould, N. G. Berry and M. J. Rosseinsky, *Angew. Chem., Int. Ed.*, 2006, **45**, 6495.
- 59 M. J. Ingleson, J. P. Barrio, J. Bacsá, C. Dickinson, H. Park and M. J. Rosseinsky, *Chem. Commun.*, 2008, 1287.
- 60 (a) L. Lin, R. Yu, W. Yang, X.-Y. Wu and C.-Z. Lu, *Cryst. Growth Des.*, 2012, **12**, 3304; (b) B. Lou, Y. Wei and Q. Lin, *CrystEngComm*, 2012, **14**, 2040.
- 61 J. Rabone, Y.-F. Yue, S. Y. Chong, K. C. Stylianou, J. Bacsá, D. Bradshaw, G. R. Darling, N. G. Berry, Y. Z. Khimiyak, A. Y. Ganin, P. Wiper, J. B. Claridge and M. J. Rosseinsky, *Science*, 2010, **329**, 1053.
- 62 C. Martí-Gastaldo, J. E. Warren, K. C. Stylianou, N. L. O. Flack and M. J. Rosseinsky, *Angew. Chem., Int. Ed.*, 2012, **51**, 11044.
- 63 C. Martí Gastaldo, AntypovD, J. E. Warren, M. E. Briggs, P. A. Chater, P. V. Wiper, G. J. Miller, Y. Z. Khimiyak, G. R. Darling, N. G. Berry and M. J. Rosseinsky, *Nat. Chem.*, 2014, 10.1038/nchem.1871.
- 64 A. P. Katsoulidis, K. S. Park, D. Antypov, C. Martí-Gastaldo, G. J. Miller, J. E. Warren, C. M. Robertson, F. Blanc, G. R. Darling, N. G. Berry, J. A. Purton, D. J. Adams and M. J. Rosseinsky, *Angew. Chem., Int. Ed.*, 2014, **53**, 193.
- 65 (a) D. N. Dybtsev, M. P. Yutkin, E. V. Peresypkina, A. V. Virovets, C. Serre, G. Férey and V. P. Fedin, *Inorg. Chem.*, 2007, **46**, 6843; (b) H. H.-M. Yeung, M. Kosa, M. Parrinello and A. K. Cheetham, *Cryst. Growth Des.*, 2013, **13**, 3705; (c) H. H.-M. Yeung and A. K. Cheetham, *Dalton Trans.*, 2014, **43**, 95.
- 66 A. J. Bailey, C. Lee, R. K. Feller, J. B. Orton, C. Mellot-Drazniéks, B. Slater, W. T. A. Harrison, P. Simoncic, A. Navrotsky, M. C. Grossel and A. K. Cheetham, *Angew. Chem., Int. Ed.*, 2008, **47**, 8634.
- 67 C. Lee, C. Mellot-Drazniéks, B. Slater, G. Wu, W. T. A. Harrison, C. N. R. Rao and A. K. Cheetham, *Chem. Commun.*, 2006, 2687.
- 68 (a) K. Uemura, S. Kitagawa, M. Kondo, K. Fukui, R. Kitaura, H.-C. Chang and T. Mizutani, *Chem.-Eur. J.*, 2002, **8**, 3586; (b) Y. Yan, S. Yang, A. J. Blake, W. Lewis, E. Poirier, S. A. Barnett, N. R. Champness and M. Schröder, *Chem. Commun.*, 2011, **47**, 9995; (c) Y.-S. Wei, K.-J. Chen, P.-Q. Liao, B.-Y. Zhu, R.-B. Lin, H.-L. Zhou, B.-Y. Wang, W. Xue, J.-P. Zhang and X.-M. Chen, *Chem. Sci.*, 2013, **4**, 1539; (d) S. Yang, L. Liu, J. Sun, K. M. Thomas, A. J. Davies, M. W. George, A. J. Blake, A. H. Hill, A. N. Fitch, C. C. Tang and M. Schröder, *J. Am. Chem. Soc.*, 2013, **135**, 4954.
- 69 G. Férey and C. Serre, *Chem. Soc. Rev.*, 2009, **38**, 1380.
- 70 (a) G. Férey, *Nat. Mater.*, 2003, **2**, 136; (b) D. Maspocho, D. Ruiz-Molina, K. Wurst, N. Domingo, M. Cavallini, F. Biscarini, J. Tejada, C. Rovira and J. Veciana, *Nat. Mater.*, 2003, **2**, 190.
- 71 G. Alberti, S. Murcia-Mascarós and R. Vivani, *J. Am. Chem. Soc.*, 1998, **120**, 9291.
- 72 S. Kitagawa and M. Kondo, *Bull. Chem. Soc. Jpn.*, 1998, **71**, 1739.
- 73 S. Kitagawa and K. Uemura, *Chem. Soc. Rev.*, 2005, **34**, 109.
- 74 (a) K. Barthelet, J. Marrot, D. Riou and G. Férey, *Angew. Chem., Int. Ed.*, 2002, **41**, 281; (b) C. Serre, F. Millange, C. Thouvenot, M. Nogués, G. Marsolier, D. Louër and G. Férey, *J. Am. Chem. Soc.*, 2002, **124**, 13519; (c) S. Surble, C. Serre, C. Mellot-Drazniéks, F. Millange and G. Férey, *Chem. Commun.*, 2006, 284; (d) C. Serre, C. Mellot-Drazniéks, S. Surblé, N. Audebrand, Y. Filinchuk and G. Férey, *Science*, 2007, **315**, 1828.
- 75 X.-L. Li, G.-Z. Liu, L.-Y. Xin and L.-Y. Wang, *CrystEngComm*, 2012, **14**, 5757.
- 76 J. P. S. Mowat, J. A. Groves, M. T. Wharmby, S. R. Miller, Y. Li, P. Lightfoot and P. A. Wright, *J. Solid State Chem.*, 2009, **182**, 2769.
- 77 M. Taddei, F. Costantino, A. Ienco, A. Comotti, P. V. Dau and S. M. Cohen, *Chem. Commun.*, 2013, **49**, 1315.
- 78 C. R. Murdock, Z. Lu and D. M. Jenkins, *Inorg. Chem.*, 2013, **52**, 2182.
- 79 (a) D. Han, F.-L. Jiang, M.-Y. Wu, L. Chen, Q.-H. Chen and M.-C. Hong, *Chem. Commun.*, 2011, **47**, 9861; (b) Z.-J. Lin, Z. Yang, T.-F. Liu, Y.-B. Huang and R. Cao, *Inorg. Chem.*, 2012, **51**, 1813; (c) H. Wu, Q. Gong, D. H. Olson and J. Li, *Chem. Rev.*, 2012, **112**, 836; (d) A. M. Plonka, D. Banerjee, W. R. Woerner, Z. Zhang, J. Li and J. B. Parise, *Chem. Commun.*, 2013, **49**, 7055; (e) J. Qian, F. Jiang, K. Su, J. Pan, L. Zhang, X. Li, D. Yuan and M. Hong, *J. Mater. Chem. A*, 2013, **1**, 10631; (f) J. Qian, F. Jiang, L. Zhang, K. Su, J. Pan, Q. Li, D. Yuan and M. Hong, *Chem. Commun.*, 2013, 10.1039/C3CC48556K; (g) J. Vaughn, H. Wu, B. Efremovska, D. H. Olson, J. Mattai, C. Ortiz, A. Puchalski, J. Li and L. Pan, *Chem. Commun.*, 2013, **49**, 5724.
- 80 (a) A. Demessence, D. M. D'Alessandro, M. L. Foo and J. R. Long, *J. Am. Chem. Soc.*, 2009, **131**, 8784; (b) W. Lu, D. Yuan, T. A. Makal, J.-R. Li and H.-C. Zhou, *Angew. Chem., Int. Ed.*, 2012, **51**, 1580; (c) S. Xiang, Y. He, Z. Zhang, H. Wu, W. Zhou, R. Krishna and B. Chen, *Nat. Commun.*, 2012, **3**, 954; (d) S. Yang, J. Sun, A. J. Ramirez-Cuesta, S. K. Callear, I. F. DavidWilliam, D. P. Anderson, R. Newby, A. J. Blake, J. E. Parker, C. C. Tang and M. Schröder, *Nat. Chem.*, 2012, **4**, 887; (e) A. M. Plonka, D. Banerjee, W. R. Woerner, Z. Zhang, N. Nijem, Y. J. Chabal, J. Li and J. B. Parise, *Angew. Chem., Int. Ed.*, 2013, **52**, 1692; (f) M. Zhang, Y.-P. Chen, M. Bosch, T. Gentle, K. Wang, D. Feng, Z. U. Wang and H.-C. Zhou, *Angew. Chem., Int. Ed.*, 2013, 10.1002/anie.201307340; (g) Z. Zhang, Y. Zhao, Q. Gong, Z. Li and J. Li, *Chem. Commun.*, 2013, **49**, 653.
- 81 (a) D. Liu and C. Zhong, *J. Mater. Chem.*, 2010, **20**, 10308; (b) M. P. Suh, H. J. Park, T. K. Prasad and D.-W. Lim, *Chem. Rev.*, 2012, **112**, 782; (c) Q. Yang, D. Liu, C. Zhong and J.-R. Li, *Chem. Rev.*, 2013, **113**, 8261.
- 82 (a) H. Furukawa, N. Ko, Y. B. Go, N. Aratani, S. B. Choi, E. Choi, A. Ö. Yazaydin, R. Q. Snurr, M. O'Keeffe, J. Kim and O. M. Yaghi, *Science*, 2010, **329**, 424; (b) Y. Yan, A. J. Blake, W. Lewis, S. A. Barnett, A. Dailly, N. R. Champness and M. Schröder, *Chem.-Eur. J.*, 2011, **17**, 11162; (c) H. Deng, S. Grunder, K. E. Cordova, C. Valente, H. Furukawa, M. Hmadeh, F. Gándara, A. C. Whalley, Z. Liu, S. Asahina, H. Kazumori, M. O'Keeffe, O. Terasaki, J. F. Stoddart and O. M. Yaghi, *Science*, 2012, **336**, 1018.
- 83 Z.-J. Lin, T.-F. Liu, B. Xu, L.-W. Han, Y.-B. Huang and R. Cao, *CrystEngComm*, 2011, **13**, 3321.

- 84 Y.-Q. Lan, H.-L. Jiang, S.-L. Li and Q. Xu, *Adv. Mater.*, 2011, **23**, 5015.
- 85 C. Zhan, C. Zou, G.-Q. Kong and C.-D. Wu, *Cryst. Growth Des.*, 2013, **13**, 1429.
- 86 A. Schoedel, A. J. Cairns, Y. Belmabkhout, L. Wojtas, M. Mohamed, Z. Zhang, D. M. Proserpio, M. Eddaoudi and M. J. Zaworotko, *Angew. Chem., Int. Ed.*, 2013, **52**, 2902.
- 87 F.-Y. Yi, S. Dang, W. Yang and Z.-M. Sun, *CrystEngComm*, 2013, **15**, 8320.
- 88 M. Wu, F. Jiang, W. Wei, Q. Gao, Y. Huang, L. Chen and M. Hong, *Cryst. Growth Des.*, 2009, **9**, 2559.
- 89 R. Yun, Z. Lu, Y. Pan, X. You and J. Bai, *Angew. Chem., Int. Ed.*, 2013, **52**, 11282.
- 90 Y.-Q. Lan, S.-L. Li, H.-L. Jiang and Q. Xu, *Chem.-Eur. J.*, 2012, **18**, 8076.
- 91 Z. Liang, J. Du, L. Sun, J. Xu, Y. Mu, Y. Li, J. Yu and R. Xu, *Inorg. Chem.*, 2013, **52**, 10720.
- 92 (a) Z.-J. Lin, T.-F. Liu, X.-L. Zhao, J. Lü and R. Cao, *Cryst. Growth Des.*, 2011, **11**, 4284; (b) W. Zhuang, D. Yuan, D. Liu, C. Zhong, J.-R. Li and H.-C. Zhou, *Chem. Mater.*, 2011, **24**, 18; (c) Y.-Q. Lan, H.-L. Jiang, S.-L. Li and Q. Xu, *Inorg. Chem.*, 2012, **51**, 7484; (d) Y.-S. Xue, Y. He, S.-B. Ren, Y. Yue, L. Zhou, Y.-Z. Li, H.-B. Du, X.-Z. You and B. Chen, *J. Mater. Chem.*, 2012, **22**, 10195.
- 93 (a) A. P. Nelson, O. K. Farha, K. L. Mulfort and J. T. Hupp, *J. Am. Chem. Soc.*, 2008, **131**, 458; (b) O. K. Farha and J. T. Hupp, *Acc. Chem. Res.*, 2010, **43**, 1166.
- 94 Y.-S. Xue, Y. He, L. Zhou, F.-J. Chen, Y. Xu, H.-B. Du, X.-Z. You and B. Chen, *J. Mater. Chem. A*, 2013, **1**, 4525.
- 95 Z.-J. Lin, T.-F. Liu, Y.-B. Huang, J. Lü and R. Cao, *Chem.-Eur. J.*, 2012, **18**, 7896.
- 96 Y.-X. Tan, Y.-P. He and J. Zhang, *Inorg. Chem.*, 2012, **51**, 9649.
- 97 (a) T. Li, D.-L. Chen, J. E. Sullivan, M. T. Kozlowski, J. K. Johnson and N. L. Rosi, *Chem. Sci.*, 2013, **4**, 1746; (b) P. Nugent, Y. Belmabkhout, S. D. Burd, A. J. Cairns, R. Luebke, K. Forrest, T. Pham, S. Ma, B. Space, L. Wojtas, M. Eddaoudi and M. J. Zaworotko, *Nature*, 2013, **495**, 80.
- 98 J. Qian, F. Jiang, D. Yuan, X. Li, L. Zhang, K. Su and M. Hong, *J. Mater. Chem. A*, 2013, **1**, 9075.
- 99 T. M. McDonald, D. M. D'Alessandro, R. Krishna and J. R. Long, *Chem. Sci.*, 2011, **2**, 2022.
- 100 (a) X. Si, C. Jiao, F. Li, J. Zhang, S. Wang, S. Liu, Z. Li, L. Sun, F. Xu, Z. Gabelica and C. Schick, *Energ Environ. Sci.*, 2011, **4**, 4522; (b) L. Du, Z. Lu, K. Zheng, J. Wang, X. Zheng, Y. Pan, X. You and J. Bai, *J. Am. Chem. Soc.*, 2012, **135**, 562; (c) J.-S. Qin, D.-Y. Du, W.-L. Li, J.-P. Zhang, S.-L. Li, Z.-M. Su, X.-L. Wang, Q. Xu, K.-Z. Shao and Y.-Q. Lan, *Chem. Sci.*, 2012, **3**, 2114; (d) B. Liu, R. Zhao, G. Yang, L. Hou, Y.-Y. Wang and Q.-Z. Shi, *CrystEngComm*, 2013, **15**, 2057.
- 101 M. Dinca and J. R. Long, *J. Am. Chem. Soc.*, 2007, **129**, 11172.
- 102 J. Duan, Z. Yang, J. Bai, B. Zheng, Y. Li and S. Li, *Chem. Commun.*, 2012, **48**, 3058.
- 103 B. Zheng, H. Liu, Z. Wang, X. Yu, P. Yi and J. Bai, *CrystEngComm*, 2013, **15**, 3517.
- 104 Z. Wang, B. Zheng, H. Liu, X. Lin, X. Yu, P. Yi and R. Yun, *Cryst. Growth Des.*, 2013, **13**, 5001.
- 105 B. Zheng, J. Bai, J. Duan, L. Wojtas and M. J. Zaworotko, *J. Am. Chem. Soc.*, 2010, **133**, 748.
- 106 B. Zheng, Z. Yang, J. Bai, Y. Li and S. Li, *Chem. Commun.*, 2012, **48**, 7025.
- 107 B. Li, Z. Zhang, Y. Li, K. Yao, Y. Zhu, Z. Deng, F. Yang, X. Zhou, G. Li, H. Wu, N. Nijem, Y. J. Chabal, Z. Lai, Y. Han, Z. Shi, S. Feng and J. Li, *Angew. Chem., Int. Ed.*, 2012, **51**, 1412.
- 108 P. Cui, Y.-G. Ma, H.-H. Li, B. Zhao, J.-R. Li, P. Cheng, P. B. Balbuena and H.-C. Zhou, *J. Am. Chem. Soc.*, 2012, **134**, 18892.
- 109 H. J. Park and M. P. Suh, *Chem. Sci.*, 2013, **4**, 685.
- 110 M. Fujita, Y. J. Kwon, S. Washizu and K. Ogura, *J. Am. Chem. Soc.*, 1994, **116**, 1151.
- 111 (a) D. Farrusseng, S. Aguado and C. Pinel, *Angew. Chem., Int. Ed.*, 2009, **48**, 7502; (b) A. Corma, H. Garcia and F. X. L. Xamena, *Chem. Rev.*, 2010, **110**, 4606; (c) M. Ranocchiari and J. A. van Bokhoven, *Phys. Chem. Chem. Phys.*, 2011, **13**, 6388; (d) A. Dhakshinamoorthy, M. Opanasenko, J. Čejka and H. Garcia, *Adv. Synth. Catal.*, 2013, **355**, 247.
- 112 S. Hasegawa, S. Horike, R. Matsuda, S. Furukawa, K. Mochizuki, Y. Kinoshita and S. Kitagawa, *J. Am. Chem. Soc.*, 2007, **129**, 2607.
- 113 (a) Y. Liu, R. Zhang, C. He, D. Dang and C. Duan, *Chem. Commun.*, 2010, **46**, 746; (b) X.-M. Lin, T.-T. Li, L.-F. Chen, L. Zhang and C.-Y. Su, *Dalton Trans.*, 2012, **41**, 10422.
- 114 Q.-R. Fang, D.-Q. Yuan, J. Sculley, J.-R. Li, Z.-B. Han and H.-C. Zhou, *Inorg. Chem.*, 2010, **49**, 11637.
- 115 J. S. Seo, D. Whang, H. Lee, S. I. Jun, J. Oh, Y. J. Jeon and K. Kim, *Nature*, 2000, **404**, 982.
- 116 M. Wang, M.-H. Xie, C.-D. Wu and Y.-G. Wang, *Chem. Commun.*, 2009, 2396.
- 117 D. Dang, P. Wu, C. He, Z. Xie and C. Duan, *J. Am. Chem. Soc.*, 2010, **132**, 14321.
- 118 P. Wu, C. He, J. Wang, X. Peng, X. Li, Y. An and C. Duan, *J. Am. Chem. Soc.*, 2012, **134**, 14991.
- 119 C. Zhu, G. Yuan, X. Chen, Z. Yang and Y. Cui, *J. Am. Chem. Soc.*, 2012, **134**, 8058.
- 120 W. Xuan, C. Ye, M. Zhang, Z. Chen and Y. Cui, *Chem. Sci.*, 2013, **4**, 3154.
- 121 Y. Nagao, M. Fujishima, R. Ikeda, S. Kanda and H. Kitagawa, *Synth. Met.*, 2003, **133–134**, 431.
- 122 M. Sadakiyo, T. Yamada and H. Kitagawa, *J. Am. Chem. Soc.*, 2009, **131**, 9906.
- 123 X. Liang, F. Zhang, W. Feng, X. Zou, C. Zhao, H. Na, C. Liu, F. Sun and G. Zhu, *Chem. Sci.*, 2013, **4**, 983.
- 124 S. C. Sahoo, T. Kundu and R. Banerjee, *J. Am. Chem. Soc.*, 2011, **133**, 17950.
- 125 R. M. P. Colodrero, P. Olivera-Pastor, E. R. Losilla, M. A. G. Aranda, L. Leon-Reina, M. Papadaki, A. C. McKinlay, R. E. Morris, K. D. Demadis and A. Cabeza, *Dalton Trans.*, 2012, **41**, 4045.
- 126 R. M. P. Colodrero, P. Olivera-Pastor, E. R. Losilla, D. Hernández-Alonso, M. A. G. Aranda, L. Leon-Reina, J. Rius, K. D. Demadis, B. Moreau, D. Villemin, M. Palomino, F. Rey and A. Cabeza, *Inorg. Chem.*, 2012, **51**, 7689.
- 127 F. Costantino, A. Donnadio and M. Casciola, *Inorg. Chem.*, 2012, **51**, 6992.
- 128 J. M. Taylor, K. W. Dawson and G. K. H. Shimizu, *J. Am. Chem. Soc.*, 2013, **135**, 1193.

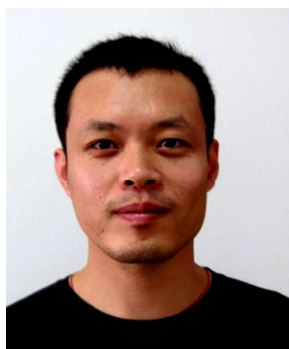




This review presents the recent developments of FL-MOFs, including their structures and applications in gas adsorption, catalysis and proton conduction.



*Dr. Zu-Jin Lin was born in Fujian province, P. R. China. He got his BSc from Fuzhou University in 2007 and received his PhD in Inorganic Chemistry from the Fujian Institute of Research on the Structure of Matter (FJIRSM), Chinese Academy of Sciences (CAS) in 2012 under the guidance of professor Rong Cao. Then, he joined the FJIRSM as an assistant researcher. His current research interests focus on the catalysis and gas adsorption in porous materials including metal-organic frameworks and porous organic polymers.*



*Dr. Jian Lü received Ph.D. from Fujian Institute of Research on the Structure of Matter (FJIRSM), Chinese Academy of Sciences, in 2008 under the supervision of Prof. Rong Cao. After one year as postdoctoral researcher in Politecnico di Milano (Italy) with Prof. Pierangelo Metrangolo and Prof. Giuseppe Resnati, he joined in Cao's research group at FJIRSM and was promoted to associate professor in 2010. He held a Sino-British incoming research fellow in the University of Nottingham (UK) with Prof. Martin Schröder in 2012-2013. His research interest includes coordination and supramolecular chemistry, crystalline functional materials for storage, separation, catalysis etc.*



*Maochun Hong graduated from Fuzhou University in 1978 and received his M.S. degree from FJIRSM, Chinese Academy of Sciences in 1981. He was a research fellow at Michigan University and Illinois University, USA in 1985–1987, and worked as a visiting scientist at Newcastle University, United Kingdom in 1992–1993. He was a Full Professor of Chemistry at FJIRSM, CAS since 1994. In 1998, he worked as a JSPS visiting professor in Japan, and received his Ph.D. degree from Nagoya University. His research interests focus on nano materials, crystal design and growth, supramolecular chemistry, and inorganic–organic hybrid functional materials.*



*Rong Cao was born in Fujian province, China. He obtained PhD in Fujian Institute of Research on the Structure of Matter (FJIRSM), Chinese Academy of Sciences (CAS), in 1993. Following post-doctoral experience in the Hong Kong Polytechnic University and JSPS Fellowship in Nagoya University, he became a professor at FJIRSM in 1998. Now, he is the director of FJIRSM. His main research interests include crystal engineering of coordination and supramolecular chemistry, and nano catalysis.*